UILU-ENG-80-2017

CIVIL ENGINEERING STUDIES
HYDRAULIC ENGINEERING SERIES NO. 36

UNSTEADY GUTTER FLOW INTO GRATE INLETS

by

A. OSMAN AKAN and BEN CHIE YEN

Metz Reference Room
University of Illinois
B106 NCEL
208 N. Romine Street
Urbana, Illinois 61801

DEPARTMENT OF CIVIL ENGINEERING
UNIVERSITY OF ILLINOIS AT URBANA-CHAMPAIGN
URBANA, ILLINOIS
AUGUST, 1980

UILU-ENG-80-2017

Civil Engineering Studies
Hydraulic Engineering Series No. 36

UNSTEADY GUTTER FLOW INTO GRATE INLETS

by

A. Osman Akan and Ben Chie Yen

DEPARTMENT OF CIVIL ENGINEERING
UNIVERSITY OF ILLINOIS AT URBANA-CHAMPAIGN
URBANA, ILLINOIS
AUGUST, 1980

ABSTRACT

Runoff from gutters into inlets is usually an unsteady flow phenomenon and is investigated theoretically in this study. The Saint-Venant equations describing unsteady gutter flows are solved numerically by using the method of characteristics. The discharge into the grate inlet is then determined approximately with the aid of previous experimental results. Dimensional analysis is performed to identify the nondimensional influential parameters and to guide the ranges of dimensionless variables analyzed. Design curves are proposed for a given type of gutter and grate inlet to determine the runoff intercepted by the inlet, and the use of these curves is illustrated by an example.

FOREWARD

This report is based mainly on the thesis of the same title submitted by A. O. Akan in June 1973 to the Department of Civil Engineering of the University of Illinois at Urbana-Champaign in partial fulfillment of the requirements for the degree of Master of Science. Since only a few copies of the thesis were printed and the authors have received a number of inquiries concerning research on gutter flow in recent years, it appears desirable to modify and publish this research result for public uses. Analysis of gutter flow from pavement under rainfall, which was not included in Dr. Akan's thesis, is included in this report. Therefore, Sections 2.2 and 2.4 and the last chapter are modified substantially from Akan's thesis and Chapter 5 is added. All the numerical analyses presented in this report were performed in 1972-1973. More efficient numerical solution methods have been developed since then. These more efficient methods have been reported elsewhere and they do not alter the conclusions of the gutter flow analyses. Therefore, these improved numerical techniques are not discussed in this report.

TABLE OF CONTENTS

LIST OF FIGURES

LIST OF TABLES

age

53

68

82,83

1. INTRODUCTION

Surface drainage problem can be resolved best with an accurate knowledge of the relative merits of each drainage device and the conditions under which it operates. An overdesign of a storm drainage system would be undesirable from the viewpoint of economy, while an underdesign of the system would result in functional failure and consequent damages.

Surface drainage of streets and roads can be best accomplished economically yet adequately through a judicious use of gutters and inlets. Adjacent to pavement, gutters control excessive ponding of precipitation run-off. They receive water from pavements as well as directly from rainfall or other sources and deliver it to be intercepted and disposed by use of a sub-surface sewer or surface channel system. Curb inlets, grate inlets or a combination of both are the most widely used devices to intercept the gutter flow. Although each group includes many varieties, a curb inlet, in general, may be defined as a vertical opening in the curb through which the water is removed from the gutter. The major disadvantage of curb inlets is being inefficient flow interceptors. A grate inlet is an opening in the gutter through which the water falls. From a hydraulic standpoint, they are better interceptors than curb inlets, because they are placed across the path of the flowing water. However, their efficiency as interceptors is reduced through inlet grating, which is needed to remove the foreign material like debris, trash, gravel and stones from the storm water that may cause trouble in the subsurface system. Structural stability, safety considerations and other limitations such as those imposed by vehicle wheels should also be considered in the design of these devices.

Many researchers examine the hydraulic behavior of grate inlets

experimentally and present their results with a series of curves relating the flow intercepted by a given type of inlet to the total discharge passing it. Larson and Straub [1949] investigated the flow capacity and self-cleansing abilities of some typical grate inlets, and subsequently they developed an improved grate inlet. Guillou [1959] determined the interception characteristics of four Illinois Division of Highways standard inlet grates and frames by using a full scale laboratory model. He also applied his results to typical design problems. In a report by a team of the Storm Drainage Research Project in the Department of Sanitary Engineering and Water Resources of the Johns Hopkins University, experimental results on various types of curb, grate and combined inlets were discussed and rating curves for several types of inlets used in Baltimore were presented with certain design recommendations [1956]. Wintz and Kuo [1970] studied the capacities of four standard inlets presently used by the Louisiana Department of Highways for different combinations of longitudinal and cross slopes and gave the curves relating the fraction of flow intercepted by the inlet to the total gutter flow. McNown and Tai [1972] conducted 1:3 scale model tests of the inlet system used by Kansas State Highway Commission. They observed the performance for various inlet configurations, discharges and slopes and studied the distribution of flow in the channel and the effectiveness of grate inlets and curb openings. Recently experiments were conducted at the Bureau of Reclamation for eight different types of grate inlets (Burgi and Gober, 1977). Three of these inlets were selected for further tests on their bicycle-safe and hydraulic characteristics (Burgi 1978a, 1978b). In a remarkable study by Cassidy [1966], a rational qualitative analysis of the variables governing the efficiency of a grate inlet was verified through experimental measurements. The results were presented in a

generalized dimensionless graphical fashion valid for any size grate. More discussion will be given to this work in the next chapter.

In all the previous studies on the subject, the discharge in the gutters and inlets are assumed to be constant, and the effect of flow unsteadiness is not considered. However, runoff in a gutter is, usually, initiated by a rainfall which is never steady. Besides, in addition to the peak rate of rainstorm runoff, an engineer should also be concerned with gutter flow detention and the time distribution of pollutants such as salt added to the gutter flow from snowmelt. Thus, for a realistic consideration of rainfall-runoff problems, one should account for the effect of flow unsteadiness, and for an efficient surface drainage accomplishment, it is necessary to determine the complete flow hydrograph into the inlet rather than only the peak flow rate. The purpose of this study is to show theoretically that the intercepted flow hydrograph for a grate inlet depends on the different gutter flow conditions by solving the unsteady gutter flow equations numerically using the method of characteristics.

2. HYDRAULIC CONSIDERATIONS

2.1 Gutter Flow Equations

Runoff in a street gutter, in general, is a form of spatially-varied, unsteady, open-channel flow. Exact equations describing the problem were given by Yen [1971, 1973]. However, although such equations provide a thorough understanding of the physical features of the phenomena, they are difficult to solve. Therefore, in the present study, simplified equations of motion of one-dimensional flow in a prismatic open channel with lateral flow are adopted [Strelkoff, 1969; Yen, 1973]

$$\frac{\partial Q}{\partial x} + \frac{\partial A}{\partial t} = q \tag{2.1}$$

$$\frac{1}{Ag}\frac{\partial Q}{\partial t} + \frac{2V}{Ag}\frac{\partial Q}{\partial x} + (1 - F_r^2)\frac{\partial y}{\partial x} = S_o - S_f \tag{2.2}$$

in which

A = cross sectional area of flow

x = distance along the gutter

y = average depth of flow measured normal to x

t = time

V = average velocity of flow, considered positive when flow occurs in the nominally downstream direction

Q = discharge through a cross section, signed in conformity with V

q = lateral flow ($q > 0$ for inflow) per unit length of the gutter

$F_r^2 = (Q^2/gA^3)(dA/dy)$

S_o = bottom slope of the gutter

S_f = friction slope

Equations 2.1 and 2.2 are actually a variation of the well-known Saint-Venant equations of continuity and momentum. They are also referred to as the complete dynamic wave equations because they contain all the terms describing the physics of the flow. But they are not exact because they are limited to be used with the following assumptions [Strelkoff, 1969; Yen, 1973]

a. The component of the inflow velocity vector in the main gutter flow direction is zero;
b. The velocity is uniformly distributed over the cross sectional area A;
c. The pressure distribution is hydrostatic;
d. The pattern of turbulence varies negligibly from section to section;
e. The variation of the internal normal stresses along the flow direction is negligible;
f. Flow passages are large compared with molecular dimensions so that continuity of fluid medium can be assumed;
g. At the solid boundaries all velocity components vanish;
h. Surface tension has negligible effect on the mean-flow variables;
i. Body forces other than gravity are negligble;
j. Stresses due to air on the free surface are negligible.

It is interesting to note that Eq. 2.2 is also valid for the case of no lateral inflow [Nes and Hendriks, 1971].

There are many different cross sectional shapes for street gutters.

Some of these are shown in Fig. 1. The triangular shape is one of the most commonly used and is adopted in the present study. Unsteady flows in gutters of other cross sectional shapes can be analyzed similarly.

The actual flow area in a triangular gutter is shown in Fig. 1.d and is defined by the boundary EFCD. If the cross sectional average depth of the gutter flow is y, then the flow cross sectional area A is

$$A = Ty \tag{2.3}$$

in which T is the water surface width. If an approximation of the flow cross section defined by the points E', F and C' is adopted, T can then be expressed approximately as

$$T = 2y \cot \phi \tag{2.4}$$

in which ϕ is the angle made by the gutter bottom along the lateral direction with the horizontal plane. The variations of T and y with respect to time and space are of the same order of magnitude. Consequently, in manipulating Eqs. 2.1 and 2.2 one should not regard the top width constant as often done in the literature. Substitution of Eqs. 2.3 and 2.4 into Eqs. 2.1 and 2.2, the equation of continuity and the momentum equation for a triangular gutter are

$$\frac{1}{2T}\frac{\partial Q}{\partial x} + \frac{\partial y}{\partial t} - \frac{q}{2T} = 0 \tag{2.5}$$

$$\frac{\partial Q}{\partial t} + 2V\frac{\partial Q}{\partial x} + (Ag - 2V^2T)\frac{\partial y}{\partial x} - (S_o - S_f)Ag = 0 \tag{2.6}$$

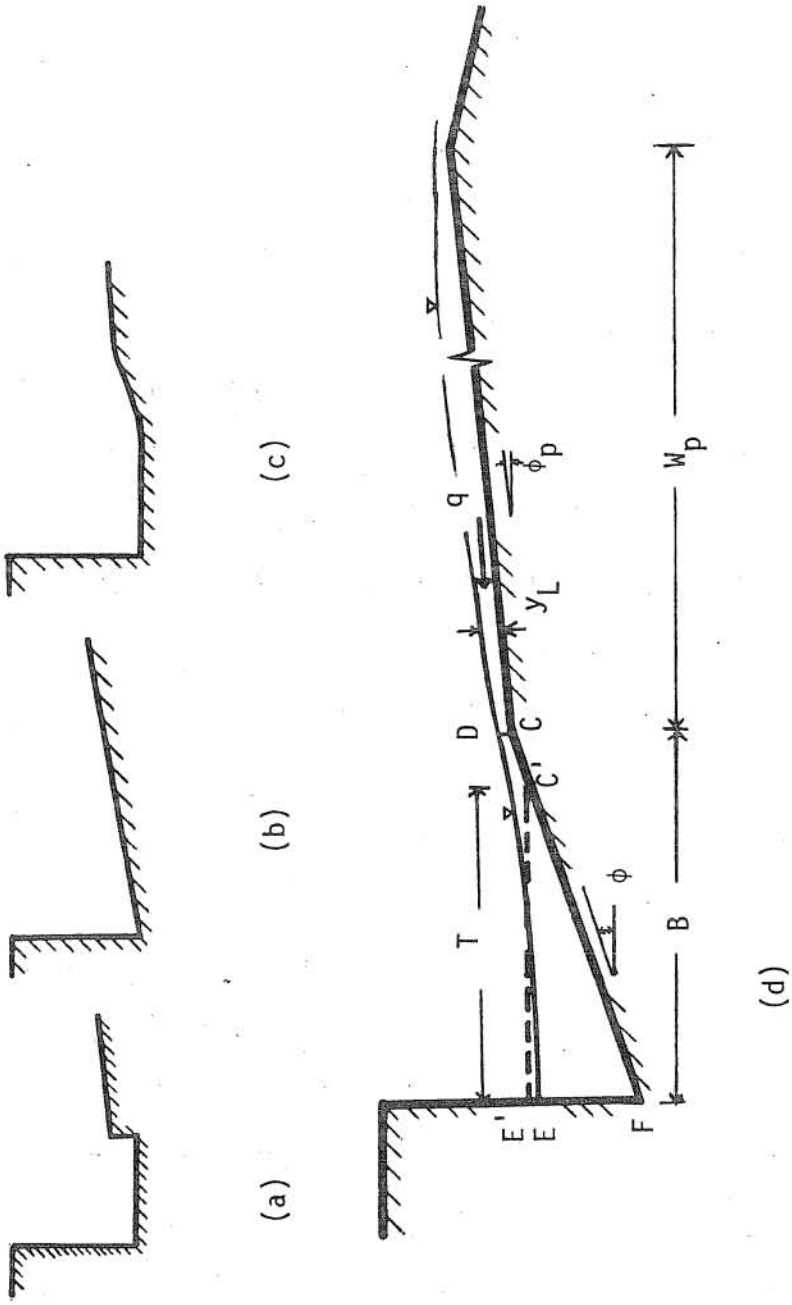

Fig. 1 Some Typical Cross Sections of Gutters

2.2 Dimensional Analysis

The flow in a gutter depends on the geometric characteristics of the gutter and pavement, the physical characteristics of the inflow, properties of the fluid, and the downstream flow condition if the flow is subcritical. The mathematical expressions describing the flow have been presented in the preceding section. However, a qualitative discussion of the flow pattern and a dimensional analysis of the factors involved will give some physical insight to the problem and will be helpful in presenting the results.

There are many different types of gutters and street pavement crown shapes. A popular type is the triangular gutter with straight pavement of constant cross slope as shown in Fig. 1d. The geometric characteristics of the gutter consists of its longitudinal slope S_o which is usually equal to the street slope, its length L_g, a measure of the roughness of the gutter surface, k, and the gutter cross-sectional parameters which consist of the gutter width B and a representative dimensionless cross sectional shape parameter, η. The pavement characteristics include its length along the transverse direction of the street, W_p, a dimensionless parameters, η_p, representing the geometric profile along its length, and the pavement surface roughness, k_p. For a constant cross slope of the pavement (or sometimes called crown slope) as shown in Fig. 1d the pavement profile parameter η_p can be expressed in terms of the angle made between the pavement and the horizontal, ϕ_p.

The inflow consists of rainfall and the carry-over inflow, if any, at the upstream end of the gutter. The rain which falls on the pavement as well as directly over the gutter has an average intensity i over its duration t_i. For the area on a street contributing to an inlet, the areal variation of i is usually small and hence assumed uniform. This assumption is made merely for

the sake of simplicity in presenting the results and can easily be removed. The temporal distribution of the rainfall is represented by a nondimensional parameter I_t. For simplicity, i considered here is assumed to be the rainfall excess, i.e., rainfall minus infiltration and other losses. This again can easily be modified and improved by including infiltration and other abstractions.

The gutter upstream carry-over inflow may be the spill-over from the previous inlet, the flow from street washing or hydrant, the water from melted snow, or, simply the flow from the upstream portion of the entire gutter which has been analyzed separately. The inflow through the upstream cross section of the gutter can be described by the peak discharge Q_{pu} and duration t_u of the inflow hydrograph together with nondimensional parameters J_t representing the time distribution of the inflow (i.e., the shape of the inflow hydrograph), and J_p, J_d, and J_v for the pressure, depth, and velocity distributions of the inflow over the upstream entrance cross section of the gutter. If the length of the gutter, L_g, is sufficiently long, the influences of the nonuniform velocity, depth, and pressure distributions at the entrance section on the flow diminish downstream along the gutter. In other words, as far as the flow through the exist section of the gutter is concerned, the flow at the entrance section behaves like a source and hence the characteristics of the inflow hydrograph is important but the effects due to J_p, J_d, and J_v can be neglected.

The fluid properties include its density, ρ, specific weight, γ, kinematic viscosity, ν, and surface tension, σ. Although surface runoffs are often sheet flows with small depth, the roughness of the surface texture of the gutters and streets together with infiltration would make the effect of surface tension negligible.

Thus, the discharge Q_o at the exit section of the gutter can be expressed as a function of the influenctial factors as

$$Q_o = F_1(t, S_o, L_g, B, \eta, k, k_p, \phi_p, W_p, t_i, i, I_t, Q_{pu}, t_u, J_t, \rho, \gamma, \nu, \delta) \tag{2.7}$$

in which t is time, δ is a dimensionless parameter representing the downstream conditions of the gutter, and F represents a function. Through dimensional analysis by applying the Buckingham π-theorem to Eq. 2.7, one obtains

$$\frac{Q_o}{iA_s} \text{ or } \frac{Q_o}{Q_s} = F_{2,3}\left(\frac{t}{t_i}, S_o, \frac{L_g}{B}, \eta, \frac{k}{B}, \frac{k_p}{B}, \phi_p, \frac{W_p}{B}, \frac{t_i i}{B}, I_t, \frac{Q_{pu} t_i}{B^3}, J_t, \frac{t_u}{t_i}, \frac{B}{g t_i^2}, \frac{B^2}{\nu t_i}, \delta\right) \tag{2.8}$$

in which $A_s = L_g (B + W_p)$ is the horizontally projected area receiving rainfall i; $Q_s = (iA_s + Q_{pu})$ is the corresponding maximum steady flow discharge; and g is the gravitational acceleration.

The physical meanings of the terms in Eq. 2.8 are as follows. To the left of the equality sign is the relative gutter discharge at its exit measured in terms of the rainfall inflow rate and the possible maximum total inflow rate, respectively. To the right of the equality sign, the first term of the function indicates the time distribution of the nondimensional hydrograph. The second term accounts for the effect of the street slope on both the gutter and pavement flows. The third term is the relative length of the gutter, and as discussed previously, only when the gutter is relatively long that the effects of the velocity, depth, and pressure distributions of the gutter upstream inflow can be neglected. The fourth term represents the nondimensional cross sectional

shape of the gutter. For a rectangular gutter as shown in Fig. 1a, η can be replaced by the ratio of the drop at the pavement side to B. For a triangular gutter, η consists of the curb angle, ψ, measured from the vertical and the gutter bottom transverse angle, ϕ, made with the horizontal. The fifth and sixth terms are the relative surface roughnesses of the gutter and pavement, respectively. The seventh term is simply the cross slope of the pavement usually ranging from 1/8 to 1/2 in. per ft, i.e., 1 to 4 percent, or approximately 0.6 to 2.4 degrees. The eighth term represents the relative size of the overland surface, the ninth a measure of the amount of rainfall, and the tenth the temporal distribution of rainfall, and these three terms together is an indication of the relative importance of the lateral flow. The eleventh term is an indirect measure of the volume of the upstream inflow into the gutter relative to the volume of the gutter. The twelfth term represents the shape of the inflow hydrograph. The thirteenth term is the relative duration of gutter upstream inflow as compared to that for the rainfall and is an indication of their relative importance in determining the runoff hydrograph. The fourteenth term, obtained from the ratio γ/ρ, represents the effect of gravity, and the fifteenth term represents the effect of viscosity, and these two terms replace respectively the representative Froude and Reynolds number of the surface runoff. The sixteenth (last) term indicates the gutter downstream boundary condition.

Because the flow is unsteady and nonuniform, even for a given inflow, it may vary between turbulent and laminar and between subcritical and supercritical, depending on the time and location. Consequently it is difficult, it not impossible, to define a representative Froude or Reynolds number for the flow over the entire area and duration. Likewise, from the fluid

mechanics viewpoint, the relative surface roughness should be measured in terms of the hydraulic radius of the flow instead of B because it is the former ratio together with the Reynolds number, and to some degree with the Froude number, that the flow resistance is determined. Again, because the hydraulic radius varies from time to time and from location to location for an unsteady non-uniform flow, a physically significant hydraulic radius cannot be found for use in the dimensional analysis.

The downstream condition of the gutter flow depends on the physical properties of the inlet. If the flow is supercritical, the flow in the gutter is independent of the downstream condition as long as a one-dimensional analysis is applied. Contrarily, if the gutter flow is subcritical, the backwater effect due to the downstream condition would affect the flow in the gutter. There are two major types of inlets, namely, the grate inlets and the curb inlets. Many variations exist for each type and they are used individually as well as mixed and combined. Within the United States, none of the states have standardized the inlets. It is not possible in this study to investigate at present the different effects of the numerous various types of inlets, nor is it desirable because it is postulated that when more information become known about the inlets in the near future there will be fewer types of inlets used. For rectangular grate inlets, the parameter δ can be represented by

$$\delta = F_4(\frac{L}{W}, G_1, \delta_1) \tag{2.9}$$

in which L and W are respectively the length and width of the grate inlet, G_1 is a collective nondimensional parameter representing schematically the interior geometric pattern of the grate inlet, and δ_1 is a nondimensional symbol representing the condition at the downstream boundary of the inlet which vanishes when the flow is supercritical or completely intercepted by the inlet. For a rectangular grate inlet with parallel bars as shown in Fig. 2,

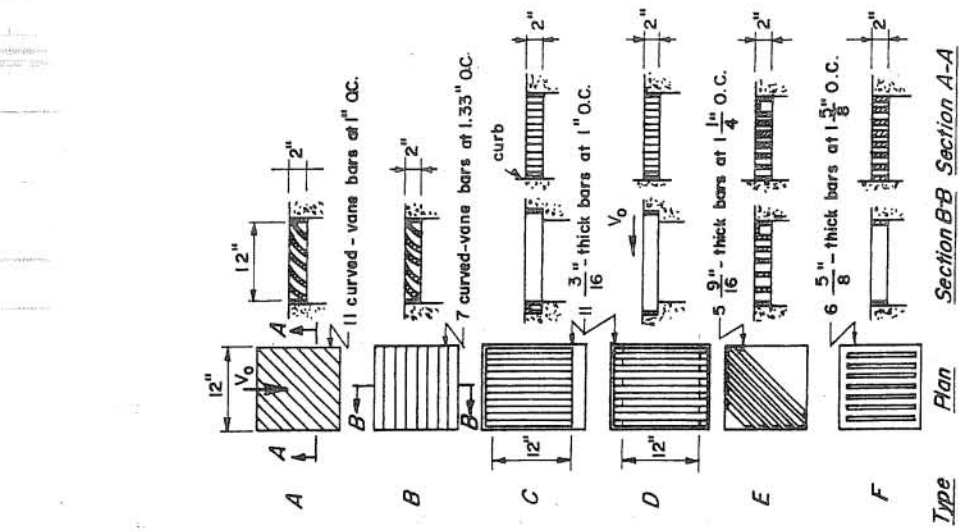

Fig. 3 Grate Inlets Tested by Cassidy[1966]

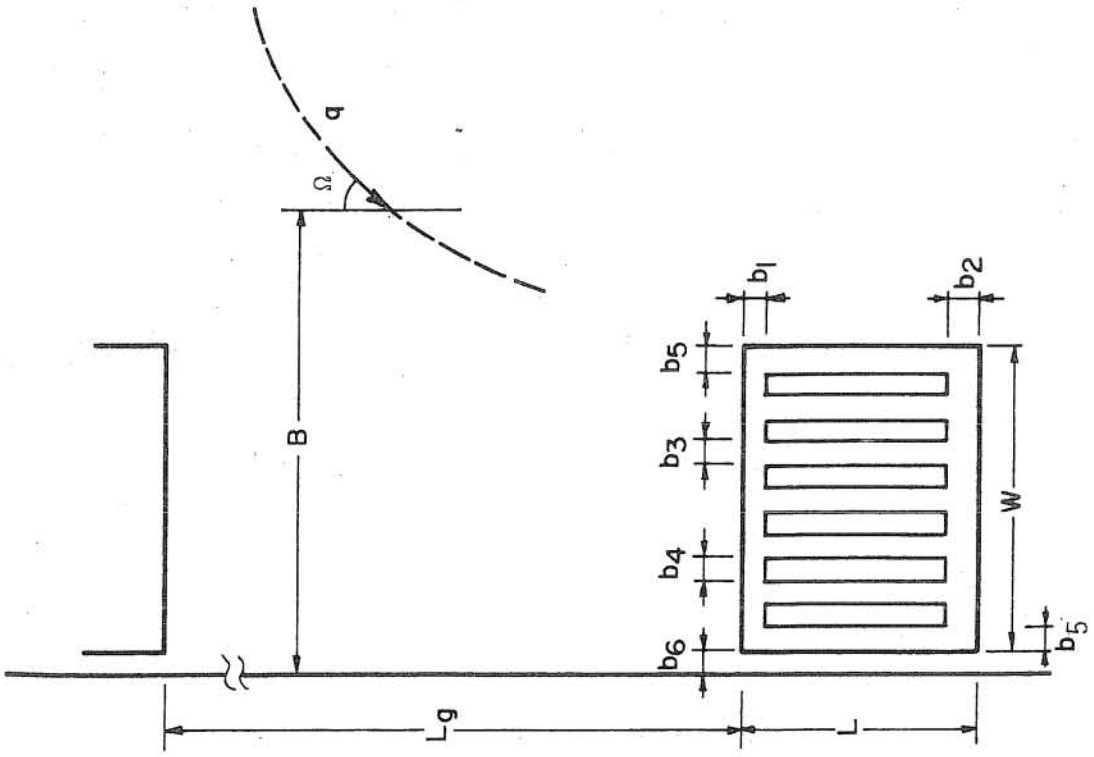

Fig. 2 Schematic of Rectangular Grate Inlet

$$G_1 = F_5\left(\frac{b_1}{W}, \frac{b_2}{W}, \frac{b_3}{W}, \frac{b_4}{W}, \frac{b_5}{W}, \frac{b_6}{W}, \eta_b\right) \tag{2.10}$$

in which b_3 is the width of the grate bars, b_4 is the opening width between the bars, b_1, b_2 and b_5 are the circumferential widths of grate frame as shown in Fig. 2, b_6 is the spacing between the grate inlet and the curb, and η_b denotes the cross sectional shape of the grate bars. For rectangular bars, η_b is replaced by the ratio of b_3 to the height of the bar, and for circular bars, η_b is replaced by the diameter of the bar. The length of the slot openning is equal to $L - b_1 - b_2$ and the opening area ratio is $[(L - b_1 - b_2)$ $b_4(W - 2b_5)/(b_3 + b_4)]/WL$. Grate inlets having other shapes and geometric patterns can be similarily represented in nondimensional forms.

Ideally, it is desirable to have the inlets intercepting all the pavement and gutter flow coming from upstream of the inlet. In reality because of the relatively steep street slope, small inlet size, or other factors, a part of the gutter flow may pass over the inlet without being intercepted, as well as the spill-over on the pavement adjacent to the inlet. If at any instant the intercepted discharge by the inlet is Q_i, the ratio Q_i/Q_o may be considered as a measure of the inlet efficiency. The gutter flow carry-over is obviously $Q_o - Q_i$. Nondimensionally, the intercepted flow, Q_i/iA_s or Q_i/Q_s, are affected by the same parameters which determine Q_o/iA or Q_o/Q_s as given in Eq. 2.8, i.e.,

$$\frac{Q_i}{iA_s} \text{ or } \frac{Q_i}{Q_s} = F_{6,7}\left(\frac{t}{t_i}, S_o, \frac{L_g}{B}, \eta, \frac{k}{B}, \frac{k_p}{B}, \phi_p, \frac{W_p}{B}, \frac{t_i i}{B}, I_t, \frac{Q_{pu} t_i}{B^3}\right.$$

$$\left. J_t, \frac{t_u}{t_i}, \frac{B}{gt_i^2}, \frac{B^2}{\nu t_i}, \delta\right) \tag{2.11}$$

Grate inlet flow discussed previously in this section considers the gutter and pavement as an integrated system of source of water for the inlet.

In addition to the rain falling directly onto the gutter, the flow from the pavement and sidewalk constitutes the lateral inflow into the gutter. The streamlines of the lateral flow near the pavement crown are along the direction of the vector sum of the crown slope and street slope, and are approximately perpendicular to the main direction of the gutter flow if the street slope is relatively small. Due to backwater effect, if the depth of the gutter flow is small the lateral inflow has an unsteady surface profile similar to M2 type curve for subcritical flow and S2 for supercritical flow. When the velocity and depth of flow in the gutter are relatively high, the lateral flow streamlines are affected and they curve towards the downstream direction of the gutter, and the unsteady backwater surface profile is similar to either M1 or S1 type. Streamlines around the grate inlet are highly curvilinear and the phenomena is too complex to be described by using a one-dimensional approach.

Two-dimensional flow simulation to represent the pavement-gutter system is rather complicated and computationally expensive. Although they are mutually related, in practice the pavement flow and gutter flow are treated as two separated entities. The pavement flow is first estimated. Subsequently, it is considered as a lateral inflow when the gutter flow is considered. In such a case the rainfall and pavement parameters, t_i, i, I_t, k_p, ϕ_p, and W_p in Eq. 2.7 are replaced by the pavement lateral flow parameters which may be represented by the lateral inflow time rate q per unit length of the gutter, the angle Ω and depth y_ℓ of the lateral flow when it enters the gutter flow, and dimensionless parameters Z_t and Z_s denoting the temporal and spatial variations of q. By assuming that Ω is nearly normal to the gutter flow, Z_t can be represented by the duration of the lateral flow t_ℓ, and ignoring the effects of y_ℓ and Z_s, the counterpart of Eq. 2.7 is

$$Q_o, Q_i = F_{8,9}(t, S_o, L_g, B, n, k, q, t_\ell, Q_{pu}, t_u, J_t, \gamma/\rho, \nu, \delta) \qquad (2.12)$$

Accordingly, using B and t_ℓ as the repeating variables,

$$\frac{Q_o}{Q_s} \text{ or } \frac{Q_i}{Q_s} = F_{10,11}\left(\frac{t}{t_\ell}, S_o, \frac{L_g}{B}, n, \frac{k}{B}, \frac{qt_\ell}{B^2}, \frac{Q_{pu}t_\ell}{B^3}, \frac{t_u}{t_\ell}, J_t, \frac{B}{gt_\ell^2}, \frac{B^2}{\nu t_\ell}, \delta\right) \qquad (2.13)$$

in which $Q_s = (qL_g + Q_{pu})$.

For a rectangular grate inlet (Fig. 2) connected to a vertical-curb triangular cross section gutter (Fig. 1d) receiving water from a spatially and temporally constant q for $t > 0$ and the upstream inflow $Q_{pu} \neq 0$, replacing t_ℓ by t_u as the repeating time variable in Eq. 2.13 and with the aid of Eq. 2.9 and cross-multiplication of some of the nondimensional terms, one obtains

$$\frac{Q_o}{Q_{pu}}, \text{ or } \frac{Q_i}{Q_{pu}} =$$

$$F_{12,13}\left(\frac{t}{t_u}, S_o, \frac{L_g}{B}, S_g, \frac{k}{B}, \frac{qL_g}{Q_{pu}}, \frac{Q_{pu}t_u}{B^2L_g}, J_t, \frac{Q_{pu}}{\sqrt{gS_g^2W^5}}, \frac{Q_{pu}}{W\nu}, \frac{W}{L}, G_1, \delta_1\right) \qquad (2.14)$$

in which $S_g = \tan\phi$ is the transverse slope of the gutter bottom.

2.3 Flow Into Grate Inlet

In order to solve Eqs. 2.5 and 2.6, it is necessary to know for a subcritical flow the flow condition at the grate inlet as the downstream boundary condition. However, the gutter flow and the flow into the inlet are interrelated. Moreover, irregular boundaries around the grate inlet make it difficult to obtain any simple general expressions describing mathematically the flow into the inlet. Therefore, at the present, assumptions must be made to provide the downstream conditions of the subcritical gutter flow. Such assumptions may be based on previous steady-flow experimental results

such as those obtained by Cassidy [1966]. A quasi-steady approximation is adopted such that the flow at the grate is assumed steady at the instant considered with the flow parameters having their instantaneous values.

Most grate inlets have their width smaller than the spread of the approaching flow in the gutter. Therefore, the flow intercepted by the inlet is usually limited to the portion of the flow over and immediately around the grate itself. The part of the flow passing directly over or around the inlet without being intercepted is called the carry-over. Although the physical nature of the flow into a grate inlet is too complex to obtain a theoretical solution even for a steady flow approximation, it is possible to clarify the physical picture by obtaining a qualitative relationship between the variables influencing the flow into the inlet. A complete relationship of this kind was given by Eqs. 2.8 and 2.11 in the preceding section, and it was reduced to Eqs. 2.13 and 2.14 through certain simplifications.

Cassidy [1966] presented a relationship between the dimensionless flow parameters in the form

$$\frac{Q_i}{Q_o} = F_{14}\left(\frac{V_o}{\sqrt{gd_o}}, \frac{L}{d_o}, \frac{d_o}{W}, G_1, S_g, S_o\right) \qquad (2.15)$$

in which d_o is the depth of flow measured at the curb and V_o is the cross sectional mean flow velocity at the gutter exit. Equation 2.15 constitutes a special form of Eq. 2.14, in that the flow is assumed to be steady (thus dropping t/t_u and J_t) and the effect of the gutter flow including the effects of lateral and upstream inflows (corresponding to the third, fifth, sixth, seventh, ninth, and tenth terms at the right hand side of Eq. 2.14) can adequately be represented

by two dimensionless terms involving V_o and d_o when the function F_{13} is divided by F_{12} to yield Q_i/Q_o.

He studied six different grate geometries shown in Fig. 3 experimentally and concluded that although S_o plays an important role in determining the gutter discharge Q_o, its effect on the relative discharge into the grate Q_i/Q_o is only secondary and indirect and hence can be neglected in Eq. 2.15. However, it should be remarked here that his experiments were conducted with supercritical flows and with very limited space for the flow to pass around the inlet.

Cassidy's results show that at relatively low values of d_o/W or $V_o/\sqrt{gd_o}$ all the flow over the grate is intercepted by the inlet and the flow pattern is relatively smooth. For each of the grate inlets tested, he gave a limiting length of the inlet at which all the water passing over it would be completely intercepted:

$$\frac{L}{d_o} = m \frac{V_o}{\sqrt{gd_o}} \qquad (2.16)$$

in which m is a coefficient depending upon the geometry of the grate inlet and is an indication of the efficiency of grate inlet.

A close examination of Cassidy's data confirms that the variation of Q_i/Q_o with $V_o/\sqrt{gd_o}$ is smaller than five percent provided $L/d_o > mV_o/\sqrt{gd_o}$. Thus by extrapolating from his data, one may obtain the flow interception curves given in Fig. 4 for the Type F grate configuration shown in Fig. 3.

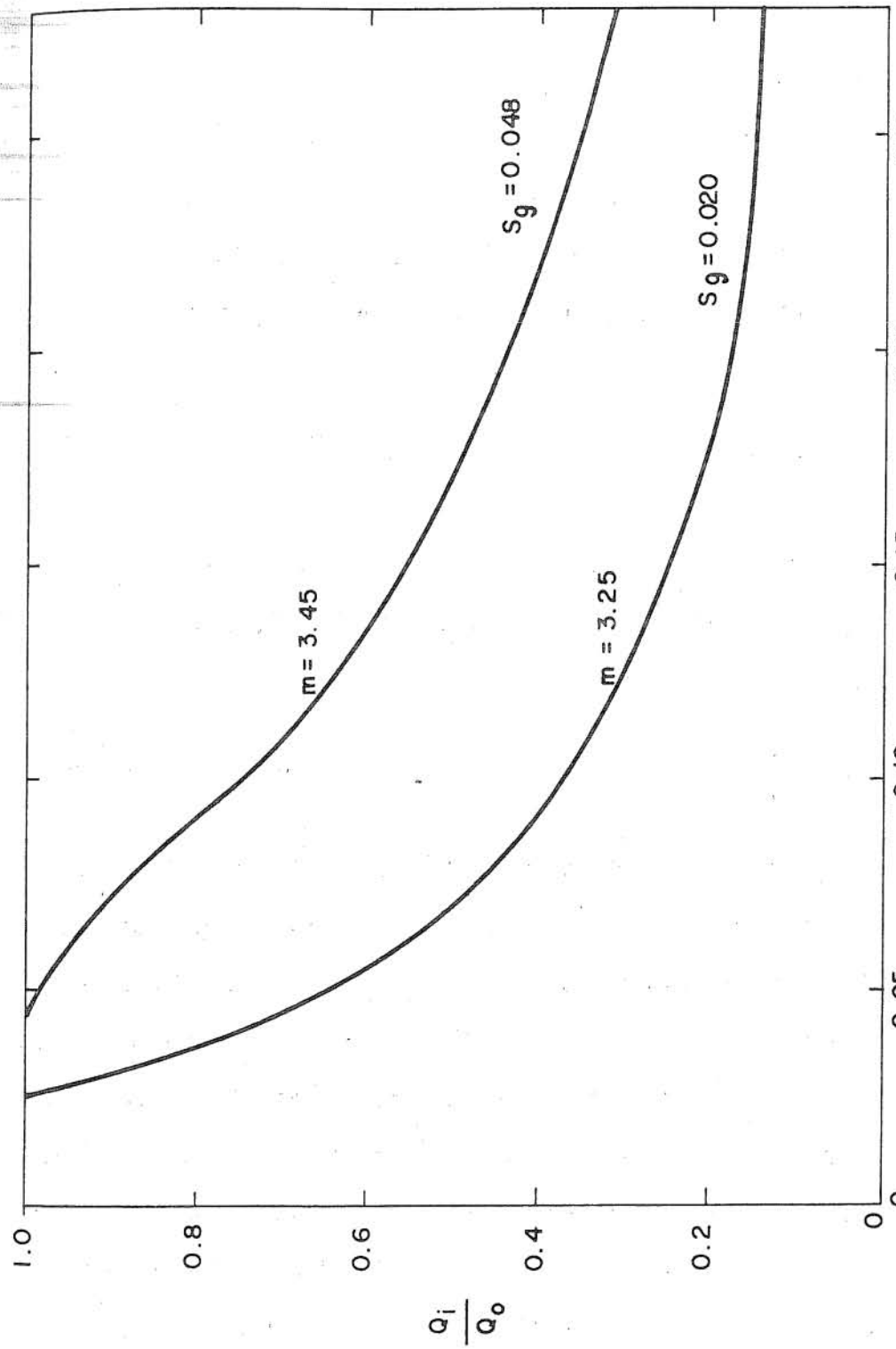

Fig. 4 Rating Curves for Type F Grate Inlet

These interception curves can be used only when L is greater than that given by Eq. 2.16.

When the grate is sufficiently long to intercept all the water passing over it as defined by Eq. 2.16, the flow into the inlet can be approximated by a free fall. Hence it is reasonable to assume that critical flow occurs at the upstream edge of the grate inlet if the approaching flow is subcritical. The specific energy head of the approaching flow is given as

$$E_o = y_o + \frac{1}{2g} \frac{Q_o^2}{A_o^2} \tag{2.17}$$

For critical flow condition, E_o is minimum for a given approach discharge Q_o [Chow, 1959; Henderson, 1966], i.e., $dE_o/dy_o = 0$. This condition combined with Eqs. 2.17 and 2.4 yields

$$Q_o = \sqrt{2gy_o^5 \cot \phi} \tag{2.18}$$

It should be noted that Cassidy used a flume with a width of 14 in. to represent the gutter while his grate inlets were 12-in. wide. Consequently triangular flow section was obtained only for small depths. At large depths he assumed that the behavior of the flow in the flume would approximately be the same as in a real triangular gutter. Moreover, he tested flow conditions for which Froude number is not less than 1.0. Therefore, the use of his experimental data in the present study when the spread of water is considerably greater than the width of the grate inlet or when the flow is subcritical is only a reluctant approximation because of lack of better information.

2.4 Evaluation of Friction Slope

In the momentum equation (Eqs. 2.2 or 2.6) the magnitude of the friction slope term is usually larger than any of the other terms, except the term containing S_o. Therefore, the method adopted to determine the value of S_f is particularly important. Inasmuch as the effects of unsteadiness and nonuniformity on the frictional resistance are not yet known quantitatively, one has to rely on the steady uniform flow formulas such as the Manning, Chezy, or Darcy-Weisbach formulas to approximate the value of S_f.

The friction slope can be expressed in the form of the Darcy-Weisbach formula as

$$S_f = \frac{f_f V^2}{8gR} \tag{2.19}$$

in which f_f is the frictional resistance coefficient, V is the cross-sectional average velocity, and R is the hydraulic radius. Following the suggestion by Chen and Chow (1968), the value of f_f may be approximated by the Weisbach resistance coefficient f given in the well known Moody diagram for steady uniform flow. Thus, for laminar flow,

$$f = C_f/\mathbb{R} \tag{2.20}$$

where C_f is a constant depending on the cross sectional shape and the Reynolds number $\mathbb{R} = VR/\nu$. For sheet flow under rainfall, the value of C_f depends on the rainfall intensity. For turbulent flow over hydraulically smooth surface, f is given by the Blasius formula

$$f = \frac{0.223}{\mathbb{R}^{0.25}} \tag{2.21}$$

and for fully developed turbulent flow over hydraulically rough surface,

$$\frac{1}{\sqrt{f}} = 2 \log \frac{2R}{k} + 1.74 \tag{2.22}$$

in which k is a length measure of the roughness size of the surface texture.

Actually, as can be seen from the moody diagram, there is a continuous transition between the laminar flow region (Eq. 2.20) and the hydraulically smooth turbulent flow region (Eq. 2.21); and again between the latter (Eq. 2.21) and the fully developed turbulent flow region (Eq. 2.22). Furthermore, the Blasius formula (Eq. 2.21) is valid only for Reynolds number smaller than 4×10^5. For turbulent flow over hydraulically smooth boundary with $\mathbb{R} > 4 \times 10^5$, the Karman-Prandtl equation

$$\frac{1}{\sqrt{f}} = 2 \log \mathbb{R} \sqrt{f} + 0.404 \qquad (2.23)$$

applies. Nevertheless, hydraulically smooth boundary turbulent flow rarely occurs on surface runoffs because of the roughness of the boundaries. Inclusion of the transitions and Eq. 2.23 in the analysis would make the computations and programming lengthy and inefficient. Therefore, for the sake of simplicity

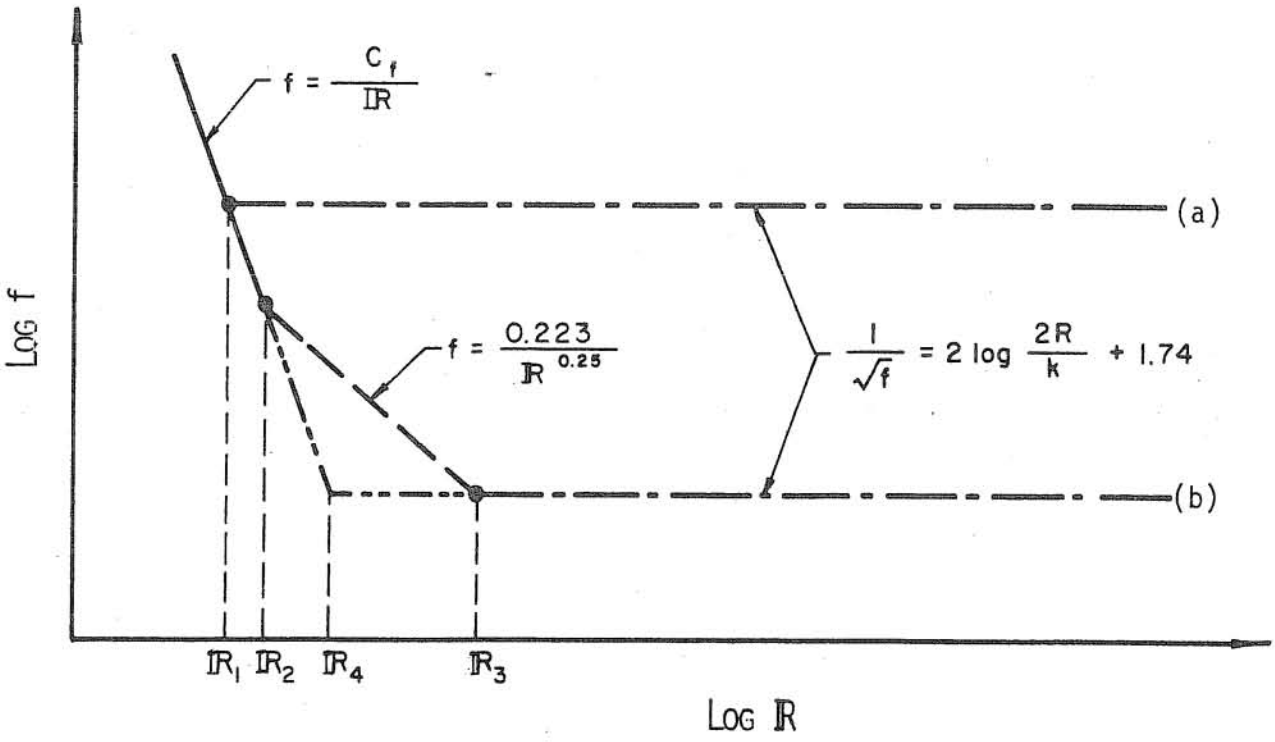

Fig. 5 Friction Coefficient Equations

without significant effect on accuracy, they are not considered in this study. And the resistance coefficient is assumed sufficiently approximate by using Eqs. 2.20, 2.21, and 2.22 as illustrated in Fig. 5.

In solving the Saint-Venant equations the Reynolds number of the flow at the cross section considered is computed and then compared with the values of the reference threshold Reynolds numbers to determine the proper resistance coefficient equation that should be used. The reference Reynolds number, $\mathbb{R}_1$, between Eqs. 2.20 and 2.22 for larger surface roughness can be obtained by solving these two equations simultaneously. Thus,

$$\mathbb{R}_1 = C_f \left(2 \log \frac{2R}{k} + 1.74\right)^2 \tag{2.24}$$

Likewise, between Eqs. 2.20 and 2.21,

$$\mathbb{R}_2 = (C_f/0.223)^{4/3} \tag{2.25}$$

and between Eqs. 2.21 and 2.22,

$$\mathbb{R}_3 = 0.633 \left(\log \frac{2R}{k} + 0.87\right)^8 \tag{2.26}$$

Note that $\mathbb{R}_4$ in Fig. 5 is a special case of $\mathbb{R}_1$ and hence Eq. 2.24 applies.

The critical value of k/R to determine which equations should be used can be found by equating Eqs. 2.24 and 2.25 to yield

$$\left(\frac{k}{R}\right)_c = 2 \times 10^{\left(0.87 - \frac{C_f^{1/6}}{0.736}\right)} \tag{2.27}$$

For $k/R > (k/R)_c$, if the Reynolds number of the flow $\mathbb{R} < \mathbb{R}_1$, Eq. 2.20 is used to give the value of f; otherwise, if $\mathbb{R} > \mathbb{R}_1$, Eq. 2.22 applies. For $k/R < (k/R)_c$, three cases exist: If $\mathbb{R} < \mathbb{R}_2$, Eq. 2.20 applies. If $\mathbb{R}_2 < \mathbb{R} < \mathbb{R}_3$, Eq. 2.21 gives the value of f. If $\mathbb{R} > \mathbb{R}_3$, Eq. 2.22 applies.

3. SOLUTION METHODS FOR UNSTEADY FLOW EQUATIONS

3.1 Mathematical Foundation of Method of Characteristics

Equations 2.5 and 2.6 form a system of hyperbolic partial differential equations. A partial differential equation is hyperbolic if it has two real characteristic directions [Ames, 1969]. This class of partial differential equations can be solved analytically only for several special cases [Kreyszig, 1972]. For the cases that analytical solutions do not exist, numerical solutions can be obtained with the aid of high-speed electronic computers.

Method of characteristics is a popular technique among the different numerical solution methods for hyperbolic partial differential equations. The basic rationale behind the method of characteristics is that the original system of hyperbolic equations can be replaced by a simpler system the coordinates of which are the characteristics [Ames, 1969]. Consider the hyperbolic system of n-coupled equations in n unknowns p^i, i = 1, 2, . . ., n,

$$\sum_{i=1}^{n} \{a_{ji} p_x^i + b_{ji} p_t^i\} + c_j = 0 \qquad j = 1, 2, \ldots, n \tag{3.1}$$

The coefficients a_{ji}, b_{ji} and c_j may be functions of x, t and p^i, and p_x^i and p_t^i are the partial derivatives of p^i with respect to x and t, respectively. The system contains differentiation in two different directions, x and t. The objective of the following analysis is to reduce this system to a simpler one in which differentiation in only one direction is involved. Equation 3.1 can be expressed in matrix form as follows

$$AP_x + BP_t + C = 0 \tag{3.2}$$

where

$$A = [a_{ji}]$$

$$B = [b_{ji}]$$

$$C = [c_j]$$

$$P_x = \frac{\partial}{\partial x}[p^i]$$

$$P_t = \frac{\partial}{\partial t}[p^i]$$

Note that A and B are each a n by n matrix, and C, P_x and P_t are column matrices. Multiplying Eq. 3.2 by a nonsingular n by n matrix T^* whose elements are to be determined later, one has

$$T^*AP_x + T^*BP_t + T^*C = 0 \tag{3.3}$$

By developing a canonical form such that $T^*A = ET^*B$ where E is a diagonal matrix with diagonal elements $e_1, e_2, \ldots, e_n$, Eq. 3.3 can be written as

$$EA^*P_x + A^*P_t + C^* = 0 \tag{3.4}$$

in which $A^* = T^*B = [a^*_{ji}]$ and $C^* = T^*C = [c^*_j]$. The j-th equation of Eq. 3.4 is

$$\sum_{i=1}^{n} a^*_{ji}\,(e_j p^i_x + p^i_t) + c^*_j = 0 \tag{3.5}$$

If $\alpha i + \beta j$ is the unit vector for which $e_j = \alpha/\beta = \cot\phi$ (Fig. 6) one obtains

$$e_j p^i_x + p^i_t = \frac{\alpha}{\beta} p^i_x + p^i_t$$

$$= \frac{1}{\beta}\{p^i_x \cos\phi + p^i_t \sin\phi\} \tag{3.6}$$

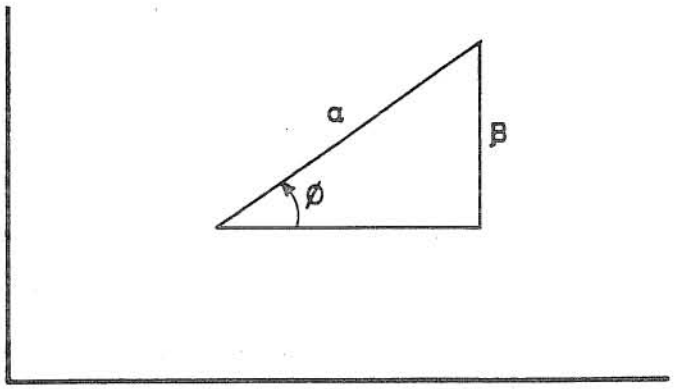

Fig. 6 Notation Used in Development of Characteristics

which is $1/\beta$ multiplied by the directional derivative of p^i in the direction defined by the unit vector $\alpha_i + \beta_j$. Hence every equation of the transformed system contains differentiation in only one direction.

The elements of the diagonal matrix E are determined by noting that $T^*A = ET^*B$ and hence

$$\sum_{k=1}^{n} (a_{ki} - e_j b_{ki})\, t_{jk} = 0 \qquad (3.7)$$

which is a system of n homogeneous linear algebraic equations for t_{jk}. For a nontrivial solution of Eq. 3.7 to exist it requires that

$$\det (A - e_j B) = 0 \qquad (3.8)$$

where the values of e_j are the eigenvalues. Elements of T^* can also be computed from Eq. 3.7 once the values of e_j are known. The direction of $\alpha_{ki} + \beta_{kj}$ for which $e_k = \alpha_k/\beta_k$ is called the characteristic direction and the n differential equations

$$\frac{dx}{dt} = e_k \qquad (3.9)$$

are called the characteristics of the system.

For hydraulic routing problems the number n in Eq. 3.7 is 2, hence the characteristics form two families of curves of one parameter. If these curves are to be used as the axes for a new curvilinear coordinate system, the following transformations can be adopted.

$$x_\alpha = \frac{\partial x}{\partial \alpha} = \frac{dx}{dt}\frac{\partial t}{\partial \alpha} = e_1 \frac{\partial t}{\partial \alpha}$$

Hence,

$$e_1 = \frac{x_\alpha}{t_\alpha} \tag{3.10}$$

Similarly,

$$e_2 = \frac{x_\beta}{t_\beta} \tag{3.11}$$

Substituting Eq. 3.10 into the quantities $e_j p_x^i + p_t^i$ one obtains

$$e_1 p_x^i + p_t^i = \frac{1}{t_\alpha}\left(\frac{\partial p^i}{\partial x}\frac{\partial x}{\partial \alpha} + \frac{\partial p^i}{\partial t}\frac{\partial t}{\partial \alpha}\right) = \frac{p_\alpha^i}{t_\alpha} \tag{3.12}$$

Likewise,

$$e_2 p_x^i + p_t^i = \frac{p_\beta}{t_\beta} \tag{3.13}$$

Hence, for n = 2, the system described by Eq. 3.4 which is equivalent to

$$a_{11}^*(e_1 p_x^1 + p_t^1) + a_{12}^*(e_1 p_x^2 + p_t^2) + c_1^* = 0 \tag{3.14}$$

$$a_{21}^*(e_2 p_x^1 + p_t^1) + a_{22}^*(e_2 p_x^2 + p_t^2) + c_2^* = 0 \tag{3.15}$$

becomes

$$a_{11}^* p_\alpha^1 + a_{12}^* p_\alpha^2 + c_1^* t_\alpha = 0 \tag{3.16}$$

$$a_{21}^* p_\beta^1 + a_{22}^* p_\beta^2 + c_2^* t_\beta = 0 \tag{3.17}$$

Equations 3.12 and 3.14 together with 3.15 and 3.15 are called the canonical

equations and constitute a simpler system than the original system of partial differential equations. Although the new system consists of four equations rather than two, it is easier to solve.

The method of characteristics consists of application of finite differences to the above mentioned canonical equations to solve them simultaneously. By knowing the fact that Eqs. 3.14 and 3.15 are to be evaluated along the characteristics, they can be expressed in the more familiar form

$$a_{11}^{*}\, dp^{1} + a_{12}^{*}\, dp^{2} + c_{1}^{*}\, dt = 0 \qquad (3.18)$$

$$a_{21}^{*}\, dp^{1} + a_{22}^{*}\, dp^{2} + c_{2}^{*}\, dt = 0 \qquad (3.19)$$

3.2 Review of Finite Differences Schemes

Finite differences technique is widely applied to solve partial differential equations. In replacing the partial differential equations with the corresponding difference quotients, certain conditions must be fulfilled. The solution of the difference equations should approach to the solution of the differential equations as the finite differences in the independent variables approach to zero. In other words, the solution must converge to the solution of the differential equations.

The use of finite differences technique has been proposed in two major classes of schemes, namely, the explicit and implicit schemes. The main distinction between the two classes is that in the former one partial differential equations are transferred into a set of linear algebraic equations from which the unknowns can be evaluated explicitly. For the implicit schemes, the difference equations may form a set of linear or nonlinear algebraic equations to be solved simultaneously. It is possible to apply the finite differences technique either directly to the original system given in the form of Eq. 3.1 or to the characteristic equations. The discussion of

finite differences schemes in characteristic equations will be prevailed until the next section. A short review of some of the direct schemes proposed in literature is given as follows.

3.2.1 Explicit Schemes

Strelkoff [1970] discussed a direct conversion of the Saint-Venant equations (Eqs. 2.1 and 2.2) to a finite difference form by expressing each space derivative and each coefficient in terms of known values. The values of the dependent unknown variables appear only in the approximations to the time derivatives (Fig. 7). The partial derivatives at a point P(x,t) in the computational grid are replaced by forward finite differences along the t-axis and central finite differences along the x-axis.

$$p_x^i = \frac{p^i(k+1,j) - p^i(k-1,j)}{2\,\Delta x}$$

$$p_x^i = \frac{p^i(k,j+1) - p^i(k,j)}{\Delta t}$$

All coefficients are evaluated at the point (x_k,t_j). With conditions known for all x along t_j, the unknown variables at (x_k,t_{j+1}) can be computed. However, such a scheme due to its large round off errors gives unstable solutions [Strelkoff, 1970; Sevuk and Yen, 1973].

Stable solutions with explicit schemes can be obtained by using staggered computational grids in the x - t plane. Strelkoff [1970] proposed such a scheme for open-channel flows. A scheme similar to Strelkoff's has been proposed by Dronkers [1969] for tidal computations. In Dronkers' scheme the following difference quotients are substituted for partial differentials (Fig. 8).

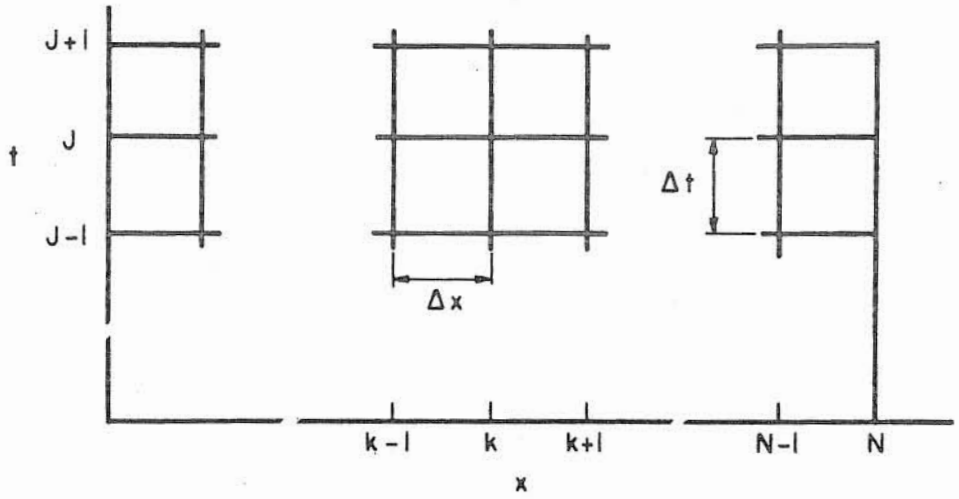

Fig. 7 Rectangular Computational Net Used in Direct Difference Scheme

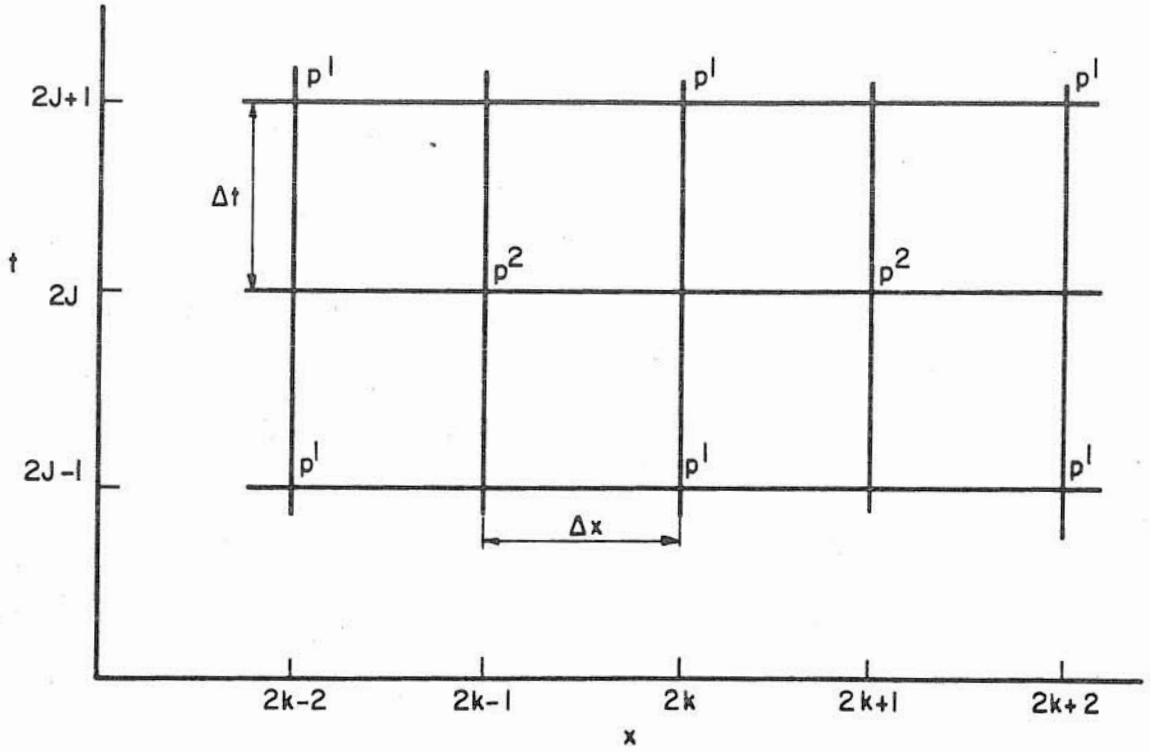

Fig. 8 Staggered Computation Net for Direct Explicit Scheme

$$p_x^1 = \frac{p^1(2k+2,2j-1) - p^1(2k-2,2j-1)}{4\,\Delta\,x}$$

$$p_t^1 = \frac{p^1(2k,2j+1) - p^1(2k,2j-1)}{2\,\Delta\,t}$$

$$p_x^2 = \frac{p^2(2k+1,2j) - p^2(2k-1,2j)}{2\,\Delta\,x}$$

$$p_t^2 = \frac{p^2(2k+1,2k+2) - p^2(2k+1,2j)}{2\,\Delta\,t}$$

Consequently, values of p^1 are computed at even points along the space axis x and at uneven points along the time axis t while the values of p^2 are computed at uneven points along x and at even time levels.

Stoker [1966] reviewed a slightly different explicit scheme in a staggered computational net. This scheme solves for the unknowns p^1 and p^2 at the same locations. However, if the solution is available at even points along the x-axis at time j, the unknowns p^1 and p^2 are computed at the uneven points of space axis x for the next time level j+1, or vice versa. The procedure progresses similarly at each time level.

3.2.2 Implicit Schemes

In the implicit schemes, x-derivatives are evaluated at the time level t = j+1. This requires simultaneous solution of a set of difference equations for all the points at the time level t = j+1 of the computational net. These algebraic equations may be linear or nonlinear. If the coefficients a_{ij}, b_{ij} and c_j in Eq. 3.1 are evaluated at the time level t = j, the equations are linear, and the solution can be accomplished through matrix algebra

techniques. If the coefficients are evaluated at t = j+1, the difference equations form a set of nonlinear algebraic equations and the solution should be obtained by use of an iteration technique.

There are many possible implicit schemes which can be used to solve partial differential equations. More popular ones are the variations of 4-point or 6-point schemes which are summarized in Fig. 9. Although all the noncentral schemes shown in Fig. 8 use forward differences along the space axis x it is possible to use backward difference schemes in a similar manner.

In a 6-point central implicit scheme proposed by Liggett and Woolhiser [1967] the following difference quotients are used (Fig. 7)

$$p_x^i = \frac{[p^i(k+1,j) - p^i(k-1,j)] + [p^i(k+1,j+1) - p^i(k-1,j+1)]}{4\,\Delta x}$$

$$p_t^i = \frac{p^i(k,j+1) - p^i(k,j)}{\Delta t}$$

The coefficients are centered at [(k+1)/2,j]. When the difference expressions are introduced into Eq. 3.1 with i = 1, 2 at each interior reach, two equations for each of the N - 2 interior points in the unknowns p^1 and p^2 are obtained. These equations form a closed system if the solution is known at the boundaries x = 1 and x = N. In order to solve these 2N - 4 nonlinear equations simultaneously an iteration technique should be used.

Dronkers [1969] proposed a 4-point forward implicit scheme in which the finite difference along the x-axis Δx is not necessarily a constant. The following difference quotients are applied to each of the 2k'th interior points along the time level t = j to convert Eq. 3.1 into a set of difference equations (Fig. 10),

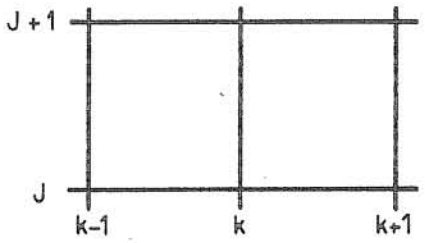

4-Point Central Implicit Scheme

$$p_x^i = \frac{p^i(k+1, j+1) - p^i(k, j+1)}{2\Delta x} + \frac{p^i(k+1, j) - p^i(k-1, j)}{2\Delta x}$$

$$p_t^i = \frac{p^i(k+1, j+1) - p^i(k+1, j)}{2\Delta t} + \frac{p^i(k, j+1) - p^i(k,j)}{2\Delta t}$$

4-Point Non-Central

$$p_x^i = \frac{p^i(k+1, j+1) - p^i(k, j+1)}{\Delta x}$$

$$p_t^i = \frac{p^i(k+1, j+1) - p^i(k+1, j)}{2\Delta t} + \frac{p^i(k, j+1) - p^i(k,j)}{2\Delta t}$$

6-Point Central

$$p_x^i = \frac{p^i(k+1, j+1) - p^i(k-1, j+1)}{4\Delta x} + \frac{p^i(k+1, j) - p^i(k-1, j)}{4\Delta x}$$

$$p_t^i = \frac{p^i(k, j+1) - p^i(k,j)}{\Delta t}$$

6-Point Non-Central

$$p_x^i = \frac{p^i(k+1, j+1) - p^i(k-1, j+1)}{2\Delta x}$$

$$p_t^i = \frac{p^i(k, j+1) - p^i(k, j)}{\Delta t}$$

Fig. 9 Summary of 6- and 4-Point Implicit Difference Schemes

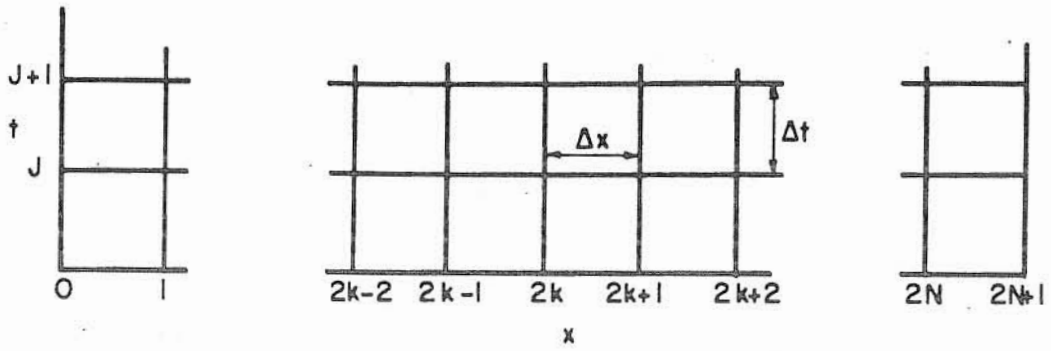

Fig. 10 Computation Net for Dronkers' Implicit Scheme

$$p_x^i = \frac{p^i(2k+1,j+1) - p^i(2k,j+1)}{(\Delta x)_{2k}}$$

$$p_t^i = \frac{p^i(2k+1,j+1) - p^i(2k+1,j) + p^i(2k,j+1) - p^i(2k,j)}{2\,\Delta\, t}$$

The coefficients are evaluated at (2k,j) to give a linear system of algebraic equations.

The selection of number points to be used in approximating the partial derivatives depends upon the accuracy required and computer expenses.

3.3 Finite Difference Schemes Applied to Method of Characteristics

The characteristic equations have been derived in Section 3.1 resulting in Eqs. 3.18 and 3.9 with k = 1 for the forward characteristic direction and Eqs. 3.19 and 3.9 with k = 2 for the backward direction. Finite difference techniques including both the explicit and implicit schemes can be applied to these equations to provide numerical solutions.

3.3.1 Explicit Schemes

Streeter and Wylie [1967] introduced an explicit scheme employing the method of finite differences in a rectangular computational net of the x - t plane. The characteristics are approximated by straight lines. By knowing the values of p^1 and p^2 along each reach when t = j, the unknown at

$t = j+1$ can be computed by the following substitutions (Fig. 11). Along the forward characteristics one has

$$dp^1 = p^1(k,j+1) - p^1(k-1,j)$$

$$dp^2 = p^2(k,j+1) - p^2(k-1,j)$$

$$dx = \Delta x$$

$$dt = \Delta t$$

Similarly, along the backward characteristics

$$dp^1 = p^1(k,j+1) - p^1(k+1,j)$$

$$dp^2 = p^2(k,j+1) - p^2(k+1,j)$$

$$dx = \Delta x$$

$$dt = \Delta t$$

The coefficients a_{11}^*, a_{12}^*, a_{21}^*, a_{22}^*; c_1^* and c_2^* are evaluated at the point (k,j).

A different type of explicit scheme called Courant's scheme [Ames, 1969] applies to the finite difference quotients to the canonical equations

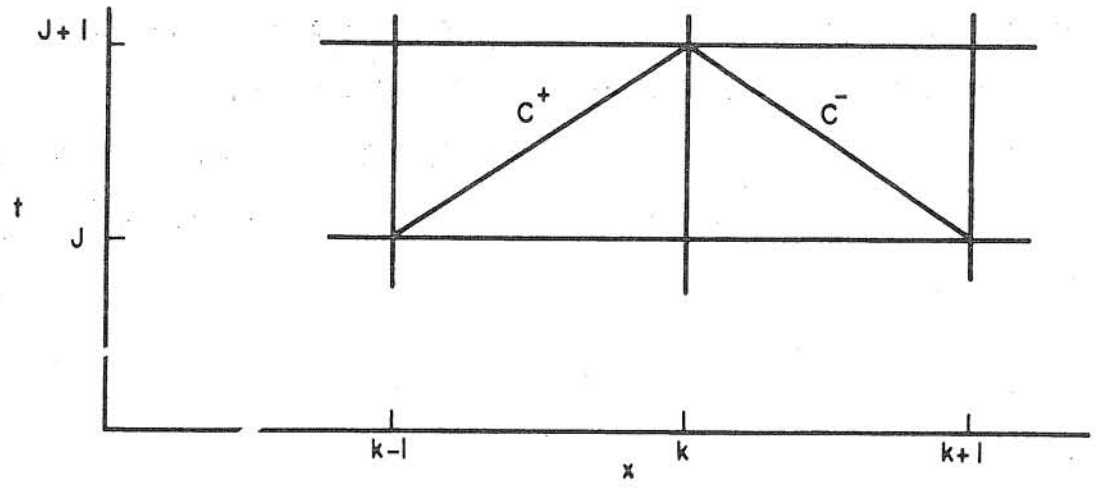

Fig. 11 Explicit Characteristic Scheme of Streeter and Wylie

in the form of Eqs. 3.14 and 3.15. The space derivative terms in Eq. 3.4 which represents the forward characteristic are replaced by

$$p_x^i = \frac{p^i(k,j) - p^i(k-1,j)}{\Delta x}$$

Equation 3.15 corresponds to the backward characteristic and the following finite difference quotients substitute the space derivatives (Fig. 11).

$$p_x^i = \frac{p^i(k+1,j) - p^i(k,j)}{\Delta x}$$

For both characteristic directions one has

$$p_t^i = \frac{p^i(k,j+1) - p^i(k,j)}{\Delta t}$$

The coefficients in Eqs. 3.14 and 3.15 are evaluated at the point (k,j) to obtain a linear system of algebraic equations.

3.3.2 Implicit Schemes

Ames [1969] reviewed a procedure which is attributable to Hartree [1958] that gives the solution on a predetermined fixed rectangular grid. Since the solution is desired at a fixed time, interpolation of dependent variables is required as the computation advances. The interpolation proposed is one-dimensional. With reference to Fig. 12, suppose solution is known at the mesh points at the time level t = j. The grid points R, S, etc. are equally spaced at the next time level t = j+1. The characteristic curves are approximated by arcs of parabolas and defined by

$$x_R - x_P = \frac{1}{2}[e_1(R) + e_1(P)]\,\Delta t$$

in the forward direction; and

$$x_R - x_Q = \frac{1}{2}[e_2(R) + e_2(Q)]\,\Delta t$$

in the backward direction. The characteristic equations are employed in the following form

$$\frac{1}{2}\left[a_{11}^{*}(R) + a_{11}^{*}(P)\right]\left[p^{1}(R) - p^{1}(P)\right] + \frac{1}{2}\left[a_{12}^{*}(R) + a_{12}^{*}(P)\right]\left[p^{2}(R) - p^{2}(P)\right] + \frac{1}{2}\left[c_{1}^{*}(R) + c_{1}^{*}(P)\right]\Delta t = 0$$

and

$$\frac{1}{2}\left[a_{21}^{*}(R) + a_{21}^{*}(Q)\right]\left[p^{1}(R) - p^{1}(Q)\right] + \frac{1}{2}\left[a_{22}^{*}(R) + a_{22}^{*}(Q)\right]\left[p^{2}(R) - p^{2}(Q)\right] + \frac{1}{2}\left[c_{2}^{*}(R) + c_{2}^{*}(Q)\right]\Delta t = 0$$

in the forward and backward directions, respectively. The last four equations are solved by an iteration technique for the unknowns $p^{1}(R)$, $p^{2}(R)$, x_p and x_Q using interpolated values at P and Q.

Another implicit scheme introduced by Streeter and Wylie [1967] gives solutions on the actual characteristic grid. Although any interpolations during the computational process is avoided, the results are obtained

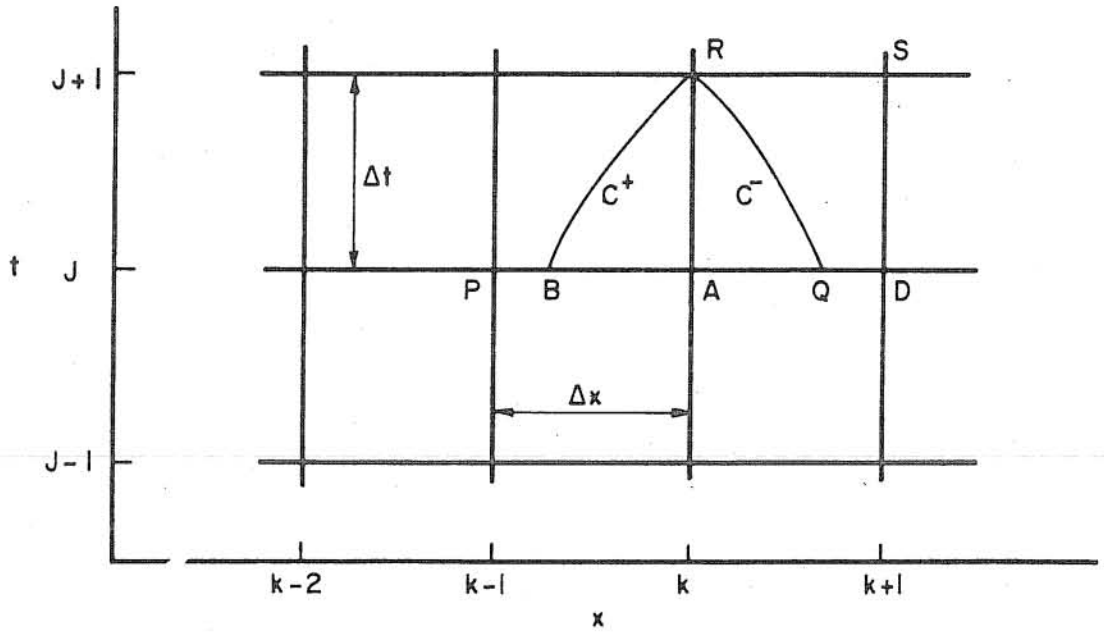

Fig. 12 Hartree's Implicit Characteristic Scheme

for odd times and distances, and some interpolation of the results may be required. With reference to Fig. 13, assume the coordinates of points R and S and the values of p^1 and p^2 at those points are known, then Eqs. 3.18 and 3.19 can be written as follows

$$a_{11}^*(R)[p^1(Q) - p^1(R)] + a_{12}^*(R)[p^2(Q) - p^2(R)] + c_1^*(R)[t_Q - t_R] = 0$$

$$x_Q - x_R = e_1(R)[t_Q - t_R]$$

and Eqs. 3.19 and 3.9 become

$$a_{21}^*(S)[p^1(Q) - p^1(S)] + a_{22}^*(S)[p^2(Q) - p^2(S)] + c_2^*(S)[t_Q - t_S] = 0$$

$$x_Q - x_S = e_2(S)[t_Q - t_S]$$

This pair of equations should then be solved for x_Q, t_Q, $p^1(Q)$ and $p^2(Q)$ simultaneously by use of an iteration technique.

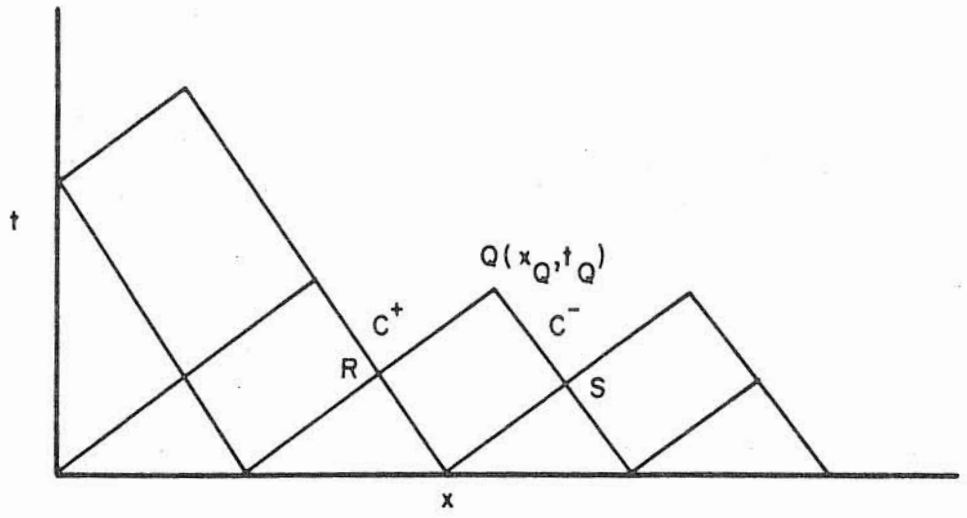

Fig. 13 Characteristic Grid of Streeter and Wylie

3.4 Application of Method of Characteristics to the Present Problem

Several schemes of the method of characteristics to solve partial differential equations have been reviewed in the preceding section. For the present study of solving the Saint-Venant equations for flow in gutters for which there is no analytical solution available, an explicit scheme of method of characteristics is selected. The major advantage of an explicit scheme over implicit schemes is being easier to program for computer use. When explicit schemes are used for problems dealing with long rivers having big depths, they may require more expensive computer runs than implicit schemes. This is due to the fact that shorter time intervals must be chosen for the former in the computational process to satisfy the stability criteria for explicit schemes. However, gutters are usually no longer than a few hundred feet, and maximum depths involved are less than one foot. Thus use of an explicit scheme for gutter flow solutions is justifiable.

3.4.1 Derivation of Characteristic Equations

Equations 2.5 and 2.6 constitute the original set of hyperbolic partial differential equations for the present study. They can be written in matrix form

$$AP_x + BP_t + C = 0 \qquad (3.2)$$

in which

$$A = \begin{bmatrix} 0 & 1/2T \\ Ag - 2V^2T & 2V \end{bmatrix}$$

$$B = \begin{bmatrix} 1 & 0 \\ 0 & 1 \end{bmatrix}$$

$$C = \begin{bmatrix} q/2T \\ -Ag(S_o - S_f) \end{bmatrix}$$

$$P_x = \frac{\partial}{\partial x} \begin{bmatrix} y \\ Q \end{bmatrix}$$

$$P_t = \frac{\partial}{\partial t} \begin{bmatrix} y \\ Q \end{bmatrix}$$

Thus, from Eq. 3.8

$$\det \begin{bmatrix} -e & \frac{1}{2T} \\ Ag - 2V^2T & 2V-e \end{bmatrix} = 0 \qquad (3.20)$$

This equation can be solved for e to give two values, $e_1 = V + c$ and $e_2 = V - c$, where $c = \sqrt{Ag/2T}$ is the celerity.

The matrix T^* of Eq. 3.3 can be evaluated by using Eq. 3.7 in its expanded form

$$(a_{11} - e_1 b_{11})t_{11} + (a_{21} - e_1 b_{21})t_{12} = 0$$

$$(a_{12} - e_1 b_{12})t_{11} + (a_{22} - e_1 b_{22})t_{12} = 0$$

For the present problem they become

$$-(V + c)t_{11} + (Ag - 2V^2T)t_{12} = 0$$

$$(1/2T)t_{11} + [2V - (V + c)]t_{12} = 0$$

which are homogeneous linear equations. Nontrivial solutions of these equations exist when Eq. 3.20 is satisfied, and t_{11} and t_{12} depend on each other. In other words, there are infinite number of solutions. Hence choosing arbitrarily $t_{11} = 1$, one can evaluate t_{12} as $t_{12} = -1/2T(V - c)$. Similarly letting $t_{21} = 1$, one obtains $t_{22} = -1/2T(V + c)$. Hence the matrix T^* becomes

$$T^* = \begin{bmatrix} 1 & -\frac{1}{2T(V - c)} \\ 1 & -\frac{1}{2T(V + c)} \end{bmatrix}$$

The matrices A^* and C^* of Eq. 3.4 can then be easily computed as

$$A^* = T^*B = \begin{bmatrix} 1 & -\frac{1}{2T(V - c)} \\ 1 & -\frac{1}{2T(V + c)} \end{bmatrix}$$

- c,

and

$$C^* = T^*C = \begin{bmatrix} \frac{q}{2T} + \frac{Ag(S_o - S_f)}{2T(V - c)} \\ \frac{q}{2T} + \frac{Ag(S_o - S_f)}{2T(V + c)} \end{bmatrix}$$

Thus the characteristic equations, Eqs. 3.18, 3.19 and 3.9, can be reduced to

$$dy - \frac{dQ}{2T(V - c)} + \left[\frac{q}{2T} + \frac{Ag(S_o - S_f)}{2T(V - c)}\right] dt = 0 \qquad (3.21)$$

$$\frac{dx}{dt} = V + c \tag{3.22}$$

$$dy - \frac{dQ}{2T(V + c)} + \left[\frac{q}{2T} + \frac{Ag(S_o - S_f)}{2T(V + c)} \right] dt = 0 \tag{3.23}$$

$$\frac{dx}{dt} = V - c \tag{3.24}$$

Equations 3.21 and 3.22 are the forward and Eqs. 3.23 and 3.24 are the backward characteristic equations.

3.4.2 Reduction to Finite Differences Form

Figure 14 shows the rectangular computational net chosen for the present study of unsteady gutter flow. The space interval Δx is kept constant while the time interval Δt is to be computed for each step as the computation processes such that the stability criteria which will be discussed in Section 3.4.5 is satisfied. Flow parameters are known at points A, C, and B from either initial conditions or previous computations. Characteristics passing through the point P are approximated by straight lines PR and PS, and they are conventionally indicated by C^+ and C^-, respectively. The slope of the C^+ characteristic is equal to $(V + c)$ and is always positive. The C^- characteristic has a slope $(V - c)$ and it may be positive or negative depending on whether the flow is supercritical or subcritical. The orientation of C^- changes accordingly.

For the critical flow situation, the C^- characteristic line coincides with the computation grid segment PC, but it is very rare to have critical flow in a gutter except at the downstream end. Thus, in the present study, it is

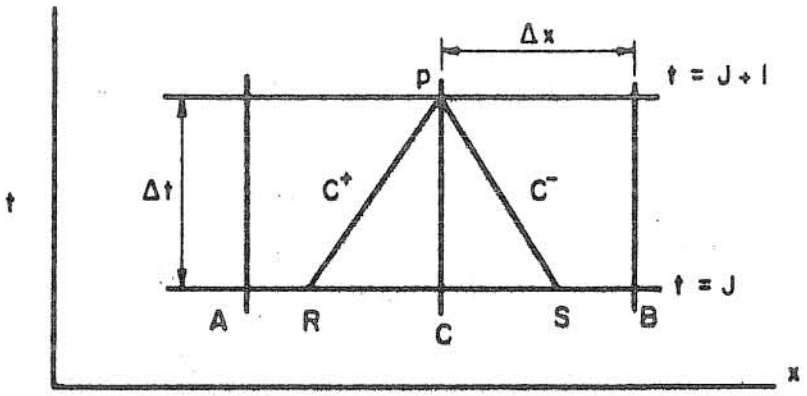

(a) Subcritical Flow

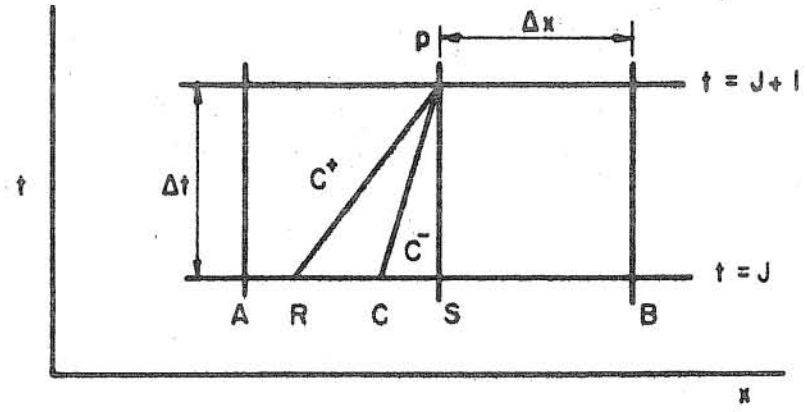

(b) Supercritical Flow

Fig. 14 Rectangular Computational Net for the Present Study

assumed that the flow is never critical at the mesh points selected for the computational grid, and the critical flow condition is used as a boundary condition at the downstream end of the gutter if the gutter flow is subcritical.

By introducing the finite difference quotients to Eqs. 3.21 and 3.22 one obtains

$$y_P - y_R - \frac{(Q_P - Q_R)}{2T_R(V_R - c_R)} + \left[\frac{q}{2T_R} + \frac{A_R g(S_o - S_{fR})}{2T_R(V_R - c_R)} \right]\Delta t = 0 \quad (3.25)$$

$$x_P - x_R = (V_R + c_R)\,\Delta t \quad (3.26)$$

whereas Eqs. 3.23 and 3.24 become

$$y_P - y_S - \frac{(Q_P - Q_S)}{2T_S(V_S + c_S)} + \left[\frac{q}{2T_S} + \frac{A_S g(S_o - S_{fS})}{2T_R(V_S + c_S)} \right] \quad (3.27)$$

$$x_P - x_S = (V_S - c_S)\,\Delta t \quad (3.28)$$

The flow conditions at the points R and S can be evaluated by linear interpolation from the known conditions at A, B, and C (Fig. 14),

$$\frac{y_C - y_R}{y_C - y_A} = \frac{x_C - x_R}{x_C - x_A} = \frac{\Delta t}{\Delta x}(V_R + c_R)$$

Likewise

$$\frac{Q_C - Q_R}{Q_C - Q_A} = \frac{\Delta t}{\Delta x}(V_R + c_R)$$

By noting that $V_R = Q_R/2y_R\cot\phi$ and $c_R = \sqrt{gy_R/2}$ one obtains

$$y_R = y_c - \frac{\Delta t}{\Delta x}(y_c - y_A)\left\{ \frac{Q_C - (Q_C - Q_A)\frac{\Delta t}{\Delta x}\sqrt{gy_R/2}}{2\cot\phi\, y_R^2 + \frac{\Delta t}{\Delta x}(Q_C - Q_A)} + \sqrt{gy_R/2} \right\} \quad (3.29)$$

$$Q_R = Q_C - (Q_C - Q_A)\frac{\Delta t}{\Delta x}(V_R + \sqrt{gy_R/2}) \quad (3.30)$$

where

$$V_R = \frac{\frac{Q_C}{Q_C - Q_A} - \frac{\Delta t}{\Delta x}\sqrt{gy_R/2}}{\frac{2y_R^2\cot\phi}{Q_C - Q_A} + \frac{\Delta t}{\Delta x}} \quad (3.31)$$

The values of Q_S and y_S can be computed similarly. For subcritical flow

$$y_s = y_C - (y_B - y_C)\frac{\Delta t}{\Delta x}\left\{ \frac{Q_C + \frac{\Delta t}{\Delta x}(Q_B - Q_C)\sqrt{gy_S}}{2y_S^2\cot\phi + \frac{\Delta t}{\Delta x}(Q_B - Q_C)} - \sqrt{gy_S/2} \right\} \quad (3.32)$$

$$Q_S = Q_C - (Q_B - Q_C)\frac{\Delta t}{\Delta x}(V_S - \sqrt{gy_S/2}) \quad (3.33)$$

where

$$V_S = \frac{\frac{Q_C}{Q_B - Q_C} + \frac{\Delta t}{\Delta x}\sqrt{gy_S/2}}{\frac{2y_S^2\cot\phi}{Q_B - Q_C} + \frac{\Delta t}{\Delta x}} \quad (3.34)$$

For supercritical flow, the conditions at S should be obtained by interpolating the flow conditions at the points A and C,

$$y_S = y_C - (y_C - y_A)\frac{\Delta t}{\Delta x}\left\{\frac{Q_C + \frac{\Delta t}{\Delta x}(Q_C - Q_A)\sqrt{gy_S/2}}{2y_S^2 \cot\phi + \frac{\Delta t}{\Delta x}(Q_C - Q_A)} - \sqrt{gy_S/2}\right\} \tag{3.35}$$

$$Q_S = Q_C - (Q_C - Q_A)\frac{\Delta t}{\Delta x}(V_S - \sqrt{gy_S/2}) \tag{3.36}$$

where

$$V_S = \frac{\frac{Q_C}{Q_C - Q_A} + \frac{\Delta t}{\Delta x}\sqrt{gy_S/2}}{\frac{2y_S^2 \cot\phi}{Q_C - Q_A} + \frac{\Delta t}{\Delta x}} \tag{3.37}$$

Equations 3.29 and 3.31 are solved for Q_R and y_R by iteration. The values of Q_S and y_S are computed from Eqs. 3.32 to 3.34 for subcritical flow or from Eqs. 3.35 to 3.37 for supercritical flow through iteration. Knowing the conditions at the points R and S, Eqs. 3.25 and 3.27 can be solved simultaneously to give the following explicit values of Q_P and y_P,

$$Q_P = \frac{2T_S T_R(V_S + c_S)(V_R - c_R)}{T_R(V_R - c_R) - T_S(V_S - c_S)}\left\{y_R - y_S + \frac{Q_S}{2T_S(V_S - c_S)} - \frac{Q_R}{2T_R(V_R - c_R)} - g\Delta t\left(\frac{T_S - T_R}{2T_S T_R}\right) + g\Delta t\left[\frac{A_S(S_o - S_{fS})}{2T_S(V_S - c_S)} - \frac{A_R(S_o - S_{fR})}{2T_R(V_R - c_R)}\right]\right\} \tag{3.38}$$

$$y_P = y_R + \frac{Q_P - Q_R}{2T_R(V_R - c_R)} - \frac{q\Delta t}{2T_R} - \frac{g\Delta t A_R}{2T_R(V_R - c_R)}(S_o - S_{fR}) \tag{3.39}$$

3.4.3 Boundary Conditions

Equations 3.38 and 3.39 together provide the solution for the flow at internal cross sections along the gutter, but they are not applicable to the end sections. Therefore, additional information should be provided at the upstream and downstream boundaries.

Inflow hydrograph provides the additional information at the upstream boundary. The inflow hydrograph is, for the sake of illustration without losing generality, arbitrarily chosen as a sine curve for the present study, i.e.,

$$Q_u = Q_{pu} \sin(\pi t/t_u) \qquad 0 \leq t \leq t_u$$
$$Q_u = 0 \qquad t \geq t_u \tag{3.40}$$

where Q_{pu} and t_u are coefficients defining peak discharge and the duration of the hydrograph. The subscript u stands for upstream boundary. The discharge Q at the upstream boundary can be obtained from Eq. 3.40 at any time level, and then the average depth may be computed from Eq. 3.25.

When the gutter flow is subcritical the downstream boundary condition is given by Eq. 2.18 , and can be used to determine the unknown variable at the downstream boundary together with Eq. 2.1 which can be transferred into finite difference form as

$$y_o = y_C - \frac{\Delta t}{\Delta x} \frac{Q_C - Q_A}{2T_C} - \frac{q \Delta t}{2T_C} \qquad (3.41)$$

The subscripts A and C correspond to the points A and C in Fig. 14, respectively, and the subscript o stands for the downstream end.

When the gutter flow is supercritical, downstream conditions have no effects on the flow. In this case, the downstream end of the gutter is treated like an internal cross section and hence Eqs. 3.38 and 3.39 can be used.

3.4.4 Initial Conditions

Continuity and momentum equations describing the unsteady gutter flows are mathematically initial value equations. Thus, an initial condition is required to start the computation after the finite differences are introduced. In a real gutter flow problem, the gutter is initially dry, that is, $y = 0$ and $Q = 0$ at any cross section along the gutter when $t = 0$.

However, such an initial condition creates singularities for numerical computations. Thus, it is necessary to assign very small but finite values to y at each cross section. In reality, before gutter flow actually starts, often there exists a thin film of water due to surface tension and local depressions. In the present study, the initial y is assumed to be uniform along the gutter having a value in the order of 10^{-4} ft. Discharge may be assumed to be initially zero provided that S_f is approximated by S_o for the first few time intervals.

3.4.5 Computational Stability Criteria

Use of finite differences techniques to solve partial differential equations may encounter computational instability problems, i.e., the solutions to the difference equations do not converge to those of the original system. In order to obtain stable results, one needs to consider certain limitations in choosing Δx and Δt values for computations.

Suppose that continuously differentiable values Q and y are specified on the noncharacteristic curve AB shown in Fig. 15. Assume also that AB is differentiable. A solution to a system of hyperbolic equations, with the prescribed values of Q and y, is uniquely determined within the region ABE bounded by the initial curve AB, the C^- characteristic AE, and the C^+ characteristic BE . Consequently, convergence at a point P within the uniqueness domain is insured.

When the solution is to be approximated at the points of the rectangular net in Fig. 14 by advancing from one row parallel to the x-axis to the next row a distance Δt from it, and the values at point P are to be computed from the known values at points A, C, and B, the point P should be located within the region bounded by the line segment AB and the C^+ and C^- characteristics drawn from A and B, respectively.

In a first-order scheme, the characteristics are approximated by straight lines defined as $\Delta t = \Delta x/(V + c)$ and $\Delta t = \Delta x/(V - c)$. Hence, if the values of $\Delta x/|V + c|$ are computed at each point on a row parallel to the x-axis, and if Δt for the next time step is chosen to be smaller than the minimum of these values, it will be insured that any point P on the next row

of the net will be within the uniqueness domain of the adjacent points A and B.

In the present scheme the values of Δx are fixed and equal while the value of Δt are obtained as the computation advances according to the above discussion, that is

$$\Delta t < \left(\frac{\Delta x}{|V + c|} \right)_{min} \tag{3.42}$$

This criteria is commonly called the Courant condition.

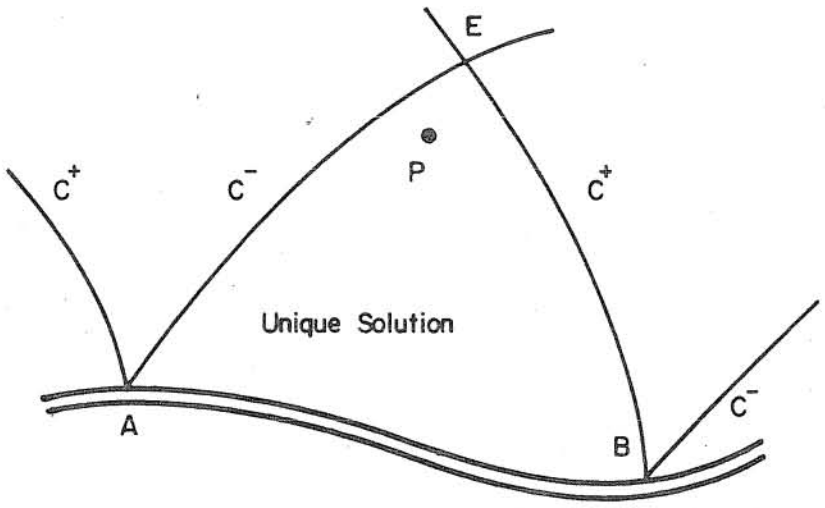

Fig. 15 Stability Criteria for Explicit Schemes

4. ANALYSIS OF FLOW FROM GUTTERS

4.1 Inflow and Gutter Conditions Analyzed

As discussed in Section 2.1, the gutter flow can be solved numerically by using the Saint-Venant equations (Eqs. 2.5 and 2.6) which has been formulated in an explicit finite-difference scheme applied to the method of characteristics as presented in Section 3.4. If the flow is subcritical, the downstream condition is assumed to be a free fall at the end of the gutter. The numerical scheme has been programmed in FORTRAN IV language and solved by using an IBM 360/75 digital computer system. With the value of Q_o thus computed, the flow into the grate inlet Q_i can be approximated by using Cassidy's [1966] experimental results relating Q_i/Q_o to other flow parameters.

In order to analyze a sufficient range of flow conditions and to present the results in a general form, guidance is taken from the result of dimensional analysis for long gutters having triangular cross section and parallel rectangular grate inlets. The case of specified constant lateral flow rate q with very long duration without considering directly the pavement flow (Eq. 2.12) is presented in this chapter. The case of considering the pavement flow from rainfall as a part of the system (Eq. 2.8) will be considered in the next Chapter. As an example of unsteady gutter flow into inlets, the Type F grate inlet (Fig. 3) tested by Cassidy [1966] is selected in the present study. For this test case, the specified nondimensional parameters are $S_g = 1/20.8 = 0.048$ or $\phi = 2.57^o$, $L_g/B = 50$, $W/L = 1$. In referring to Eq. 2.10 and Fig. 3., $b_3/W = b_5/W = 5/96$, $b_4/W = 1/12$, $b_1/W = b_2/W =$ constant, $b_6/W = 0$, $\eta_b = 5/16$, where W = 1 ft. Furthermore, the downstream boundary condition parameter is approximated by the interception curves shown in Fig. 4, and the gutter upstream inflow hydrographs are assumed to be of sine-curve shape so that the parameter

J_t in Eqs. 2.8 and 2.14 is constant. Hence, for this case of inlet and gutter without considering the pavement directly, Eq. 2.14 can be simplified for $k/B = 0.005$ as

$$\frac{Q_o}{Q_{pu}} \text{ or } \frac{Q_i}{Q_{pu}} = F_{15,16}\left(\frac{t}{t_u}, S_o, \frac{Q_{pu}}{W\nu}, \frac{Q_{pu}}{\sqrt{gS_g^2W^5}}, \frac{qL_g}{Q_{pu}}, \frac{Q_{pu}t_u}{W^2L_g}\right) \qquad (4.1)$$

Based on this equation, the ranges of flow conditions to be analysed for the Type F inlet-gutter system are determined and listed in Table 1.

The first term on the right hand side of Eq. 4.1 represents the unsteady nature of the flow into grate inlet. The second term, S_o, considers directly the effect of the longitudinal slope of the gutter. The parameter $Q_{pu}/W\nu$ being in a Reynolds-number form reflects the effect of viscosity to the gutter flow. The fourth term, in the Froude-number form, denotes the effect of gravity. The relative importance of the lateral flow is reflected by the parameter qL_g/Q_{pu}. The last term, $Q_{pu}t_u/W^2L_g$, accounts for the effect of the duration of the gutter inflow hydrograph.

For the sake of comparison of the results showing the effects of the various nondimensional independent parameters a reference condition is chosen as follows:

1. $\nu = 1.93 \times 10^{-5}$ sq ft/sec which corresponds to a water temperature 32^oF.
2. The peak discharge Q_{pu} of the sine-curve gutter inflow hydrograph is chosen based on a reference discharge $Q_r = 0.636\ Q_{pu}$ which is equal to the average discharge of the hydrograph. The value of Q_r is the discharge for a steady uniform critical flow in a gutter flowing just full with the water surface equal to B.

TABLE 1. Gutter Flow Conditions Analyzed

Run No.	Q_{pu}	t_u	q	ν	S_o	$\frac{Q_{pu}}{W\nu}$	$\frac{Q_{pu}}{\sqrt{gW^5S_g^2}}$	$\frac{qL_g}{Q_{pu}}$	$\frac{Q_{pu}t_u}{W^2L_g}$
	(cfs)	(sec)	$(10^{-3}\ \frac{cfs}{ft})$	$(10^{-5}\ \frac{ft^2}{sec})$	(10^{-4})	(10^3)			
Ref	0.132	46.0	2.10	1.93	48	6.30	484	0.63	0.152
1	0.132	46.0	2.10	1.93	12	6.30	484	0.63	0.152
2	0.132	46.0	2.10	1.93	72	6.30	484	0.63	0.152
3	0.132	46.0	2.10	1.93	96	6.30	484	0.63	0.152
4	0.132	46.0	2.10	0.75	48	1.76	484	0.63	0.152
5	0.132	46.0	2.10	1.13	48	1.16	484	0.63	0.152
6	0.132	46.0	2.10	3.10	48	0.42	484	0.63	0.152
7	0.066	92.0	1.05	1.05	48	6.30	240	0.63	0.152
8	0.099	61.4	1.57	1.57	48	6.30	360	0.63	0.152
9	0.199	30.6	3.10	3.15	48	6.30	720	0.63	0.152
10	0.132	46.0	0.00	1.93	48	6.30	484	0.00	0.152
11	0.132	46.0	1.05	1.93	48	6.30	484	0.32	0.152
12	0.132	46.0	4.20	1.93	48	6.30	484	1.26	0.152
13	0.132	23.0	2.10	1.93	48	6.30	484	0.63	0.075
14	0.132	69.0	2.10	1.93	48	6.30	484	0.63	0.228
15	0.132	92.0	2.10	1.93	48	6.30	484	0.63	0.314

Remarks: Triangular gutter, Type F grate inlet

S_g = 0.048, B/L_g = 0.05, k/B = 0.005, L/W = 1.0, W = 1.0 ft

3. The duration of the gutter inflow hydrograph t_u is chosen such that the total volume of the gutter inflow is equal to the volume of the prism defined by the gutter with length L_g, width B and lateral slope S_g.
4. The steady lateral inflow q is chosen such that qL_g is equal to Q_r. The lateral inflow which starts at t = 0 is assumed to continue after the gutter upstream inflow ceases.

The computed dimensionless hydrographs into the grate inlet for different conditions are plotted in Figs. 16 to 19 and those for the flow passing through the downstream section of the gutter in Figs. 20 to 23. In all these figures, the nondimensional parameters are kept at the values of the reference run given in Table 1 except the independent variable being considered. The effect of the reference Reynolds number on Q_i/Q_{pu} and Q_o/Q_{pu} for the range of $Q_{pu}/\nu w^2$ from 4200 to 17,600 examined has been found insignificant, therefore, the results are not plotted.

4.2 Discussion of Results

As shown in Figs. 16 to 23, the characteristics of the gutter flow and the flow into the grate are obviously affected by the unsteadiness of the inflow. This unsteadiness effect is particularly important when the input flood waves are short and high. The attenuation effect on the input flood hydrographs as the flow propagating along the gutter can clearly be observed in Fig. 24. This attenuation is due to the detention storage in the gutter. The flow shown in Fig. 24 is for the reference condition listed in Table 1. Starting from dry gutter, immediately after the upstream and lateral inflows are introduced, the water depth is building up in the gutter. At the upstream part of the gutter the inflow wave is propagating and being attenuated towards downstream as shown by the left part of the depth profile

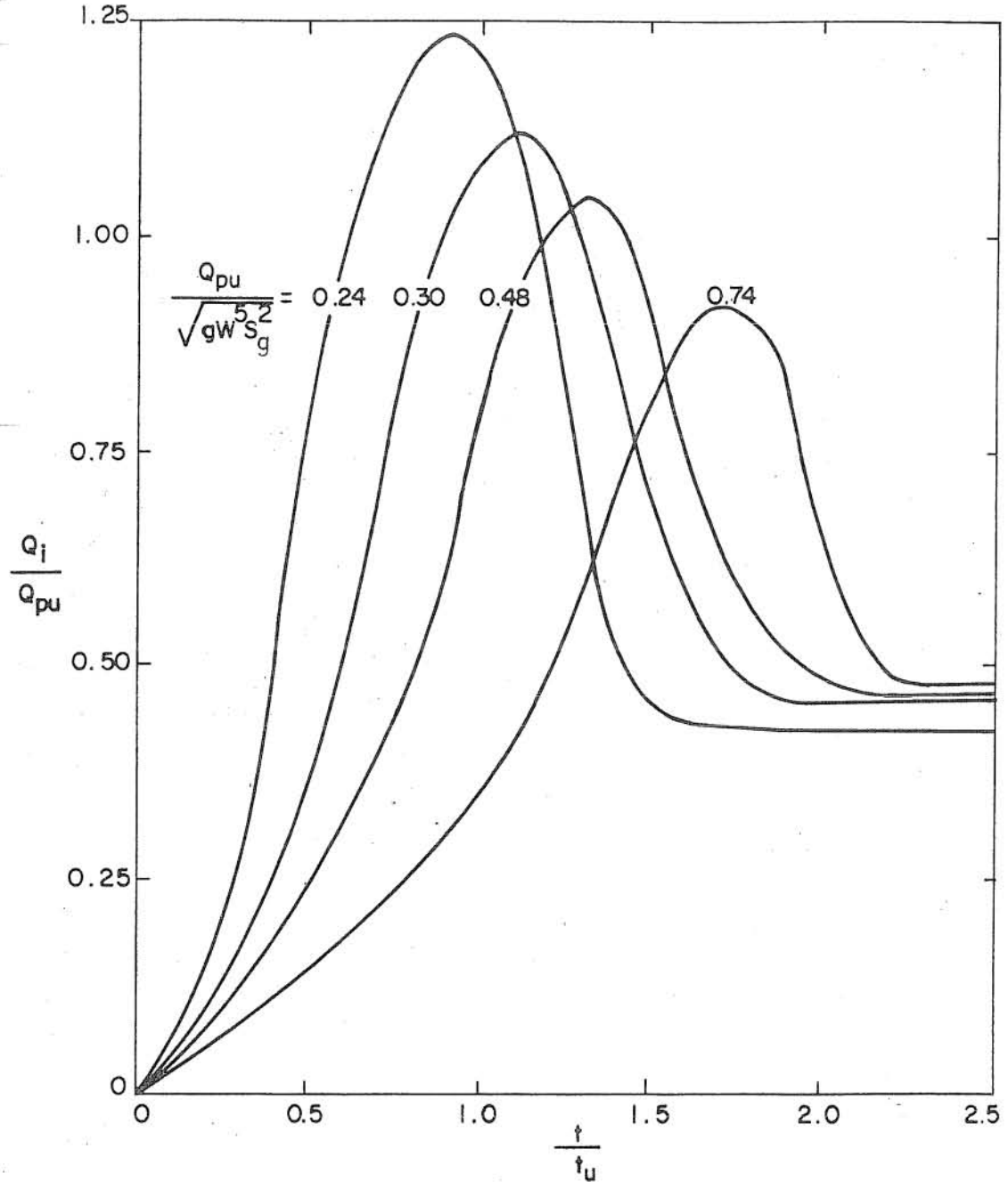

Fig. 16 Effect of $Q_{pu}/\sqrt{gW^5S_g^2}$ on Flow into Grate Inlet

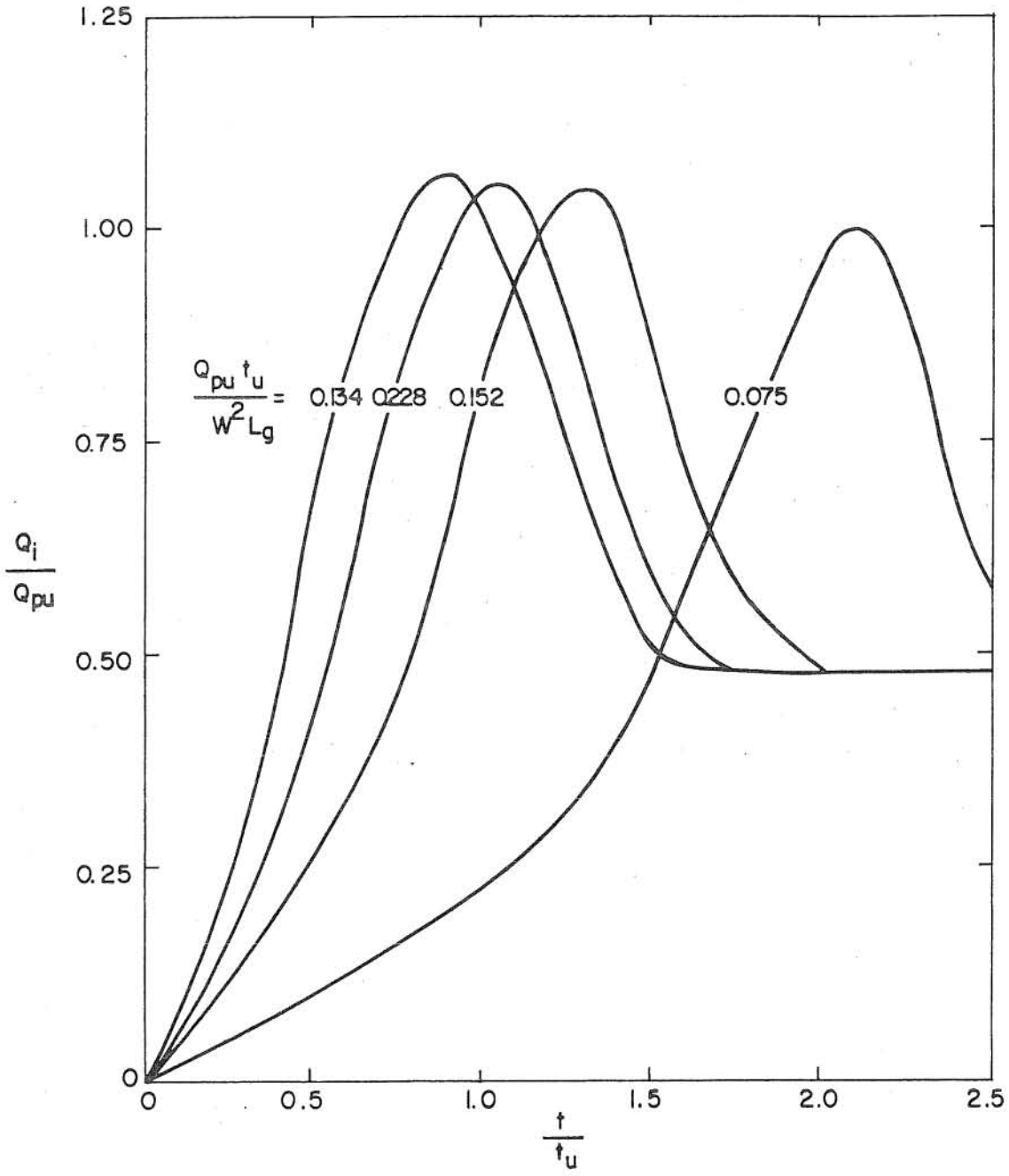

Fig. 17 Effect of Duration of Inflow on Flow into Grate Inlet

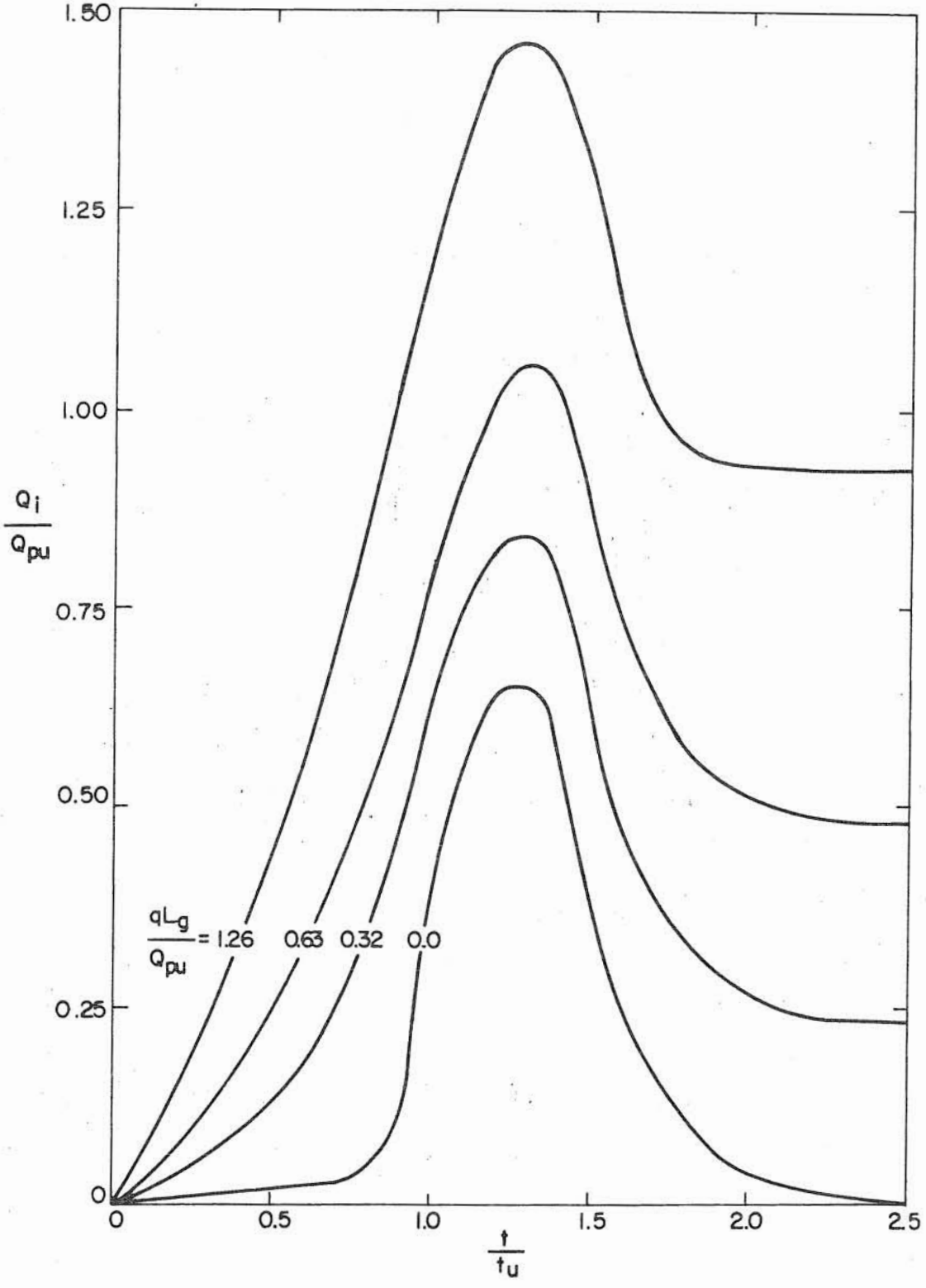

Fig. 18 Effect of Lateral Flow on Flow into Grate Inlet

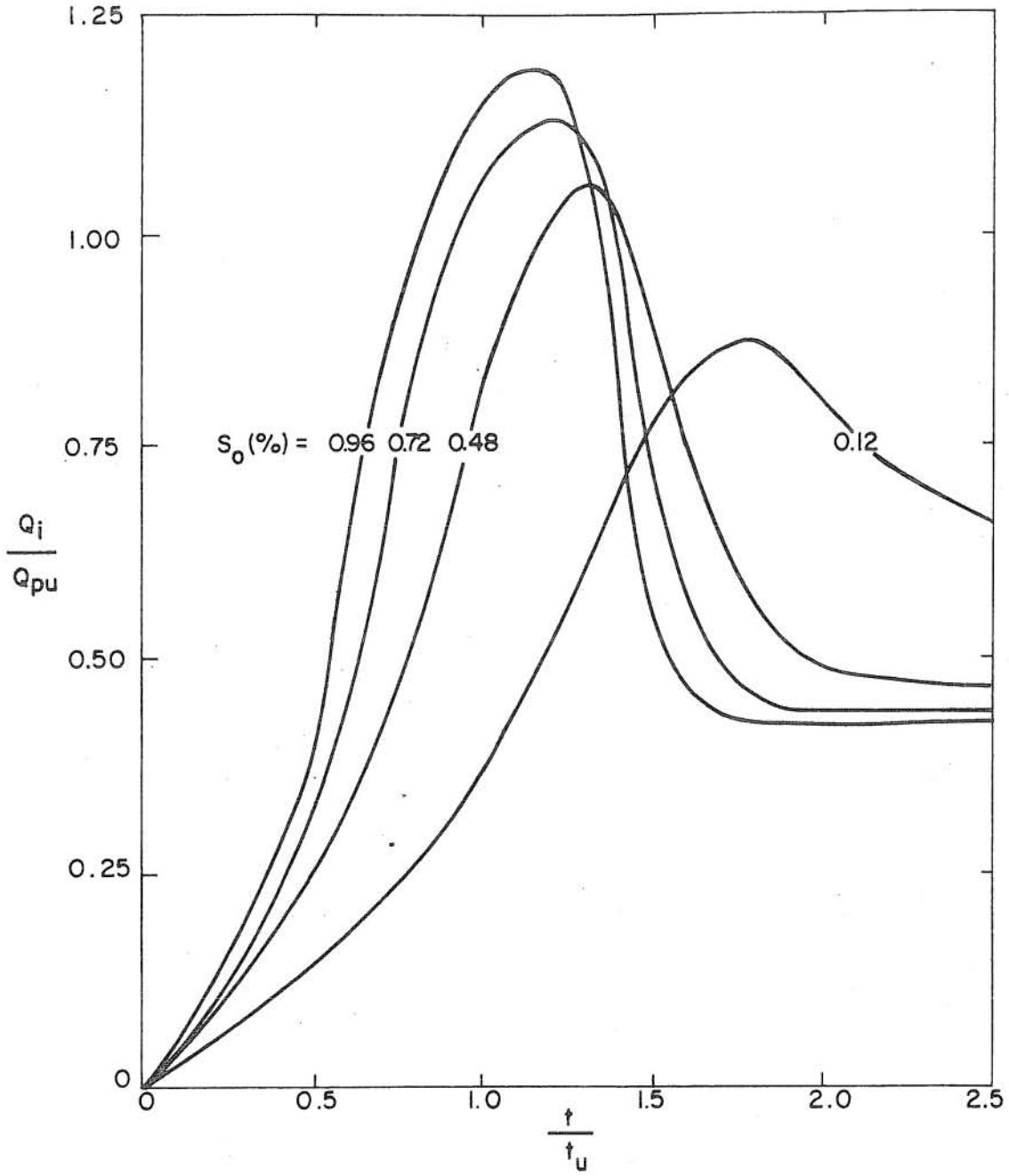

Fig. 19 Effect of Gutter Slope on Flow into Grate Inlet

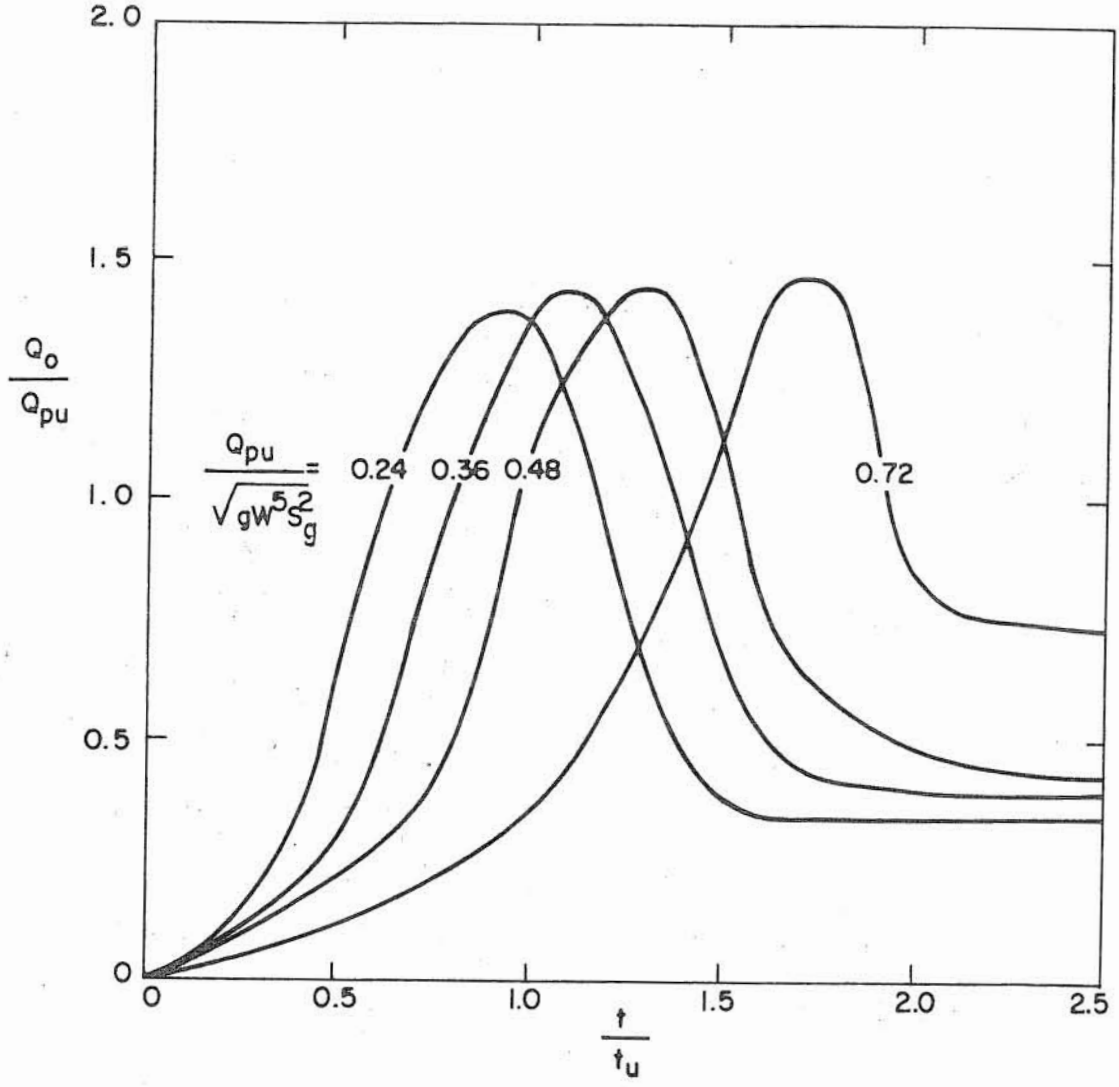

Fig. 20 Effect of $Q_{pu}/\sqrt{gW^5S_g^2}$ on Total Gutter Outflow

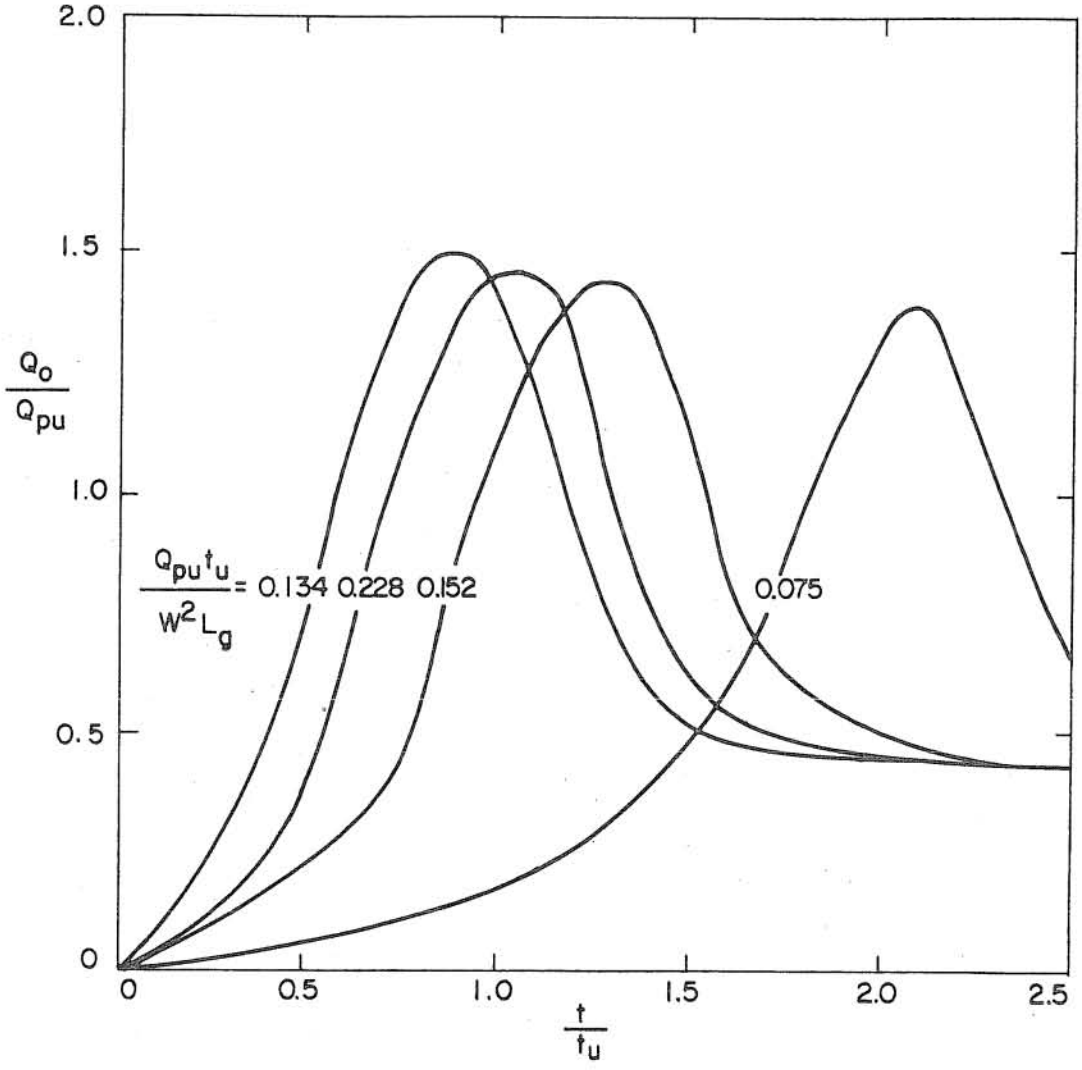

Fig. 21 Effect of Duration of Inflow on Total Gutter Outflow

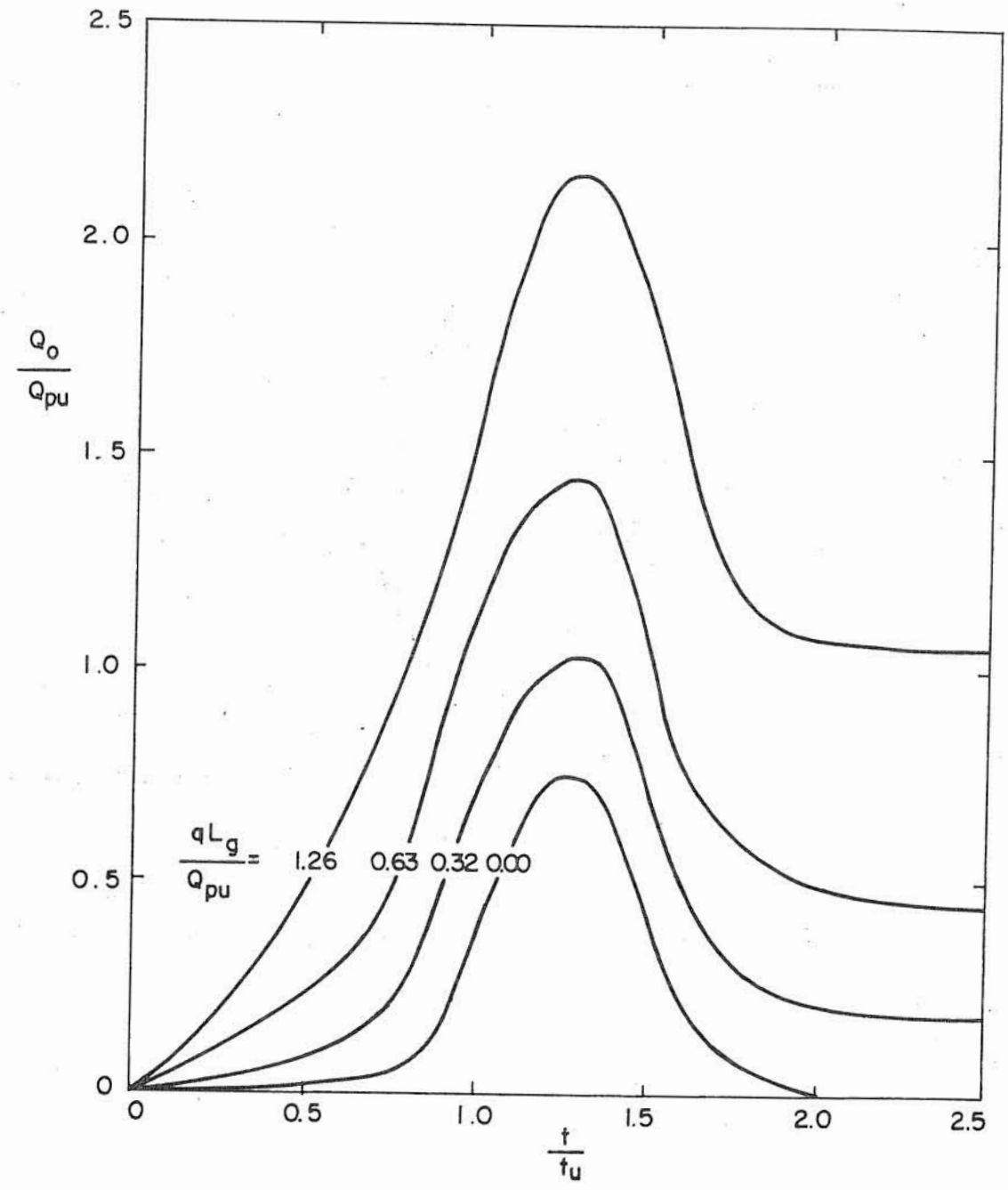

Fig. 22 Effect of Lateral Flow on Total Gutter Outflow

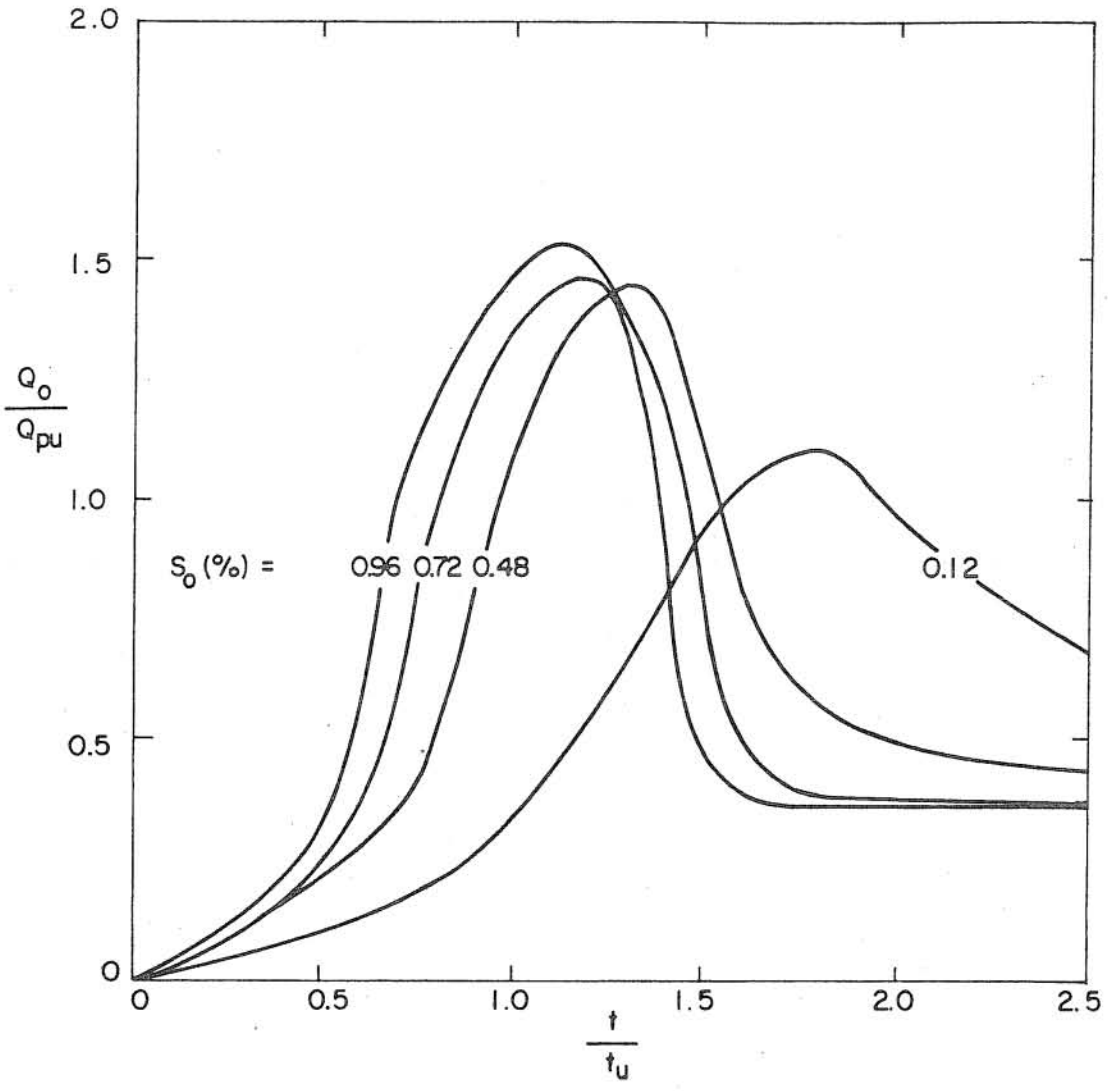

Fig. 23 Effect of Gutter Slope on Total Gutter Outflow

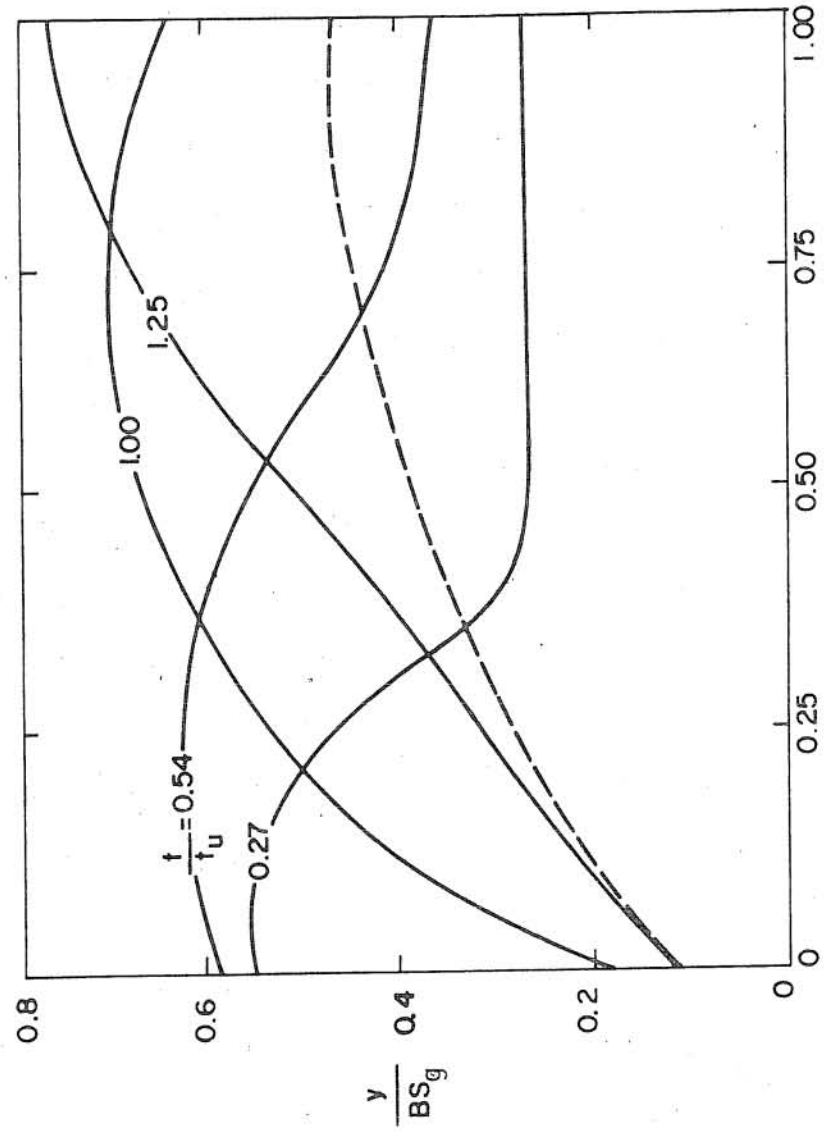

Fig. 24 Flow Propagating Along the Gutter

at t/t_u = 0.27. The downstream part of this surface profile is a straight line of constant depth, simply because the flow is supercritical and hence there is no downstream backwater effect. Consequently the depth is building up as a result of constant q and subsequently an equal flow rate at any cross section before the upstream inflow flood wave arrives at that section. At t/t_u = 0.54 the inflow wave from upstream already covers most of the length of the gutter and the flow peak has already moved into the gutter. At t/t_u = 1.0 the depth in the downstream part of the gutter continues to rise. The maximum depth is increasing as the time elapses and the flood wave propagates downstream. This is because of the effect of the lateral inflow with qL_g/Q_{pu} = 0.636. At t/t_u = 1.32, Q_o reaches its maximum; the depth reaches its maximum slightly earlier, at t/t_u = 1.25; and after that the flood in the gutter starts to recede to its steady flow condition with constant lateral flow q into the gutter. This steady flow profile is shown in Fig. 24 in dash line and is similar to a S-3 type backwater curve but with discharge varying along the gutter, i.e., steady spatially varied flow. The critical and normal depths at the downstream end of the gutter for the reference steady flow discharge qL_g is $y_c/BS_g = y_n/BS_g = 0.50$.

In each of the Figs. 16 to 23, as mentioned previously, only one nondimensional independent parameter is allowed to vary while others are kept constant at the values of the reference condition given in Table 1 so that the effect of each independent influential nondimensional parameters can be studied individually. As shown in Figs. 17 and 21, there is little effect of the relative gutter upstream inflow duration t_uQ_{pu}/W^2L_g on the magnitude of the relative outflow peak discharges. However, the relative time of occurrence of the peak discharge t_p/t_u is delayed considerably as

the nondimensional duration decreases. This is obviously due to smaller total inflow volume for a shorter duration as compared to the volume of the gutter when completely filled, and consequently the relative delay of the peak outflow.

The effect of the parameter $Q_{pu}/\sqrt{gW^5S_g^2}$ on the gutter flow and intercepted flow is indicated in Figs. 16 and 20. For a greater relative gravity force, the inflow reaches the grate inlet at a shorter time with less attenuation. Alternatively, from Fig. 16, for a given gutter and inlet and a given duration of the gutter inflow hydrograph, the greater the value of Q_{pu} the more the volume of inflow. With a constant detention storage capacity of the gutter, the large amount of inflow would produce a higher hydraulic gradient and smaller resistance per unit mass of the flow as compared to the case of a smaller inflow. Consequently, it is expected that the flow attenuation is smaller and flowing faster for the large flood than for the smaller one.

As shown in Figs. 18 and 22, the relative rate of outflow from the gutter as well as the inflow into the grate inlet is related directly to the relative amount of lateral flow into the gutter. However, the computer results show that for the conditions considered the effect of lateral flow on the relative time distribution of the gutter and inlet flows are small. This is due partly to the approximation of one-dimensional approach used in this analysis. It should also be noted here that the lowest curve in Figs. 18 and 22 with $q = 0$ is the case of no lateral flow corresponding to situations such as street washing, hydrant flashing, and snow melting at upstream.

It is apparent that for otherwise identical conditions, the steeper the gutter slope, the faster the inflow will be conveyed to the inlet with less attenuation. This is indeed the case as shown

nondimensionally in Figs. 19 and 23. When the gutter slope is flat, the flow may be subcritical in the entire gutter over the whole period of runoff. However, when the gutter is steep, the flow becomes supercritical. As discussed in Sec. 3.4.3, the downstream boundary conditions used in the numerical solution are different for subcritical and supercritical flows at the downstream end of the gutter. For the curves in Fig. 19 and 23, the flow is subcritical for gutter slope of 0.0012, whereas for slopes of 0.0048, 0.0072 and 0.0096 at peak discharge in the neighborhood of the downstream of the gutter the flow is supercritical.

Since the flow from the gutter may pass over or flow around the inlet without being intercepted, the ratio Q_i/Q_o indicating the efficiency of the inlet is not necessarily equal to unity. In fact, for the Type F grate inlet and the gutter and flow conditions investigated, this ratio of Q_i/Q_o is always smaller than unity. For most of these cases investigated, there may indeed be some carry over of water passing through the inlet without being intercepted as L/W = 1 and B/W = 2, i.e., the gutter width is wider than the grate inlet width and the inlet is not very long. Nevertheless, it should be mentioned here that the values of Q_i are computed by using Cassidy's [1966] experimental results of Q_i/Q_o while d_o and Q_o at the downstream end of the gutter are determined by solving the Saint-Venant equations with the assumed downstream boundary conditions. Cassidy's data were obtained from steady flows and from a 12-in. wide inlet in a 14-in. wide narrow flume allowing only limited amount of water to flow around the inlet to be carried downstream. Thus the computed results of Q_o/Q_{pu} shown in Figs. 20 to 23 are presumably more accurate than the corresponding values for Q_i/Q_{pu} shown in Figs. 16

to 19. One would also expect that for supercritical approaching flow the computed Q_i based on Cassidy's data is overestimated whereas for subcritical approaching flow it is underestimated. The underestimate of Q_i for subcritical approaching flow is due partly to the assumed boundary condition of critical depth at the cross section the gutter joins the inlet in the numerical solution. Because of the geometry of the inlet, the critical depth actually occurs somewhere downstream from the upper edge of the openings of the inlet and the flow is highly disturbed and curvilinear. However, a careful examination of the computed results indicates that the error due to change of flow regimes at the downstream boundary of the gutter although not negligible, is not appreciable, particularly if the approaching flow is supercritical. A final test on the reliability of the theoretical results, of course, hinges on their agreement with future experimental results.

Based on his data, Cassidy indicated that for steady flow Q_i/Q_o is not a function of S_o which may be true for his narrow flume. A comparison of Figs. 19 and 23 gives the value of Q_i/Q_o which indicates that S_o is an important factor for the conditions investigated in the present study. It should also be noted here that although the computed gutter flow depth y and velocity V are not presented for the sake of brevity, the values of d_o can be obtained by using Figs. 16 to 23 and Fig. 4 and subsequently V_o can be obtained.

Although the dimensionless hydrographs in Figs. 16 to 23 gives better physical picture on the hydraulic phenomena of unsteady gutter flow into inlets, from a practical viewpoint, the peak flow rate Q_{pi} into the grate inlet and its time of occurrence t_p are of more interests.

TABLE 2. Comparison of Peak Discharges for Unsteady and Steady Flows

Run No.	Q_{po}/Q_{pu}		Q_{pi}/Q_{pu}	
	Unsteady	Steady	Unsteady	Steady
Ref	1.45	1.63	1.05	1.15
1	1.11	1.63	0.87	1.15
2	1.39	1.63	1.13	1.15
3	1.53	1.63	1.21	1.15
4	1.45	1.63	1.05	1.15
5	1.45	1.63	1.05	1.15
6	1.45	1.63	1.05	1.15
7	1.40	1.63	1.25	1.45
8	1.44	1.63	1.12	1.06
9	1.46	1.63	0.93	0.99
10	0.75	1.00	0.65	0.75
11	1.06	1.31	0.84	0.90
12	2.15	2.27	1.46	1.60
13	1.39	1.63	1.00	1.15
14	1.47	1.63	1.00	1.15
15	1.47	1.63	1.06	1.15

Thus the numerical results are replotted in Figs. 25 to 28 for dimensionless Q_{pi} and t_p relative to the reference flow condition for the effects of gutter inflow magnitude and duration, of lateral flow, and of gutter slope. The dashed parts of the curves in these figures correspond to the case of subcritical approaching flow to the inlet around its peak value as discussed previously. An example of use of these curves will be given in the next section.

Another feature of interest is to compare the unsteady flow to the corresponding steady flow so that the effect of unsteadiness can be observed. The corresponding steady flow condition is selected as the steady uniform gutter flow with a discharge equal to the total maximum gutter inflow, i.e., Q_{pu} plus qL_g, which is the discharge commonly used in conventional method in design or computation of gutter flows by using the Manning or Chezy formulas. The corresponding computed results for steady and unsteady cases are given in Table 2. As it can be seen from Table 2, the steady flow approximation overestimates the flow in a gutter if the flow is actually unsteady. However, the flow intercepted by the grate may be either over- or under-estimated by the steady flow approximation.

4.3 Example Applications

Figures 25 to 28 are provided for easy determination of the relative magnitude of peak discharge into the grate inlet, Q_{pi}/Q_{pu}, and its relative time of occurrence, t_p/t_u, which are the major objectives for many practical problems. Through a systematic use of these figures, the peak discharges and its time of occurrence for different flow conditions for the given inlet and gutter geometries of different gutter slopes can be determined. The procedure will be illustrated in the following example.

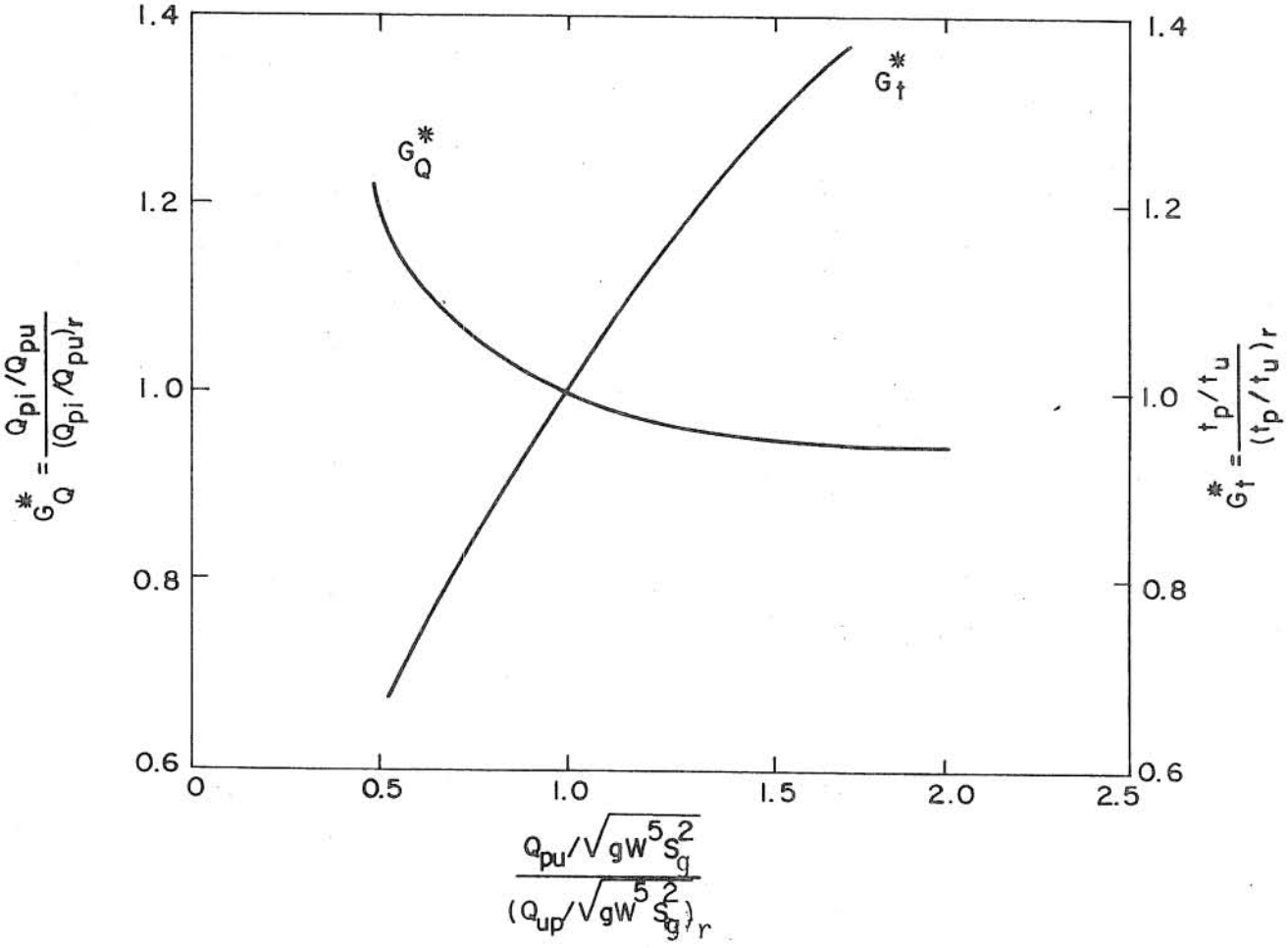

Fig. 25 Effect of $Q_{pu}/\sqrt{gW^5S_g^2}$ on Peak Discharge into Grate Inlet

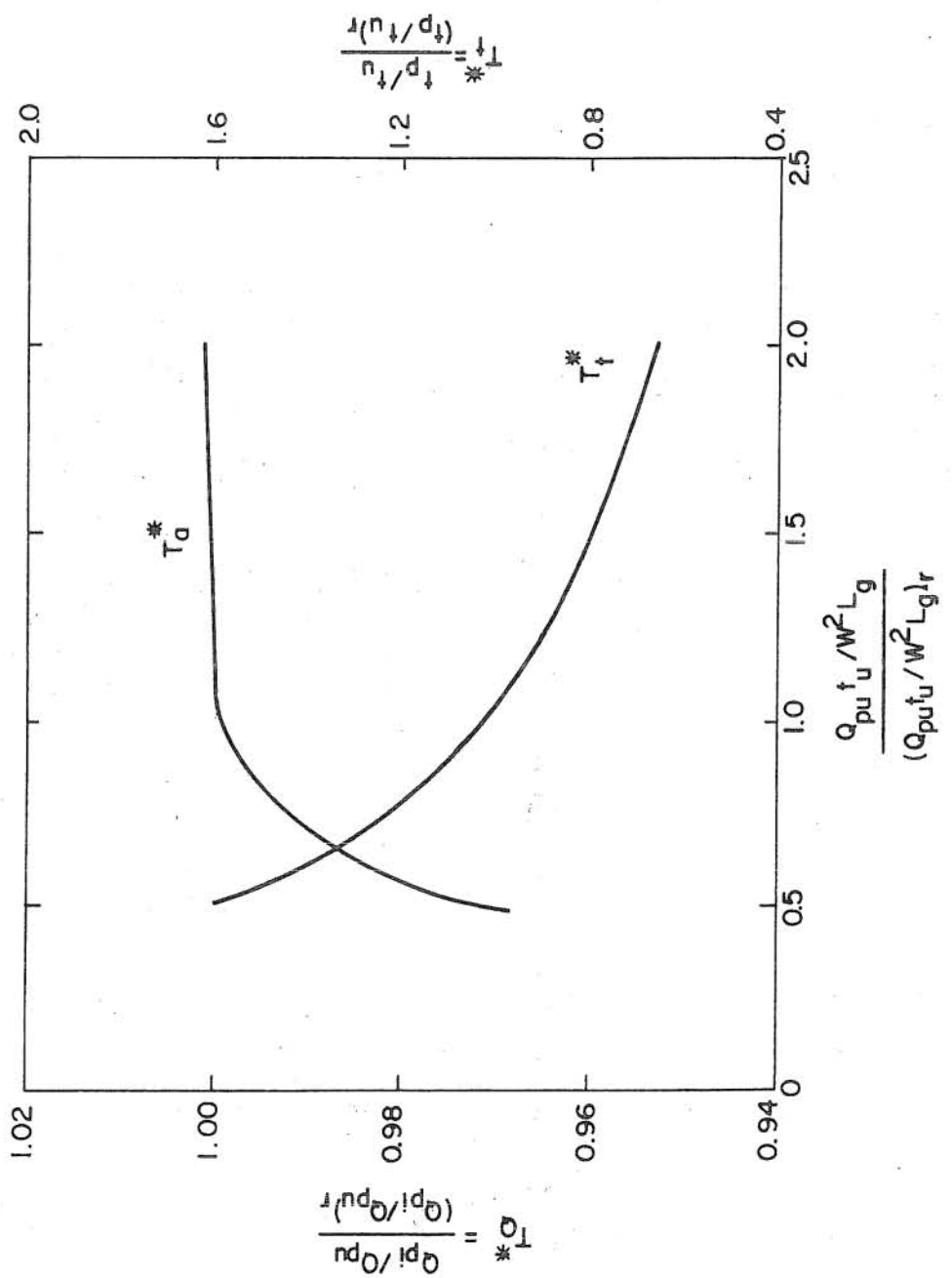

Fig. 26 Effect of $Q_{pu}t_u/W^2L_g$ on Peak Discharge into Grate Inlet

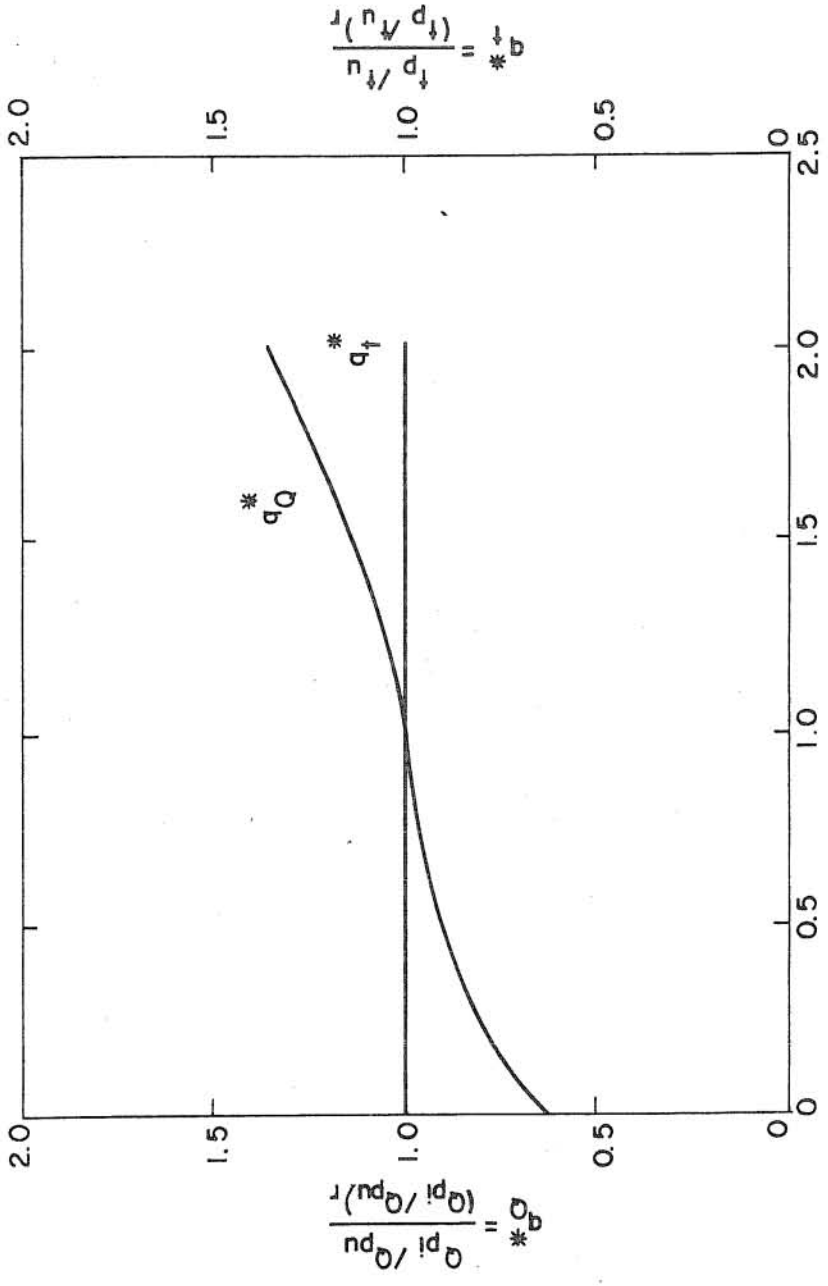

Fig. 27 Effect of Gutter Lateral Flow on Peak Discharge into Grate Inlet

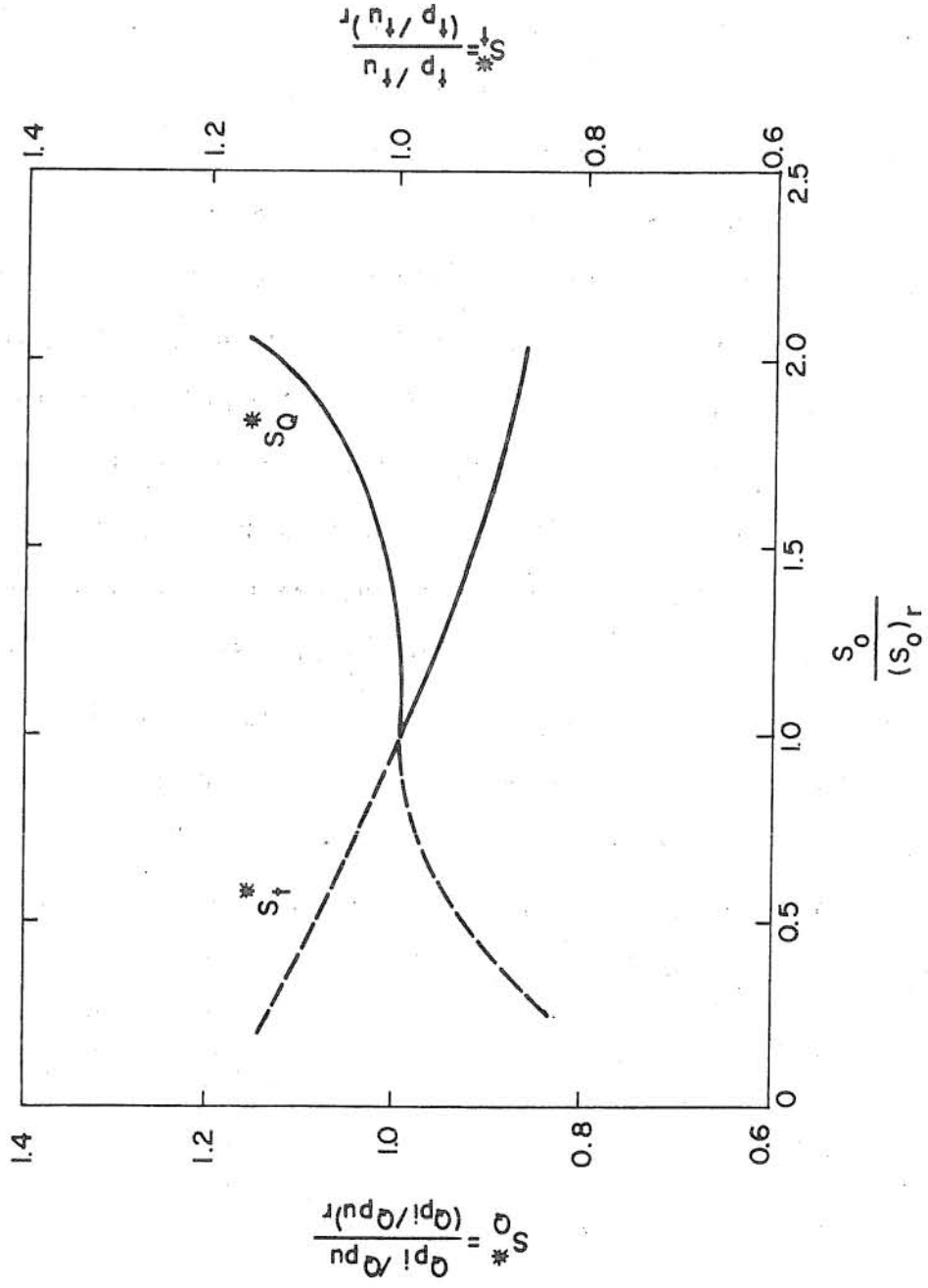

Fig. 28 Effect of Gutter Slope on Peak Discharge into Grate Inlet

Suppose a street has a gutter having slope S_o = 0.008, width B = 2.5 ft, lateral slope S_g = 0.048, and surface roughness k = 0.0125 ft. The spacing between the inlets is sufficiently long that for the sake of simplicity and saving in computation only the last reach of the gutter L_g = 50 ft is used in this example computation. The inflow into this reach from the upstream part of the gutter is assumed to have a peak discharge Q_{pu} = 0.150 cfs, a duration t_u = 80 sec, and this inflow hydrograph can be approximated by a sine curve. The lateral flow from the pavement and directly from rainfall has a steady rate q = 0.003 cfs/ft of gutter, starting at the same time of initiation of the upstream gutter inflow into this reach. Furthermore, the downstream grate inlet is of Type F with W = L = 1.25 ft. For this gutter and inlet, since S_g = 0.048, B/L_g = 0.05, k/B = 0.005, B/W = 2, and L/W = 1, Figs. 25 to 28 can be used to determine the peak discharge and its time of occurrence of the flow into the inlet as follows.

The first step is to compute the value of nondimensional parameters for the given condition:

$$Q_{pu}/\sqrt{gW^5S_g^2} = 0.314$$

$$Q_{pu}t_u/W^2L_g = 0.153$$

$$qL_g/Q_{pu} = 1.00$$

The second step is the determination of the values of the flow at the reference condition which has been discussed in Sec. 4.1:

$$y = BS_g/2 = 2.5 \times 0.048/2 = 0.060 \text{ ft}$$

$$Q_r = (2gy^5\cot^2\phi)^{1/2} = [2 \times 32.2 \times (0.06)^5 \times (20.6)^2]^{1/2} = 0.145 \text{ cfs}$$

$$Q_{pu} = Q_r/0.636 = 0.145/0.636 = 0.23 \text{ cfs}$$

$$q = Q_r/L_g = 0.145/50 = 0.0029 \text{ cfs/ft}$$

$$A = By = 2.5 \times 0.06 = 0.150 \text{ ft}^2$$

$$V = Q_r/A = 0.145/0.150 = 0.97 \text{ fps}$$

$$P = B(1+S_g^2)^{1/2} + 2y = 2.5 + 2 \times 0.06 = 2.62 \text{ ft}$$

$$R = A/P = 0.057 \text{ ft}$$

$$f = 1/(2 \log 2R/k + 1.74)^2 = 0.0746$$

$$S_o = S_f = 0.0048$$

Hence, for the reference condition,

$$(Q_{pu}/\sqrt{gW^5S_g^2})_r = 0.484$$

$$(Q_{pu}t_u/W^2L_g)_r = 0.152$$

$$(qL_g/Q_{pu})_r = 0.63$$

$$(S_o)_r = 0.0048$$

Thus,

$$\frac{Q_{pu}/\sqrt{gW^5S_g^2}}{(Q_{pu}/\sqrt{gW^5S_g^2})_r} = 0.65$$

Therefore, from Fig. 25, $G_Q^* = 1.09$, $G_t^* = 0.77$. Likewise, since

$$\frac{Q_{pu}t_u/W^2L_g}{(Q_{pu}t_u/W^2L_g)_r} = 1.01$$

from Fig. 26, $T_Q^* = 1.0$, $T_t^* = 1.0$;

$$\frac{qL_g/Q_{pu}}{(qL_g/Q_{pu})_r} = 1.58$$

from Fig. 27, $q_Q^* = 1.17$, $q_t^* = 1.0$; and

$$\frac{S_o}{(S_o)_r} = 1.67$$

from Fig. 28, $S_Q^* = 1.04$, $S_t^* = 0.895$. Knowing $(Q_{pi}/Q_{pu})_r = 0.105$ from Fig. 16, 17, 18 or 19, one can find Q_{pi}/Q_{pu} as follows

$$Q_{pi}/Q_{pu} = (Q_{pi}/Q_{pu})_r\, G_Q^*\, T_Q^*\, q_Q^*\, S_Q^* = 1.393$$

hence,

$$Q_{pi} = 1.393\, Q_{pu} = 0.21 \text{ cfs}$$

Similarly, by knowing $(t_p/t_u)_r = 1.32$ from any of Figs. 16 to 19

$$t_p/t_u = (t_p/t_u)_r \; G_t^* \; T_t^* \; q_t^* \; S_t^* = 0.91$$

and

$$t_p = 0.91 \; t_u = 72.77 \text{ sec}$$

It should be mentioned here that this result is by no means exact but sufficiently accurate for engineering purposes. The approximation involved include those in the numerical solutions to produce Figs. 25-28 and the assumption that the peak discharge and its time of occurrence can be computed by using the respective geometric products of G^*, T^*, q^*, and S^*.

5. ANALYSIS OF FLOW FROM GUTTER AND PAVEMENT UNDER RAIN

5.1 Flow from Pavement and Gutter into Inlet

The factors affecting runoff from gutters into inlets have been discussed in the preceding chapter for the case of constant lateral flow, q, into the gutter. In this chapter the investigation is extended to include unsteady pavement flow under rainfall. Strictly from a theoretical viewpoint, it is interesting and accurate to apply the Saint-Venant equations to the pavement flow as to the gutter flow. However, this approach would require a scheme to account for the ever changing internal boundary condition between the gutter and pavement flows and hence necessitates a trial-and-error computational scheme requiring large amount of computations. Contrarily, nonlinear kinematic-wave models disregard the downstream boundary condition whether the pavement flow is subcritical or supercritical, and hence solutions for pavement flow can be obtained independent of the gutter flow and only relatively simple computations are needed, particularly if the pavement conditions are identical along the street. The kinematic wave result is understandably less accurate than that from the Saint-Venant equations. Nonetheless, it is considerably more reliable than the results of linear kinematic-wave models such as the Manning formula or the Izzard or Horton methods.

Because of its shallow depth, pavement flow resistance is subject to much greater influence of the rainfall than the gutter flow. In view of the considerable savings in computational time and cost for the nonlinear kinematic-wave model and the lack of accurate information on unsteady flow resistance under rainfall, it is judged that from a practical viewpoint the accuracy gained by using the Saint-Venant equations for the pavement flow does not offset their disadvantages at this stage of research, and hence the nonlinear kinematic-wave model is adopted as the mathematical simulation for the pavement flows.

The kinematic-wave equations representing the pavement flow are a simplification and approximation of the Saint-Venant equations (Eqs. 2.1 and 2.2). With the friction slope, S_f, evaluated by using the Darcy-Weisbach formula (Eq. 2.19), they can be written as

$$\frac{\partial Q_1}{\partial x} + \frac{\partial y}{\partial t} = i \tag{5.1}$$

$$S_p = \frac{f Q_1^2}{8gy^3} \tag{5.2}$$

in which Q_1 denotes the discharge per unit width of the pavement flow path; y is the depth of the flow; i is the rainfall intensity having a dimension of length per unit time with appropriate units; $S_p = \tan \phi_p$ is the pavement crown slope; and f is Weisbach's resistance coefficient, evaluated as indicated in Fig. 5.

In this study Eqs. 5.1 and 5.2 are solved by using the method of characteristics. The characteristic equations are obtained in a manner similar to that described in Section 3.4. However, it should be noted that backward characteristics do not exist in a kinematic wave. A forward characteristic is defined by

$$\frac{dx}{dt} = 24 \frac{S_p g}{C_f \nu} y^2 \tag{5.3}$$

for laminar flow; and

$$\frac{dx}{dt} = \left(3 \log \frac{2y}{k_p} + 3.48\right) (8gS_p y)^{\frac{1}{2}} \tag{5.4}$$

for turbulent flow. The expression

$$\frac{dy}{dt} = i \tag{5.5}$$

is valid along the forward characteristic.

Finite difference equations for pavement flow are written with reference to Fig. 14 as

$$y_R = y_C - 24 \frac{gS_p}{C_f \nu} \frac{\Delta t}{\Delta x} (y_C - y_A)\, y_R^2 \tag{5.6}$$

for laminar flow; and

$$y_R = y_C - (8gS_p)^{\frac{1}{2}} \frac{\Delta t}{\Delta x} \left(3 \log \frac{2y_R}{k_p} + 3.48\right) y_R^{\frac{1}{2}} \tag{5.7}$$

for turbulent flow. After calculating the interpolated value of y_R from Eq. 5.6 or Eq. 5.7, by trial-and-error, solution is advanced to the next time step with

$$y_p = y_R + i\, \Delta t \tag{5.8}$$

Upstream boundary and initial conditions for pavement flow are represented by a zero depth condition.

The gutter flow, however, is still simulated by the Saint-Venant equations as in the preceding chapter. These equations are nondimensionalized by using the gutter width B and rainfall duration t_i.

The numerical analysis has been performed by applying the first-order explicit scheme of the method of characteristics discussed in Section 3.4 to the nondimensional Saint-Venant equations for the gutter flow and nondimensionalized nonlinear kinematic-wave equations for the pavement flow. The nondimensional parameters considered are guided by Eqs. 2.8 and 2.11. Again the case of Cassidy's [1966] Type F grate inlet used in Chapter 4 as an example is adopted here. With specified values of ϕ, L_g/B, W/L, b_1/W, b_2/W, b_3/W, b_4/W, b_5/W, b_6/W, η_b, and J_t as given in Section 4.1, with $\phi_p = \phi = 2.57^o$, and assuming a constant I_t for uniform temporal distribution of rainfall and insignificant effect of $B^2/\nu t_i$, Eqs. 2.8 and 2.11 can be simplified as

$$\frac{Q_o}{iA_s}, \frac{Q_o}{Q_s}, \frac{Q_i}{iA_s}, \text{ or } \frac{Q_i}{Q_s} = F_{17,18,19,20}\left(\frac{t}{t_i}, S_o, \frac{k}{B}, \frac{k_p}{B}, \frac{W_p}{B}, \frac{t_u}{t_i}, \frac{Q_{pu}t_i}{B^3}, \frac{t_i i}{B}, \frac{B}{gt_i^2}\right) \quad (5.9)$$

The flow conditions analyzed are summarized in Table 3 and they cover a sufficient range of the field conditions. The results of the analysis are presented in nondimensional forms for general uses. The runoff hydrographs at the exit section of the gutter are shown in Figs. 29 to 35 for the parameters S_o, k/B, W_p/B, $Q_{pu}t_i/B^3$, t_u/t_i, $t_i i/B$, and B/gt_i^2. The variations of the relative peak discharge from the gutter, Q_{op}/Q_s, which is of practical important from a design viewpoint, are shown in Figs. 36 to 39. The hydrographs for the parameter k_p/B are not presented because the effect of this parameter is relatively small as can be seen from Fig. 37 and Table 3.

5.2 Discussion of Results

Again, as in Chapter 4, for the sake of comparison of the computed results, a reference common condition is chosen and it is listed as the first one in Table 3. For the reference flow condition, the sine-curve shape gutter upstream inflow hydrograph is so chosen that its peak discharge Q_{pu} is equal to one-half of the discharge for a steady uniform critical flow in the gutter which is flowing just full with the water surface width equal to B. The duration of the gutter inflow hydrograph, t_u, is chosen equal to 1.57 times the duration of the rainfall, t_i, and the rainfall intensity i is equal to Q_{pu}/A_s so that the total volume of the gutter upstream inflow is equal to the total volume of the lateral inflow which in turn is equal to the volume of rainfall.

In Figs. 29 to 39, the values of the nondimensional parameters, except the one being considered, are the same as those for the reference condition given in Table 3. For the results shown, the values of the parameters $L_g/B = 50$, $\phi = 0.048$ rad (approximately 2.6^o or 5%), and $B_2/\nu t_i = 9090$. Of course, effects

TABLE 3. Conditions for Pavement and Gutter Flows

S_o (%)	$\frac{k}{B}$ (10^{-3})	$\frac{k_p}{B}$ (10^{-3})	$\frac{W_p}{B}$	$\frac{t_u}{t_i}$	$\frac{Q_{pu}t_i}{B^3}$	$\frac{t_i i}{B}$ (10^{-3})	$\frac{B}{gt_i^2}$ (10^{-5})	$\frac{Q_s}{iA}$	$\frac{Q_{op}}{iA}$	$\frac{Q_{op}}{Q_s}$	$\frac{t_{op}}{t_i}$
1.06	6.0	6.0	4.22	1.57	0.227	0.87	6.94	2.00	0.99	0.49	3.15
0.20	6.0	6.0	4.22	1.57	0.227	0.87	6.94	2.00	0.26	0.13	6.30
0.30	6.0	6.0	4.22	1.57	0.227	0.87	6.94	2.00	0.36	0.18	5.55
0.50	6.0	6.0	4.22	1.57	0.227	0.87	6.94	2.00	0.53	0.26	4.56
0.70	6.0	6.0	4.22	1.57	0.227	0.87	6.94	2.00	0.66	0.33	3.81
0.80	6.0	6.0	4.22	1.57	0.227	0.87	6.94	2.00	0.71	0.36	3.65
0.90	6.0	6.0	4.22	1.57	0.227	0.87	6.94	2.00	0.79	0.40	3.45
1.20	6.0	6.0	4.22	1.57	0.227	0.87	6.94	2.00	1.04	0.52	3.00
1.06	1.0	6.0	4.22	1.57	0.227	0.87	6.94	2.00	1.73	0.87	2.30
1.06	2.0	6.0	4.22	1.57	0.227	0.87	6.94	2.00	1.45	0.73	2.55
1.06	3.0	6.0	4.22	1.57	0.227	0.87	6.94	2.00	1.30	0.65	2.75
1.06	4.0	6.0	4.22	1.57	0.227	0.87	6.94	2.00	1.17	0.58	2.90
1.06	5.0	6.0	4.22	1.57	0.227	0.87	6.94	2.00	1.06	0.53	3.05
1.06	10.0	6.0	4.22	1.57	0.227	0.87	6.94	2.00	0.86	0.43	3.50
1.06	6.0	6.5	4.22	1.57	0.227	0.87	6.94	2.00	0.98	0.49	3.15
1.06	6.0	7.0	4.22	1.57	0.227	0.87	6.94	2.00	0.98	0.49	3.15
1.06	6.0	8.0	4.22	1.57	0.227	0.87	6.94	2.00	0.97	0.48	3.15
1.06	6.0	9.0	4.22	1.57	0.227	0.87	6.94	2.00	0.95	0.48	3.15
1.06	6.0	10.0	4.22	1.57	0.227	0.87	6.94	2.00	0.94	0.47	3.15
1.06	6.0	6.0	6.0	1.57	0.227	0.87	6.94	1.745	0.77	0.44	3.15
1.06	6.0	6.0	9.0	1.57	0.227	0.87	6.94	1.522	0.56	0.37	3.15
1.06	6.0	6.0	12.0	1.57	0.227	0.87	6.94	1.403	0.43	0.31	3.15
1.06	6.0	6.0	15.0	1.57	0.227	0.87	6.94	1.326	0.35	0.29	3.15

TABLE 3 (Cont'd)

S_o (%)	$\frac{k}{B}$ (10^{-3})	$\frac{k_p}{B}$ (10^{-3})	$\frac{W_p}{B}$	$\frac{t_u}{t_i}$	$\frac{Q_{pu}t_i}{B^3}$	$\frac{t_i i}{B}$ (10^{-3})	$\frac{B}{gt_i^2}$ (10^{-5})	$\frac{Q_s}{iA}$	$\frac{Q_{op}}{iA}$	$\frac{Q_{op}}{Q_s}$	$\frac{t_{op}}{t_i}$
1.06	6.0	6.0	4.22	0.75	0.227	0.87	6.94	2.00	0.46	0.23	3.15
1.06	6.0	6.0	4.22	1.00	0.227	0.87	6.94	2.00	0.64	0.37	3.15
1.06	6.0	6.0	4.22	2.00	0.227	0.87	6.94	2.00	1.10	0.55	3.30
1.06	6.0	6.0	4.22	3.00	0.227	0.87	6.94	2.00	1.25	0.63	3.64
1.06	6.0	6.0	4.22	4.00	0.227	0.87	6.94	2.00	1.29	0.65	3.97
1.06	6.0	6.0	4.22	1.57	0.100	0.87	6.94	1.44	0.44	0.30	3.67
1.06	6.0	6.0	4.22	1.57	0.150	0.87	6.94	1.66	0.61	0.37	3.45
1.06	6.0	6.0	4.22	1.57	0.300	0.87	6.94	2.32	1.04	0.45	3.11
1.06	6.0	6.0	4.22	1.57	0.350	0.87	6.94	2.54	1.26	0.49	3.04
1.06	6.0	6.0	4.22	1.57	0.450	0.87	6.94	2.98	1.33	0.45	2.96
1.06	6.0	6.0	4.22	1.57	0.600	0.87	6.94	3.65	1.70	0.47	2.81
1.06	6.0	6.0	4.22	1.57	0.750	0.87	6.94	4.30	2.05	0.48	2.61
1.06	6.0	6.0	4.22	1.57	0.227	0.174	6.94	6.00	2.94	0.49	3.50
1.06	6.0	6.0	4.22	1.57	0.227	0.435	6.94	3.00	1.45	0.48	3.35
1.06	6.0	6.0	4.22	1.57	0.227	1.740	6.94	1.50	0.70	0.47	2.85
1.06	6.0	6.0	4.22	1.57	0.227	2.610	6.94	1.33	0.60	0.45	2.65
1.06	6.0	6.0	4.22	1.57	0.227	4.000	6.94	1.22	0.57	0.46	2.17
1.06	6.0	6.0	4.22	1.57	0.227	6.000	6.94	1.14	0.62	0.54	1.79
1.06	6.0	6.0	4.22	1.57	0.227	0.87	9.71	2.00	0.50	0.25	3.90
1.06	6.0	6.0	4.22	1.57	0.227	0.87	8.77	2.00	0.62	0.31	3.65
1.06	6.0	6.0	4.22	1.57	0.227	0.87	7.77	2.00	0.89	0.44	3.35
1.06	6.0	6.0	4.22	1.57	0.227	0.87	5.83	2.00	1.08	0.54	2.95
1.06	6.0	6.0	4.22	1.57	0.227	0.87	2.50	2.00	1.50	0.75	2.14
1.06	6.0	6.0	4.22	1.57	0.227	0.87	1.66	2.00	1.64	0.82	1.91
1.06	6.0	6.0	4.22	1.57	0.227	0.87	0.50	2.00	1.90	0.95	1.43
1.06	6.0	6.0	4.22	1.57	0.227	0.87	0.20	2.00	1.90	0.95	1.18

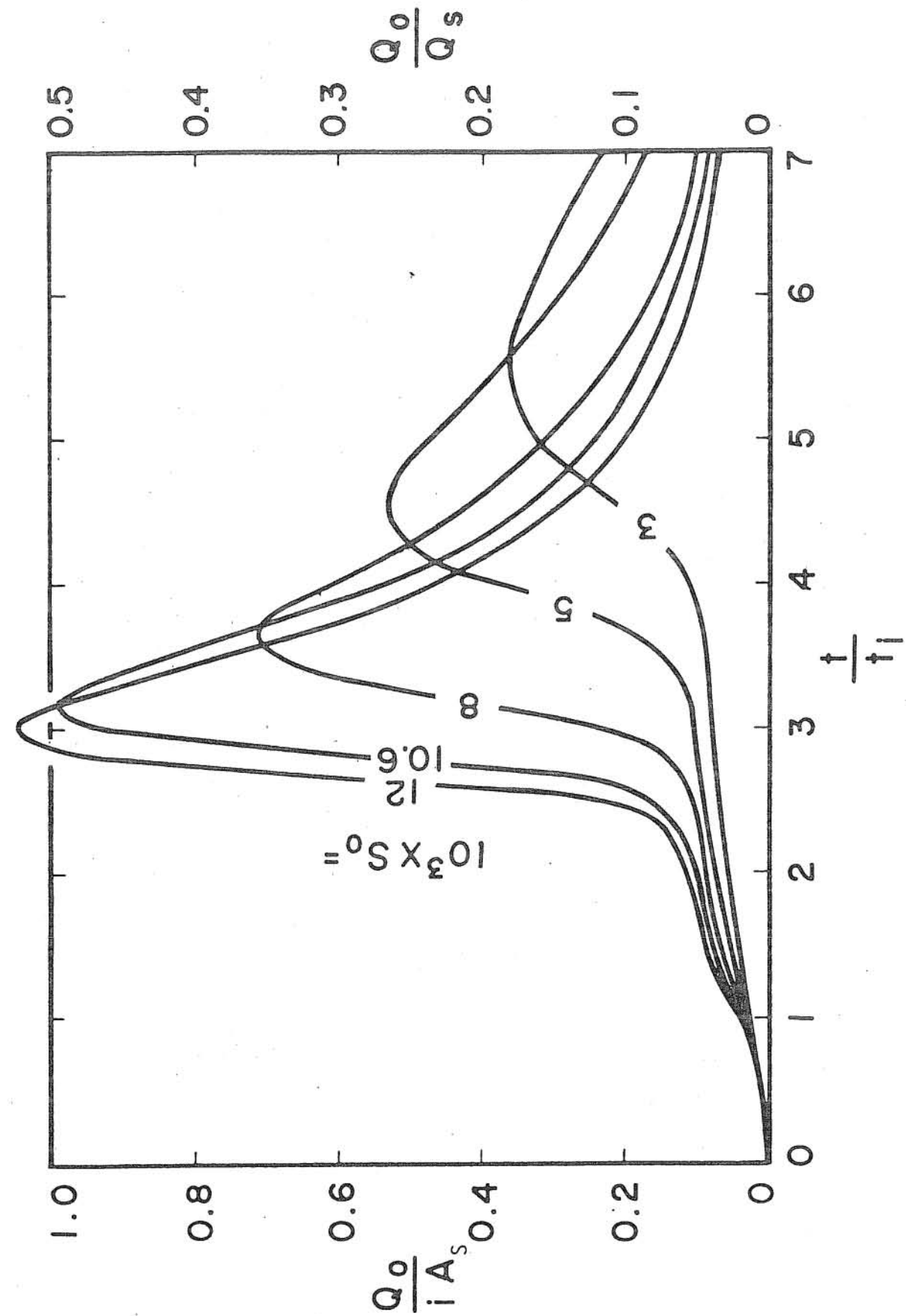

Fig. 29 Hydrographs at Gutter Exit for Different Street Slopes

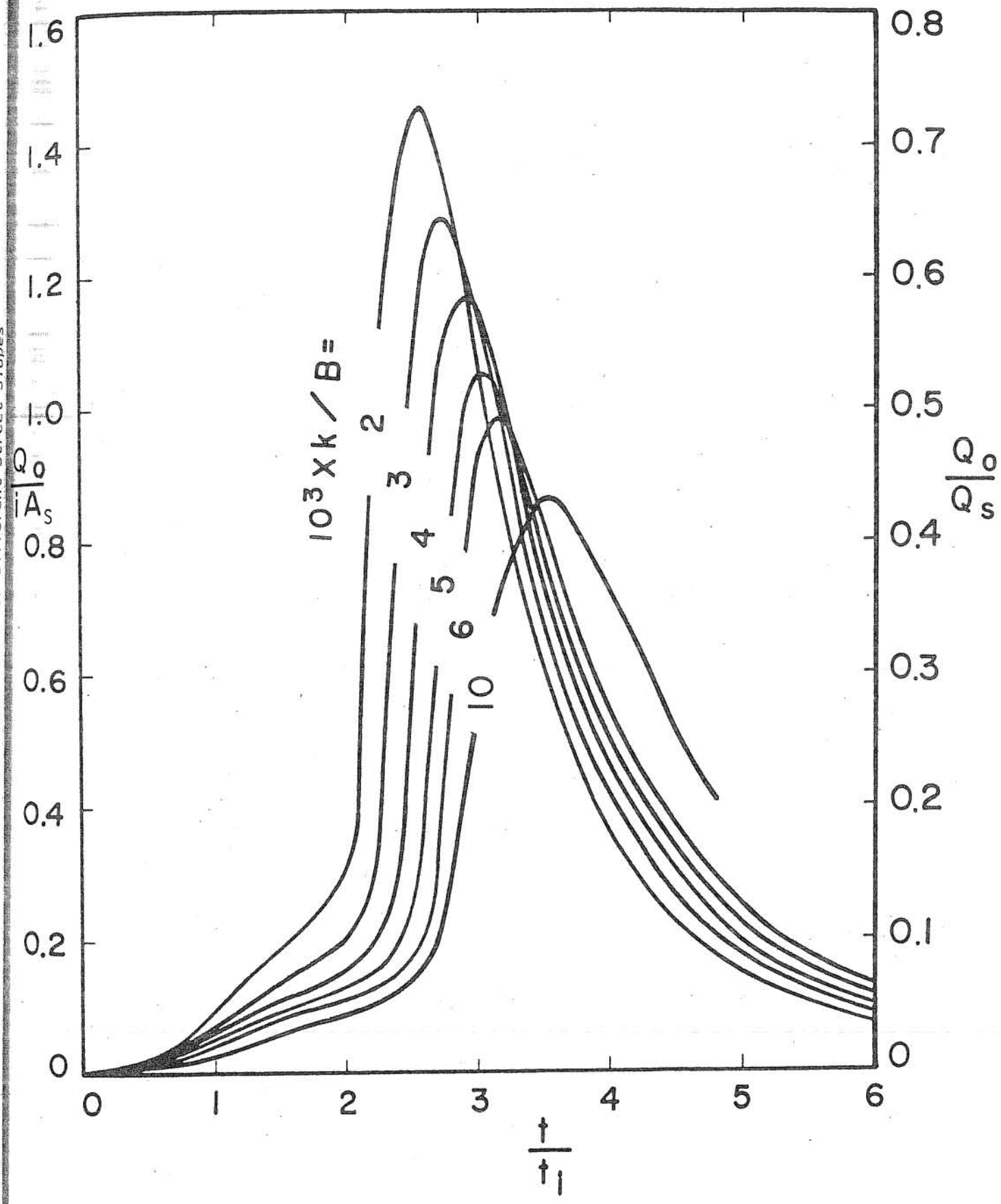

Fig. 29 Hydrographs at Gutter Exit for Different Street Slopes

Fig. 30. Hydrographs at Gutter Exit for Different Gutter Surface Roughnesses

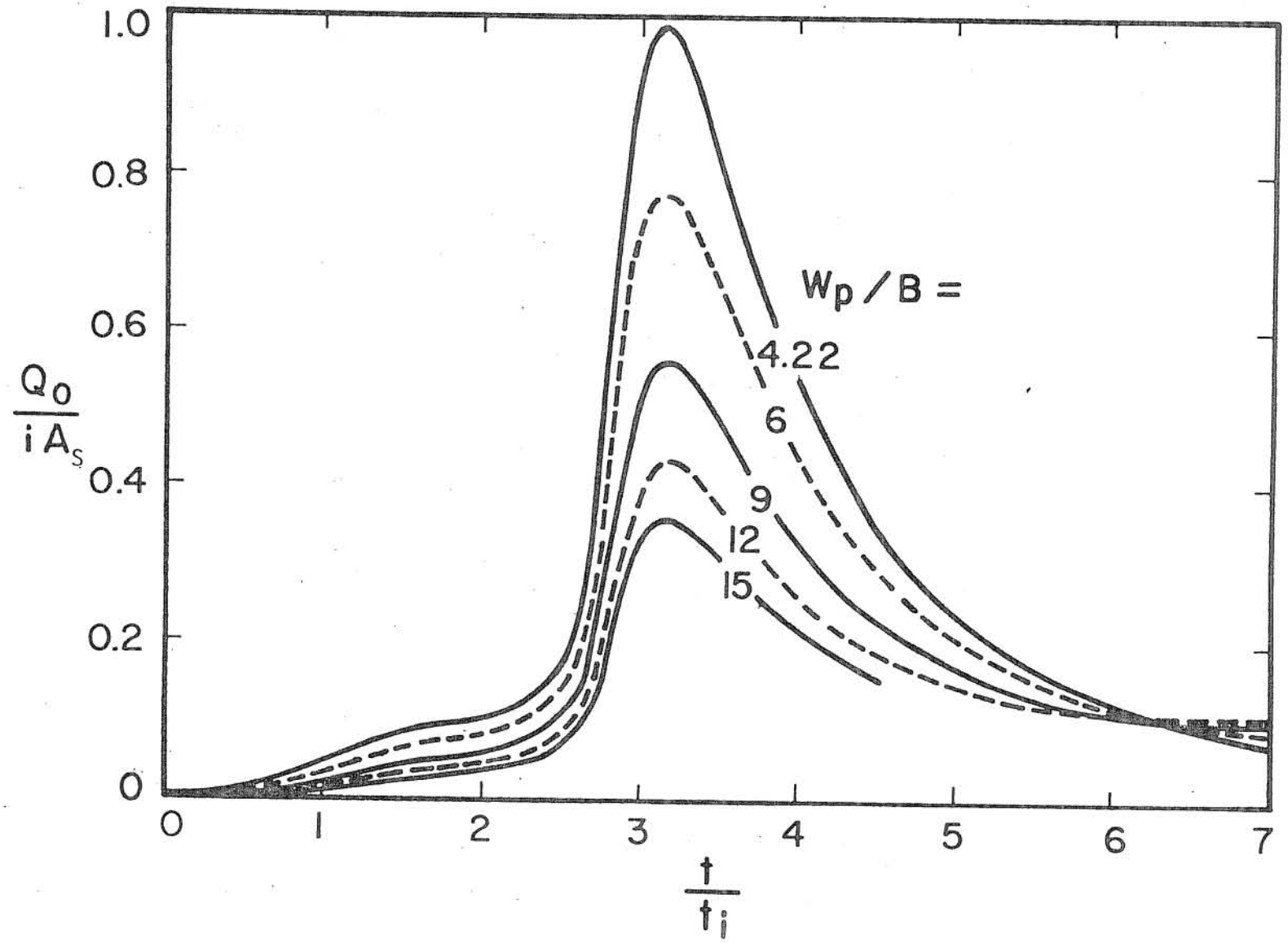

Fig. 31 Hydrographs at Gutter Exit for Different Pavement Widths (a) Q_o/iA_s vs. t/t_i

Fig. 31 Hydrographs at Gutter Exit for Different Pavement Widths (a) Q_o/iA_s vs. t/t_i

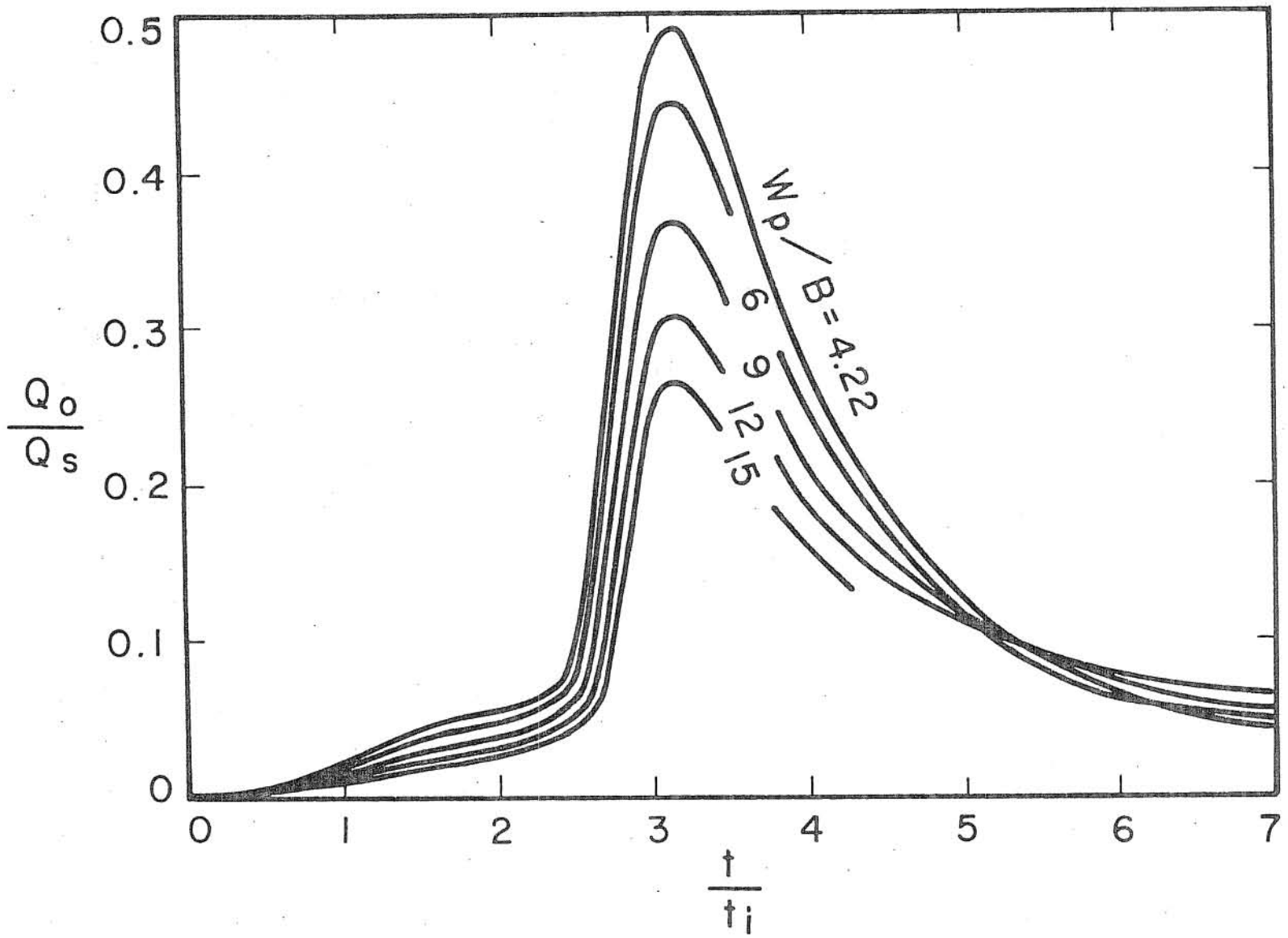

Fig. 31 (b) Q_o/Q_s vs. t/t_i

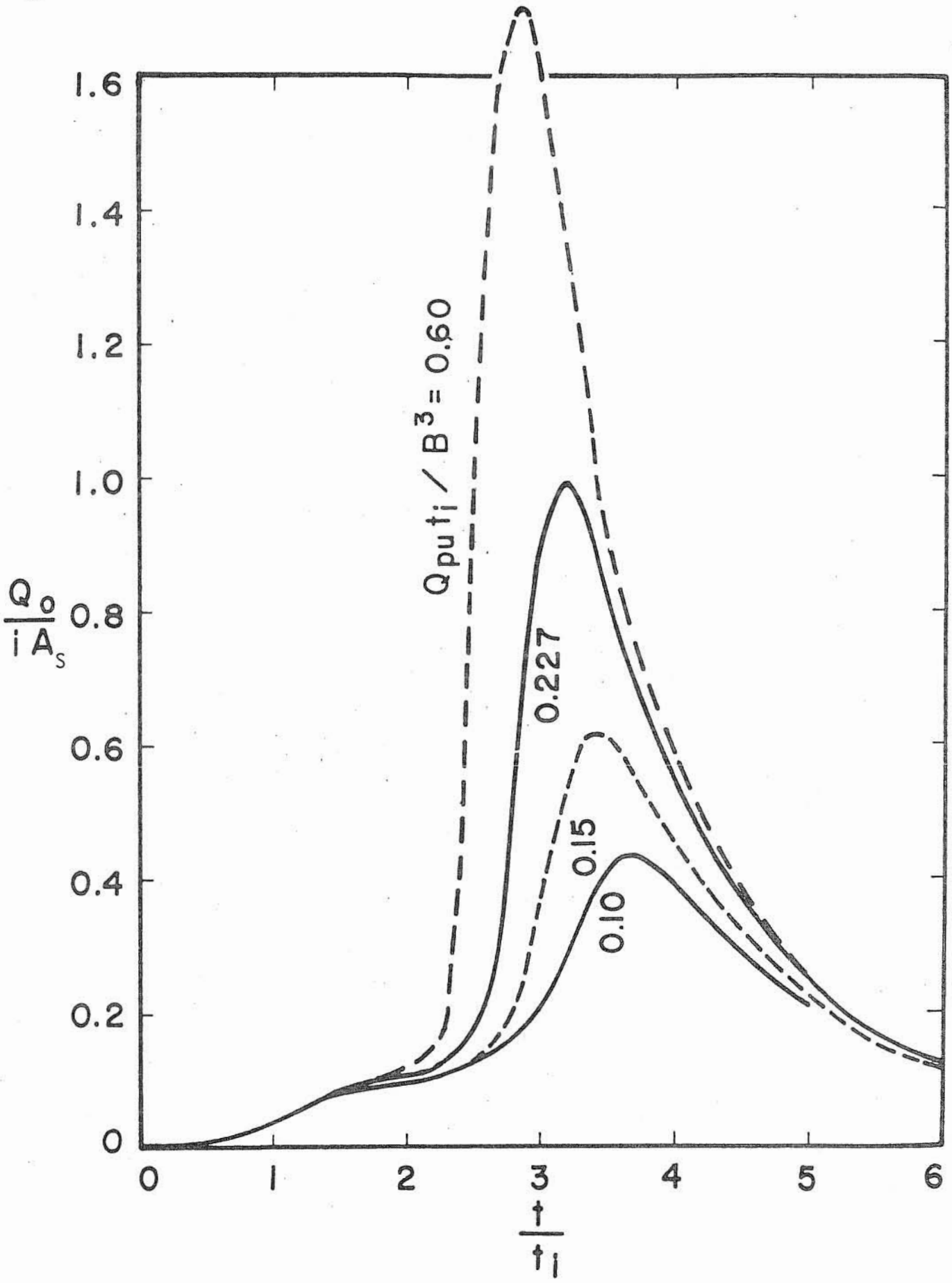

Fig. 32 Hydrographs at Gutter Exit for Different Upstream Inflow Rates
(a) Q_o/iA_s vs. t/t_i

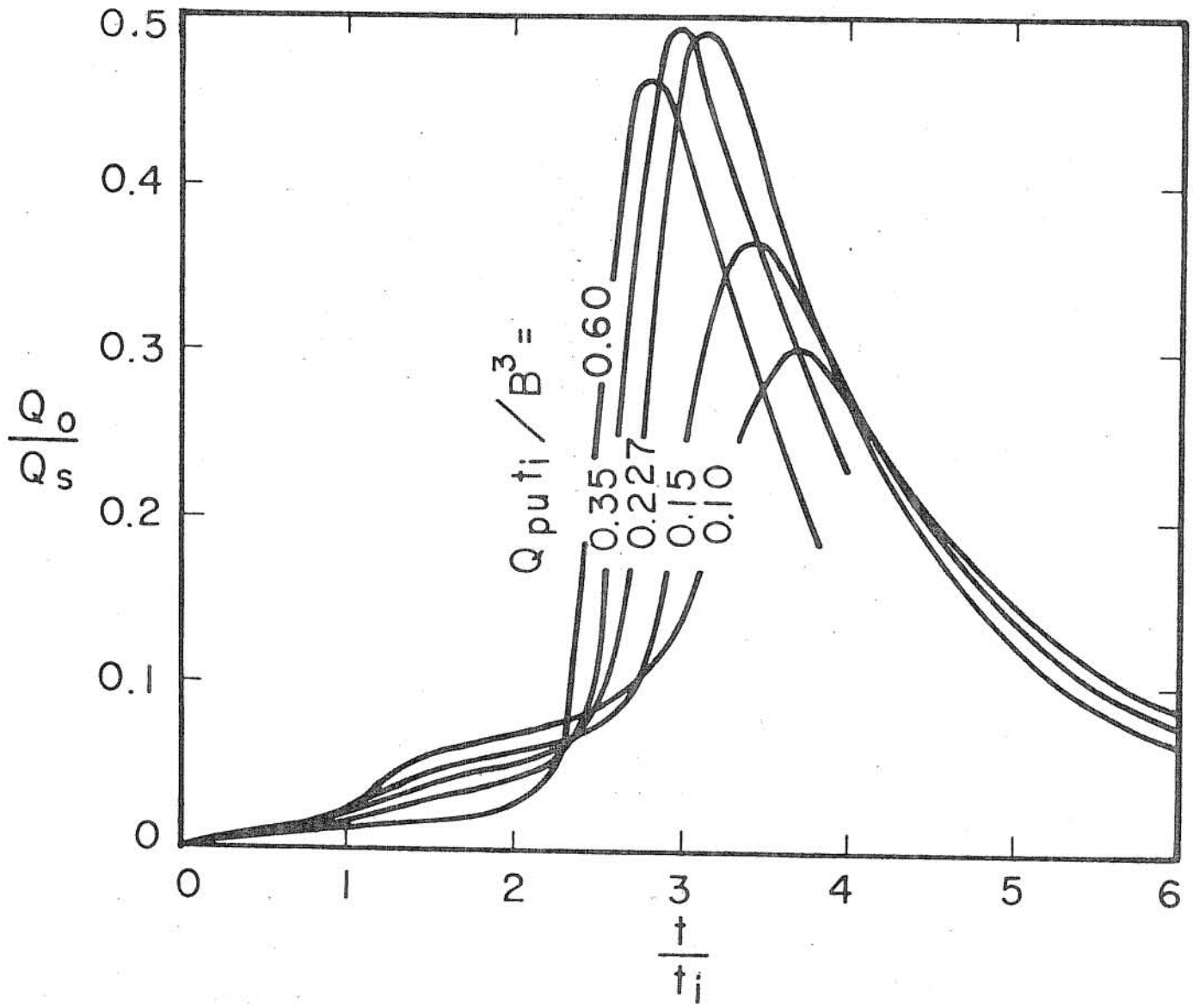

Fig. 32 (b) Q_o/Q_s vs. t/t_i

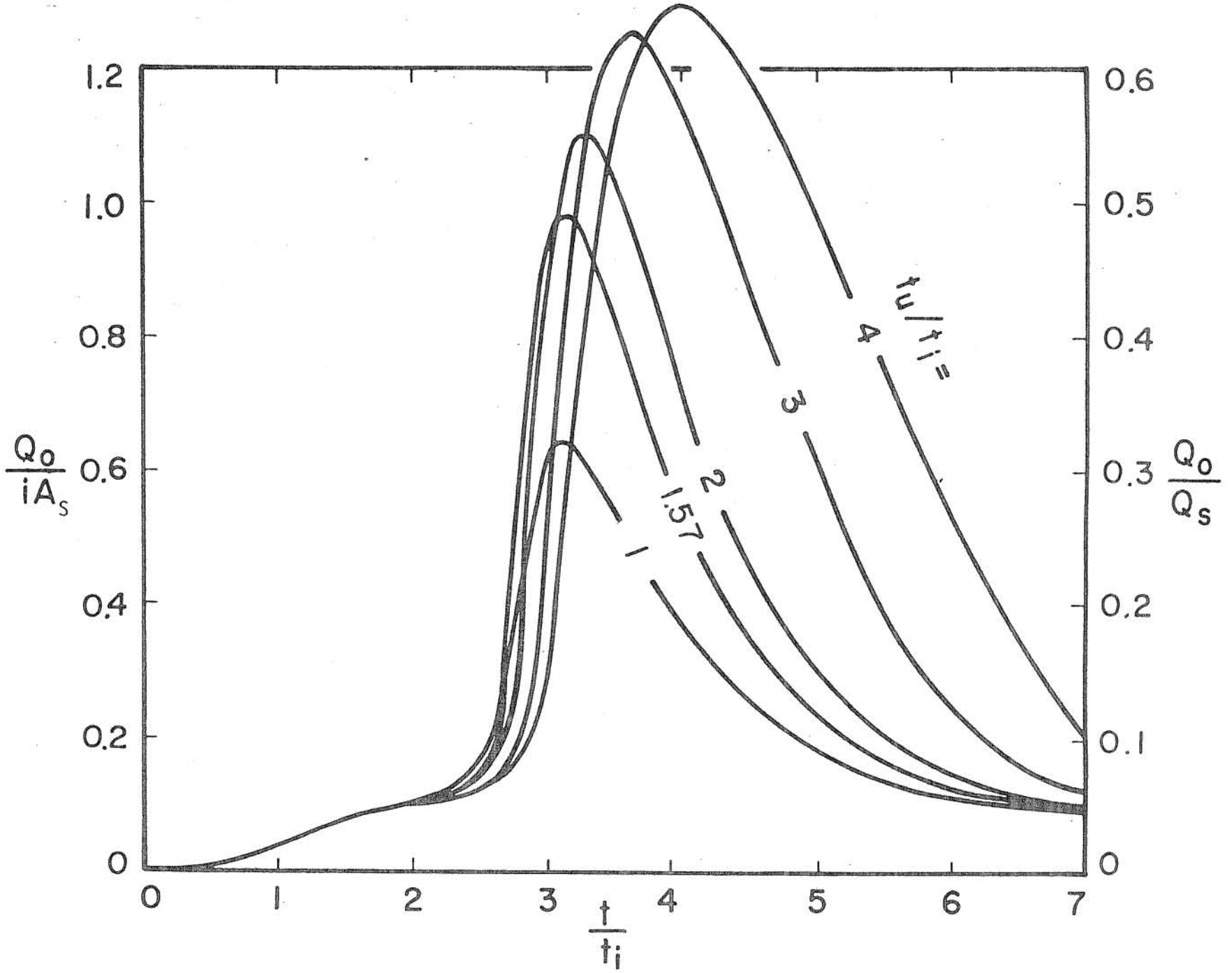

Fig. 33 Hydrographs at Gutter Exit for Different Upstream Inflow Durations

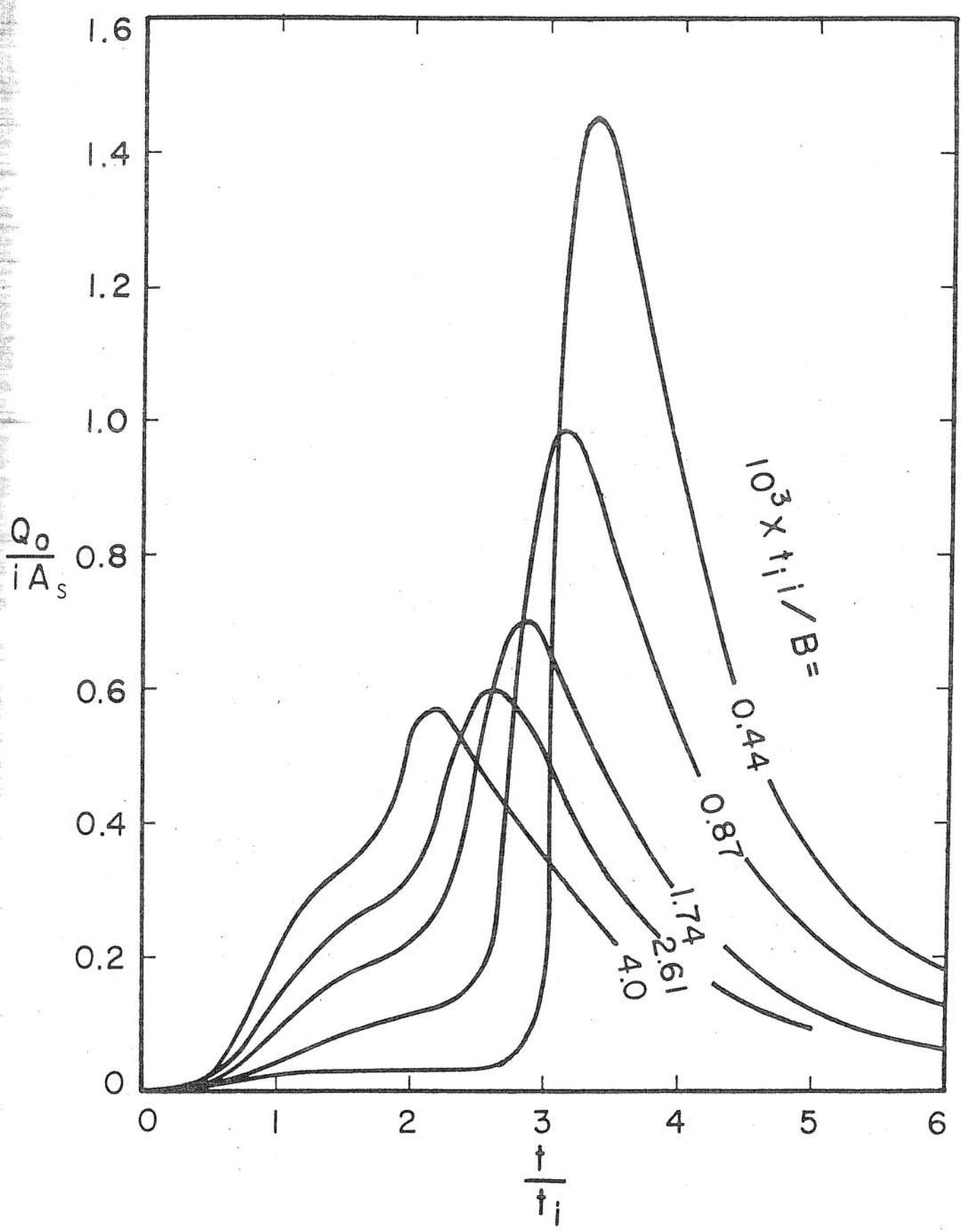

Fig. 33 Hydrographs at Gutter Exit for Different Upstream Inflow Durations

Fig. 34 Hydrographs at Gutter Exit for Different Rainfall Intensities
(a) Q_o/iA_s vs. t/t_i

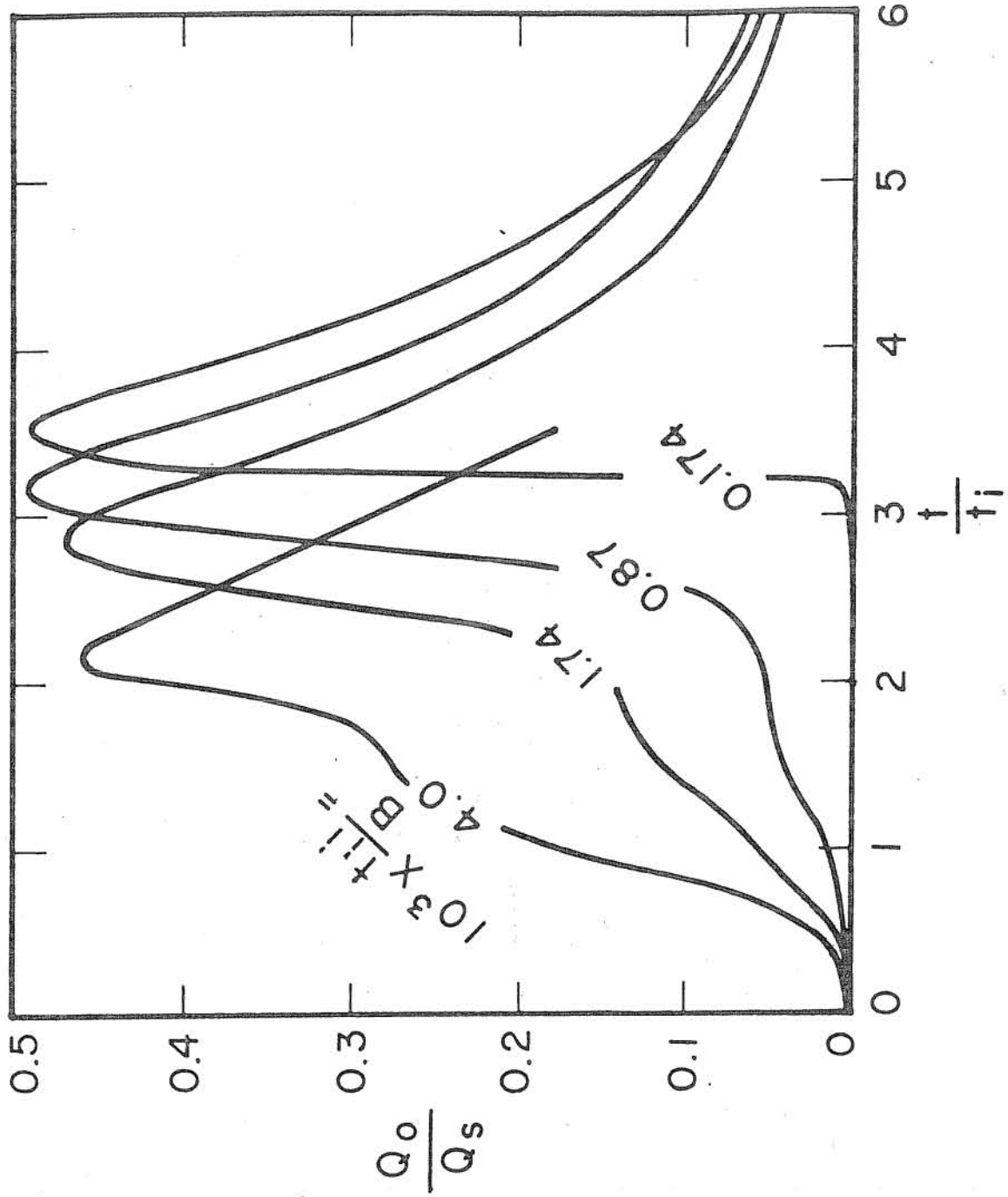

Fig. 34 (b) Q_o/Q_s vs. t/t_i

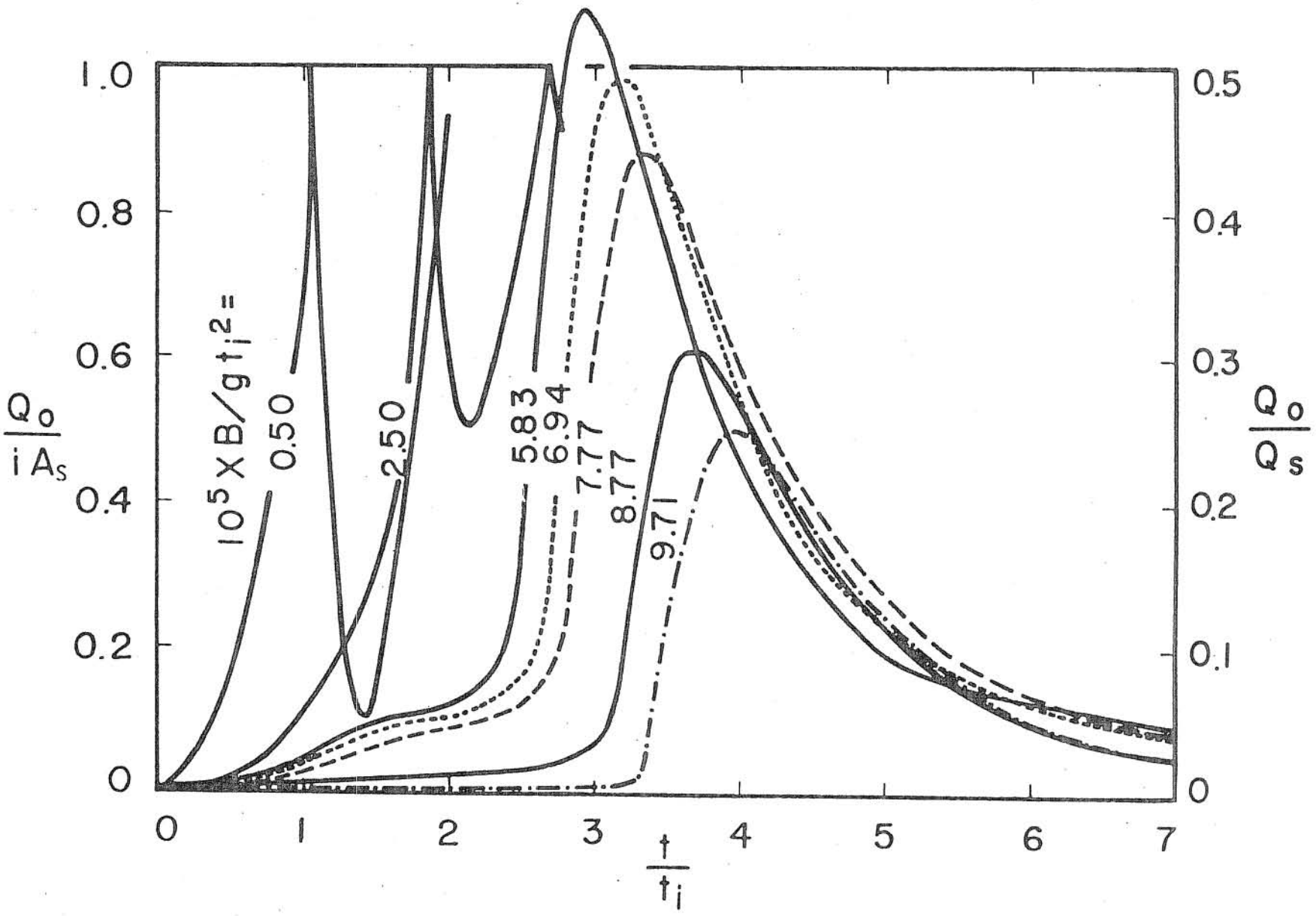

Fig. 35 Hydrographs at Gutter Exit for Different Gravitational Effects

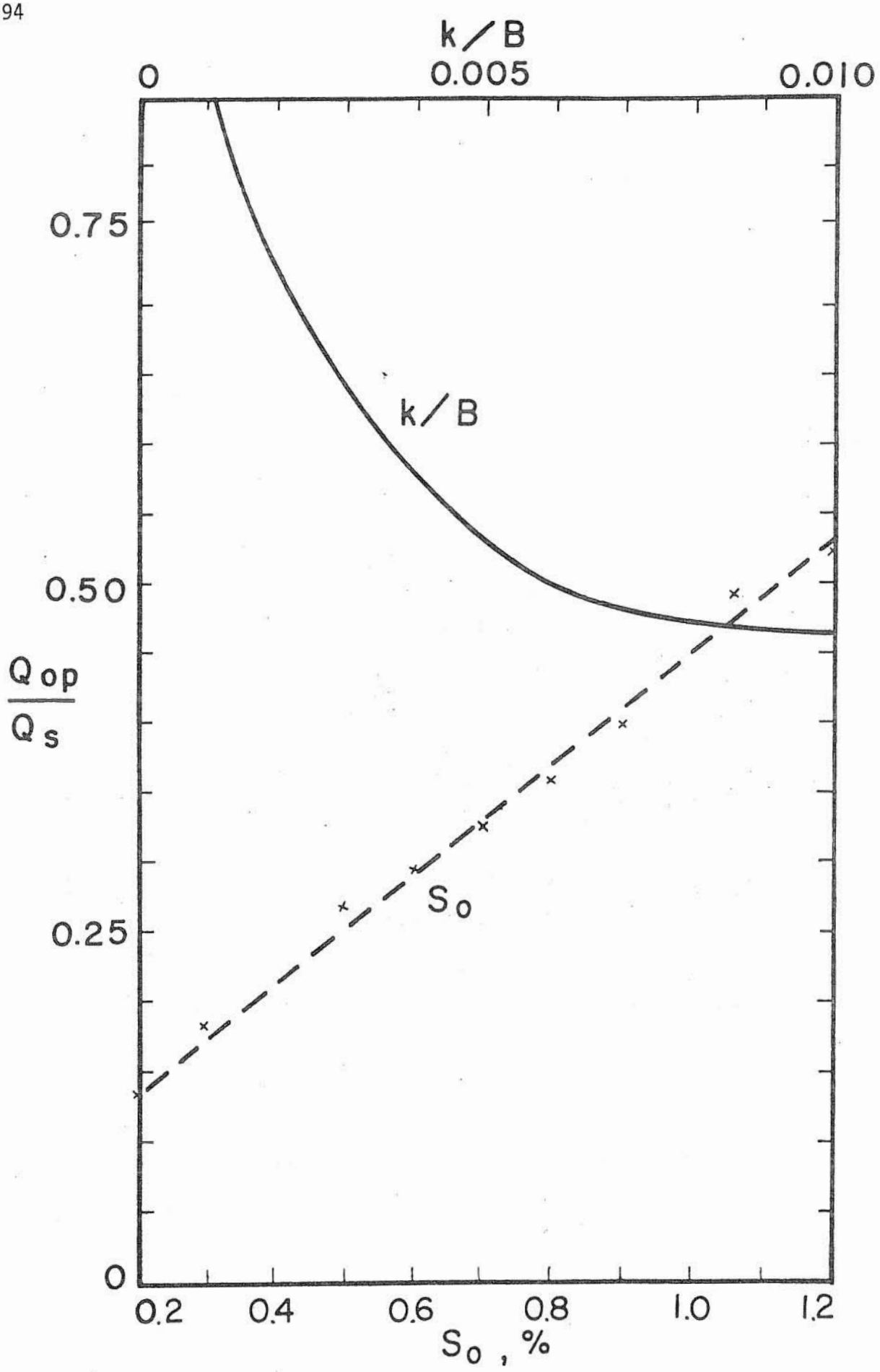

Fig. 36 Variations of Peak Discharge from Gutter with Gutter Characteristics

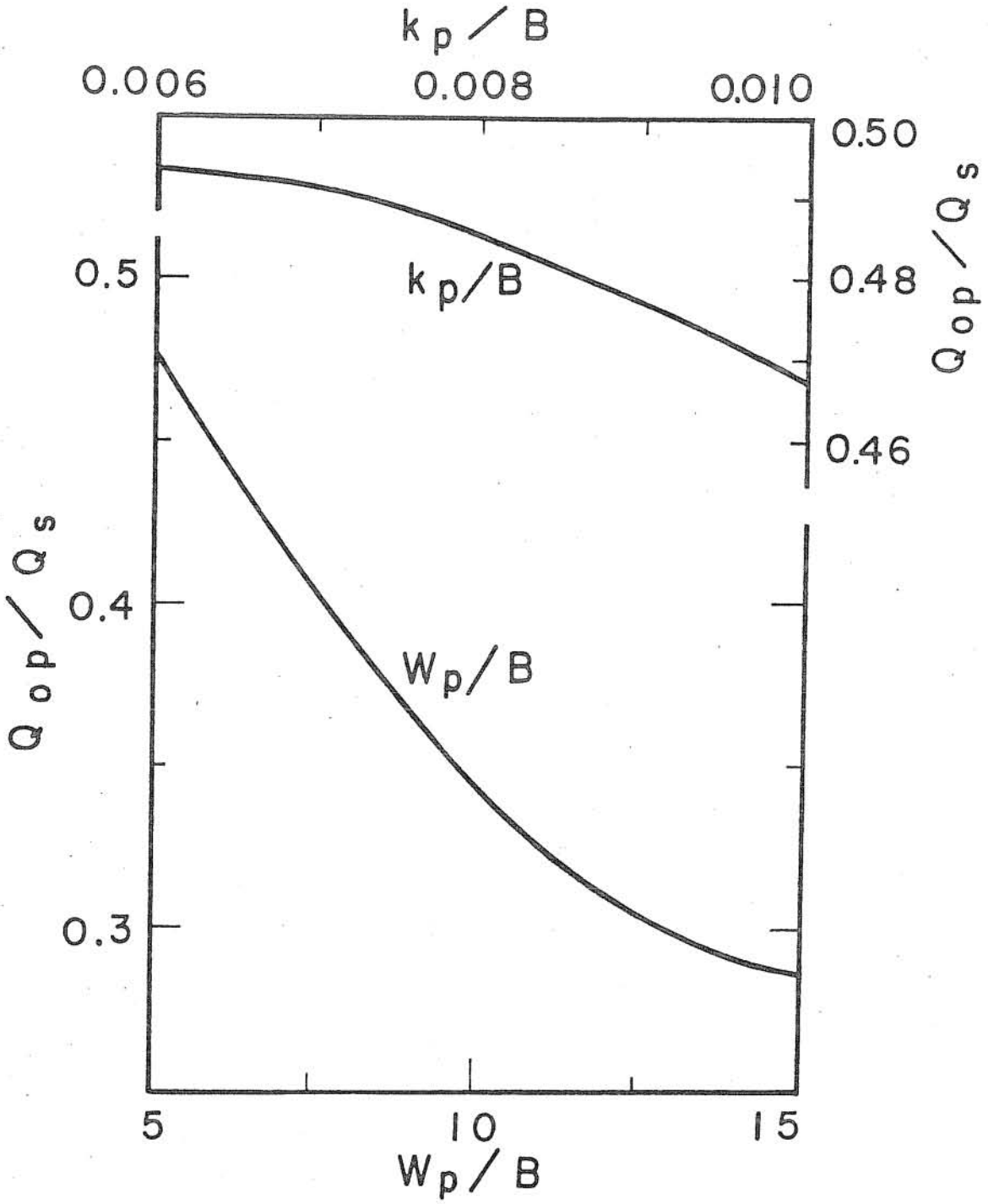

Fig. 37 Variations of Peak Discharge from Gutter with Pavement Characteristics

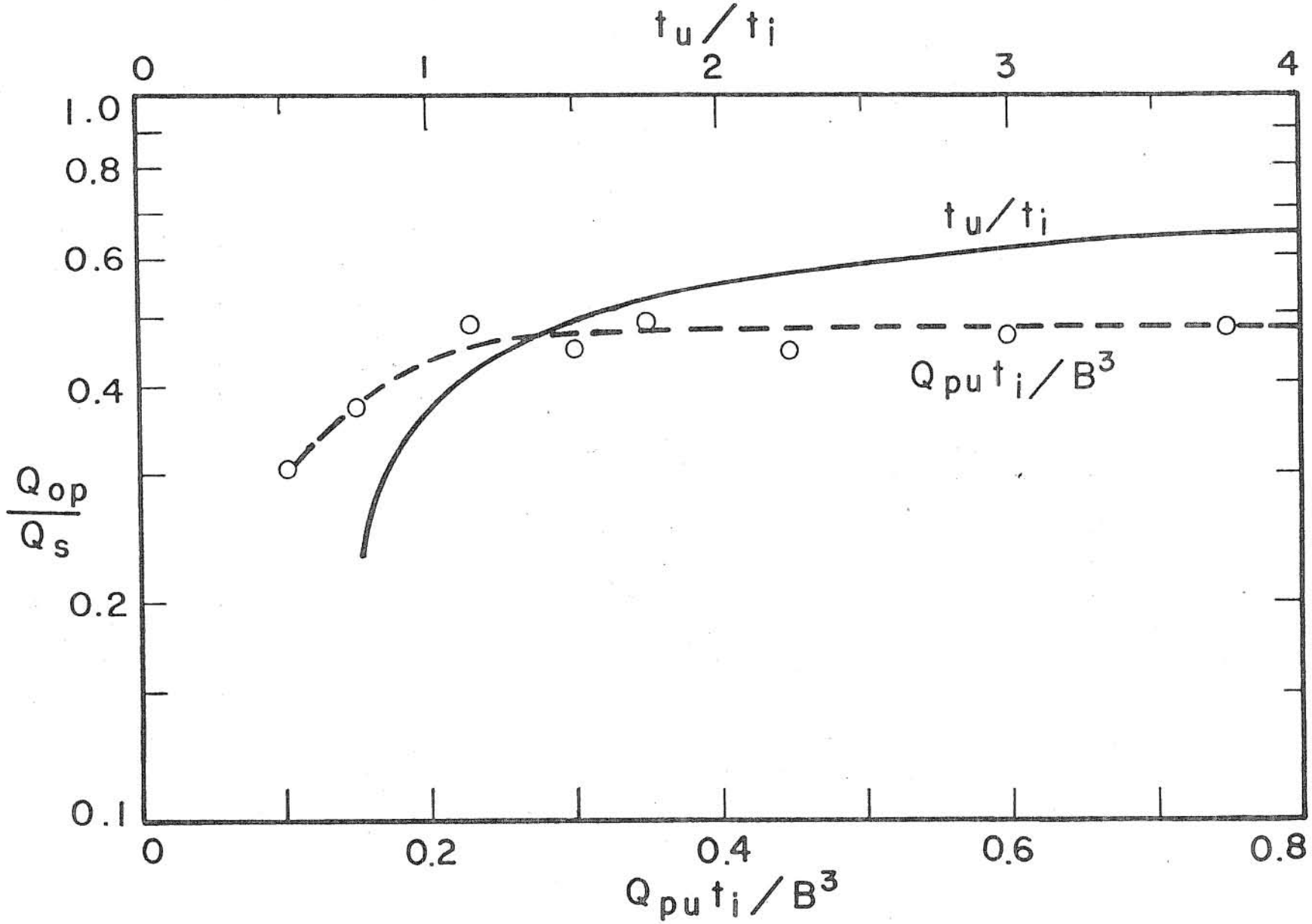

Fig. 38 Variations of Peak Discharge from Gutter with Upstream Inflow Characteristics

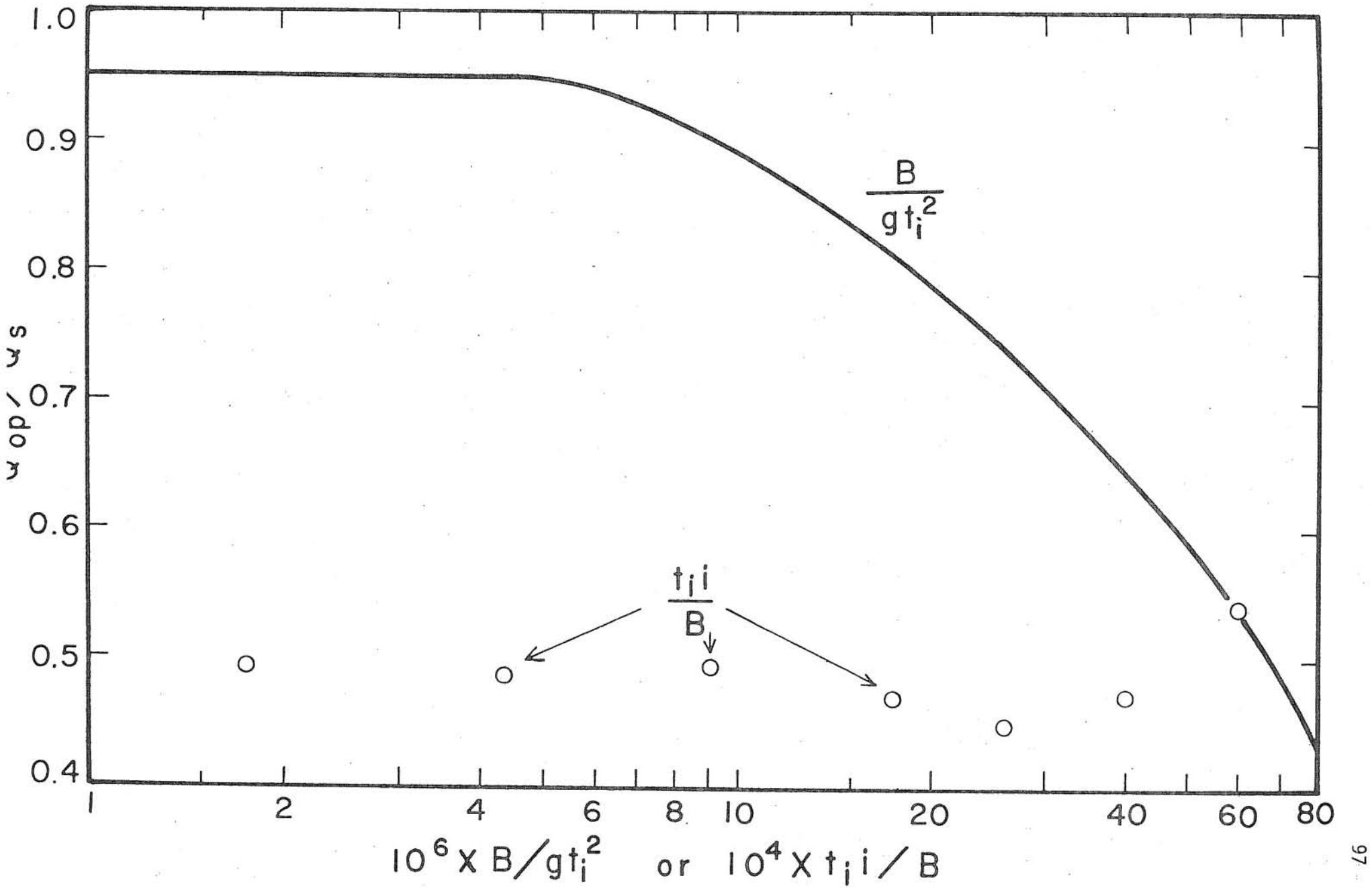

Fig. 39 Variations of Peak Discharge from Gutter with Relative Rainfall Intensity and Gravitation Effect

of these three parameters can also be evaluated numerically if desired. However, as discussed previously, the effect of L_g/B is indirect as long as it is not too small so that the upstream inflow behaves like a source. The value of ϕ is arbitrary chosen as that used by Cassidy [1966]. As to $B^2/\nu t_i$, this parameter actually represents the effect of viscosity. In field conditions of unsteady flow on pavement and in gutters, particularly when under rainfall, turbulence effect is dominant in determing the runoff hydrographs. Laminar flows occur only at the very beginning and near the end of runoff when the velocity is slow and the depth is small. Consequently for field conditons the effect of $B^2/\nu t_i$ is insignificant and hence not presented herewith. Alternatively, by cross multiplying the last two terms in Eq. 2.8, either $B^2/\nu t_i$ or B/gt_i^2 can be replaced by ν^2/gB^2 which indicates the relative importance of viscous effect as compared to the gravity effect.

Because the nonlinear kinematic-wave approximation is used in evaluating the pavement flow, understandably some of the calculated results do not fall exactly on a smooth line as one would hope. For such cases the computed points are plotted as in Figs. 36, 38, and 39 to illustrate the deviations. However, it is believed that from a practical viewpoint these deviations are not significant. Particularly, the method presented in this chapter is a considerable improvement from the Manning or Chezy formulas and the Izzard and Horton methods commonly used in estimating pavement and gutter flows.

From the computed results as shown in Figs. 29 to 39, it can be seen that the effect of flow unsteadiness is quite important. Should a steady-flow approach be adopted as in common practice, the design discharge would be $Q_s = Q_{pu} + iA_s$. As shown by the computed values of Q_{op}/Q_s (Figs. 36 to 39), the peak discharge from the gutter is alwasy smaller than Q_s, and significantly, the reduction is more for smaller relative gutter upstream inflow. In other words, presumably the runoff coefficient in the rational formula commonly used should account for, among other things, the effect of detention storage on the

surface. In engineering practice, the runoff coefficient is selected independent of the intensity and duration of the rainfall, whereas the computed results show the contrary.

However, as shown in Fig. 39, the effects of rainfall duration and intensity of the relative gutter peak outflow Q_{op}/Q_s are not as dominant as those by S_o, k/B, W_p/B, and t_u/t_i. Obviously, with increasing street slope, S_o, the surface detention storage decreases and the value of Q_{op}/Q_s increases, and the runoff hydrograph becomes steeper and with a shorter runoff time, as shown in Fig. 29. Increase in surface roughness of the gutter retards the flow and consequently reduces Q_{op}/Q_s as shown in Figs. 30 and 36. However, as the value of k/B increases, its affect on changing the gutter flow decreases. The effect of W_p/B on Q_{op}/Q_s is somewhat similar to that of k/B in that increasing W_p/B results in decreasing Q_{op}/Q_s at a decreasing rate as shown in Figs. 31 and 37.

6. CONCLUSIONS

Flow in a street gutter is essentially unsteady because of the time varying nature of rainfall and other inputs. The unsteady gutter flow can be described mathematically and approximately by the Saint-Venant equations and solved by using the method of characteristics or other finite difference methods.

The factors affecting the gutter flow and discharge into the grate inlet can be identified by using dimensional analysis. The numerical results reveal that for a given grate inlet, the outflow of the gutter and the flow intercepted by the inlet are affected by the nondimensional parameters of rainfall or lateral flow into the gutter, and a Froude number-form parameter; and these effects are more obvious when the gutter slope increases.

The conventionally adopted uniform steady flow approach to determine the gutter flow considering only the peak inflow rate usually results in an overdesign of the gutter size and overestimates the amount of water into the grate inlet for a given rainfall of finite duration. Moreover, in the steady-flow approach, the information obtained is incomplete since the time distribution of flow which is important in design and operation of storm systems is missing.

The conditions used in the numerical investigation are limited to a triangular gutter with a particular type of grate inlet, a sine wave-type upstream inflow and a uniform rainfall. Other conditions can be investigated similarly. Design curves of the kind presented in Figs. 24 to 27 and 36 to 39 can be established for different types of gutters and grate inlets for practical uses.

A weakness in this theoretical analysis of unsteady gutter flow into grate inlet is that for subcritical gutter flow the downstream boundary condition is given by assuming a quasi-steady condition at the inlet in order to use previous experimental results. Further study on this aspect and experimental verification of the theoretical results are most desirable.

REFERENCES

1. Ames, W. F., Numerical Methods for Partial Differential Equations, Barnes and Nobel Inc., New York, 1969, pp. 165-215.

2. Burgi, P. H., "Bicycle-Safe Grate Inlet Study, Vol. 2, Hydraulic Characteristics of Three Selected Grate Inlets on Continuous Grades," Report No. FHWA-RD-78-4, Federal Highway Administration, Washington, D.C., May 1978a.

3. Burgi, P. H., "Bicycle-Safe Grate Inlet Study, Vol. 3, Hydraulic Characteristics of Three Selected Grate Inlets in a Sump Condition," Report No. FHWA-RD-78-70, Federal Highway Administration, Washington, D.C., September 1978b.

4. Burgi, P. H., and Gober, D. E., "Bicycle-Safe Grate Inlets Study, Vol. 1, Hydraulic and Safety Characteristics of Selected Grate Inlets on Continuous Grades," Report No. FHWA-RD-77-24, Federal Highway Administration, Washington, D.C., June 1977.

5. Cassidy, J. J., "Generalized Hydraulic Characteristics of Grate Inlets," Highway Research Record No. 123, 1966, pp. 36-48.

6. Chen, C. L. and Chow, V. T., "Hydrodynamics of Mathematically Simulated Surface Runoff," Hydraulic Engineering Series No. 18, Department of Civil Engineering, University of Illinois at Urbana-Champaign, August 1968, 132 p.

7. Chow, V. T., Open-Channel Hydraulics, McGraw-Hill Book Co., New York, 1959, pp. 41-83.

8. Dronkers, J. J., "Tidal Computations for Rivers, Coastal Areas, and Seas," Journal of the Hydraulics Division, ASCE, Vol. 95, No. HY1, January 1969, pp. 29-77.

9. Guillou, J. C., "The Use and Efficiency of Some Gutter Inlet Grates," Engineering Experiment Station Bulletin No. 450, University of Illinois at Urbana-Champaign, 1959, 68 p.

10. Hartree, D. R., Numerical Analysis, Oxford University Press, New York, 1958.

11. Henderson, F. M., Open Channel Flow, The McMillan Co., New York, 1966, pp. 35-45.

12. Kreyszig, E., Advanced Engineering Mathematics, John Wiley and Sons, Inc., New York, 1972, pp. 415-60.

13. Larson, C. L. and Straub, L. G., "Grate Inlets for Surface Drainage of Streets and Highways," St. Anthony Falls Hydraulic Laboratory Bulletin No. 2, University of Minnesota, Jun 1949, 30 p.

14. Liggett, J. A. and Woolhiser, D. A., "Difference Solutions of the Shallow-Water Equation," Journal of the Engineering Mechanics Division, ASCE, Vol. 93, No. EM2, April 1967, pp. 39-71.

15. McNown, J. S. and Tai, C., "Balanced Storm Drainage," Report, Water Resources Research Institute, University of Kansas, 1972, 37 p.

16. Nes, T. J. J. S. and Hendriks, M. H., "Analysis of Linear Distributed Model of a Surface Runoff," Report No. 1, Laboratory of Hydraulics and Catchment Hydrology, Agricultural University, Wageningen, The Netherlands, January 1971, 129 p.

17. Sevuk, A. S and Yen, B. C., "A Comparative Study on Flood Routing Computation," Proceedings, IAHR International Symposium on River Mechanics, Vol. 3, Bangkok, Thailand, January 1973, pp. 275-90.

18. Stoker, J. J., Water Waves, Interscience Publishers, Inc., New York, 1966, pp. 451-505.

19. Storm Drainage Research Project, "The Design of Stormwater Inlets," Department of Sanitary Engineering and Water Resources, The Johns Hopkins University, Baltimore, 1956, 193 p.

20. Streeter, V. L. and Wylie, E. B., Hydraulic Transients, McGraw-Hill Book Co., New York, 1967, pp. 238-59.

21. Strelkoff, T., "One Dimensional Equations of Open-Channel Flow," Journal of the Hydraulics Division, ASCE, Vol. 95, No. HY3, May 1969, pp. 861-76.

22. Strelkoff, T., "Numerical Solution of Saint-Venant Equations," Journal of the Hydraulics Division, ASCE, Vol. 96, No. HY1, January 1970, pp. 223-52.

23. Wintz, W. A., and Kuo, Y. H., "A Study of Storm-Water Inlet Capacities," Report, Louisiana State University, Baton Rouge, 1970, 95 p.

24. Yen, B. C., "Spatially Varied Open-Channel Flow Equations," Research Report No. 51, Water Resources Center, University of Illinois at Urbana-Champaign, December 1971, 63 p.

25. Yen, B. C., "Open-Channel Flow Equations Revisited," Journal of the Engineering Mechanics Division, ASCE, Vol. 99, No. EM5, October 1973, pp. 979-1009.

NOTATION

A	cross sectional area of flow
A_s	surface area drained, $= L_g(B + W_p)$
a_{ij}	coefficients in Eq. 3.1
B	gutter width
b_{ij}	coefficients in Eq. 3.1
$b_1, b_2, b_3, b_4, b_5, b_6$	length dimensions of grate inlet as shown in Fig. 2
C_f	flow resistance constant, depending on cross sectional shape and rainfall intensity, to compute f for laminar flow
C^+	forward characteristics
C^-	backward characteristics
c	celerity of gravity wave
c_j	coefficients in Eq. 3.1
d_o	depth of flow measured at curb at cross section just upstream from grate inlet
E_o	specific energy head of flow at the cross section just upstream from grate inlet
e_k	k-th characteristic direction

F_i	function
F_r	Froude number
f	Weisbach resistance coefficient
G_l	nondimensional shape and pattern parameter of grate inlet
G_Q^*	correction factor for Q_{pi}
G_t^*	correction factor for t_p
g	gravitational acceleration
I_t	nondimensional parameter describing temporal distribution of rainfall
i	rainfall intensity
J_t	nondimensional parameter describing the shape of gutter upstream inflow hydrograph
k	roughness size of gutter surface texture
k_p	roughness size of pavement surface texture
L	length of grate inlet
L_g	gutter length
m	measure of interception efficiency of grate inlet
P	wetted perimeter
p^i	i-th dependent variable in Eq. 3.1
Q	discharge through a cross section

Q_i	discharge into grate inlets
Q_o	discharge at the cross section just upstream from grate inlet
Q_1	discharge per unit width of pavement
Q_{pi}	peak discharge into grate inlet
Q_{po}	peak outflow rate of gutter
Q_{pu}	peak gutter inflow at upstream
Q_r	a reference gutter discharge
Q_s	a reference discharge, = $iA_s + Q_{pu}$
q	lateral discharge per unit length
R	hydraulic radius
$\mathbb{R}$	Reynolds number
S_g	lateral slope of gutter
S_o	longitudinal slope of gutter
S_f	frictional slope of flow
S_p	crown slope of pavement, = $\tan \phi_p$
S_Q^*	correction factor for Q_{pi}
S_t^*	correction factor for t_p
T	surface width of gutter flow at a cross section
T_Q^*	correction factor for Q_{pi}

T_t^*	correction factor for t_p
t	time
t_i	duration of rainfall
t_ℓ	duration of lateral flow
t_u	duration of gutter upstream inflow
t_p	time of occurrence of Q_{pi}
V	cross sectional average velocity of gutter flow
V_o	average velocity of flow at downstream section of gutter
W	width of grate inlet
W_p	length of pavement
x	longitudinal distance
y	average depth of flow at a cross section
y_L	depth of lateral inflow
y_u	characteristic depth of gutter upstream inflow
Z_s	parameter describing spatial distribution of lateral inflow
Z_t	parameter describing temporal distribution of lateral inflow
α	forward characteristic direction
β	backward characteristic direction
γ	specific weight of water

Δt	time interval in a computational net
Δx	space interval in a computational net
δ	nondimensional parameter denoting downstream condition of gutter
δ_1	nondimensional parameter denoting downstream condition of grate inlet
η	nondimensional parameter representing the cross sectional shape of gutter
η_b	nondimensional shape parameter for grate bars
ν	kinematic viscosity of water
ρ	density of water
ϕ	angle between lateral direction of gutter bottom and horizontal; also used in Fig. 6 for method of characteristics
ψ	curb angle with respect to vertical
Ω	horizontally projected angle between main gutter flow direction and velocity vector of lateral inflow.